NSK

Cover photos:
   Automatic transmission

Contents

Technical Articles

Unique Fatigue Failure of Spherical Roller Bearings and Life-Enhancing Measures
Part I: Unique Fatigue Failure of Spherical Roller Bearings

Tohru Ueda and Kouji Ueda
Corporate Research & Development Center

ABSTRACT

It is well known that, in general, fatigue flaking of rolling elements can be classified as either subsurface originated flaking or surface originated flaking. Subsurface originated flaking is usually associated with ideal lubrication conditions and long bearing life. Surface originated flaking occurs when lubrication conditions are poor, resulting in relatively short life.[1)-3)] However, in the case of spherical roller bearings, surface originated fatigue failure can sometimes occur when the bearing is operating under ideal lubricating conditions. Consequently, spherical roller bearing life is relatively short compared to other bearing types. In this article, the mechanism of surface originated fatigue failure of spherical roller bearings will be clarified. We will also discuss how tangential force generated by rolling friction between rolling elements and raceways severely affects bearing life.

1. Introduction

Rolling elements in a spherical roller bearing are able to accommodate minor relative misalignment between the outer ring and the inner ring. This feature makes spherical roller bearings the best choice where operating conditions entail large radial loading and enhanced handling due to the integration of outer and inner rings as well as high resistance to mounting errors and impact loads. This is why spherical roller bearings are widely used for machinery in iron and steel works, roll necks in papermaking machinery, and for construction equipment, as well as for vehicles and other various applications.

In recent years, the cleanliness of bearing material has improved and rolling fatigue life has been enhanced under conditions of non-metallic inclusions in the material and ideal lubricating conditions. Meanwhile, rolling bearing life is still often calculated using the following formula based on the 1947 Lundberg and Palmgren theory (L-P theory), [4), 5)] which proposes that bearing failure originates with inclusions in the material:

$$L = \left[\frac{C}{F} \right]^p \quad \text{...} (1)$$

Where, L: Basic rating life (10^6 rev)
$\quad$ F: Dynamic equivalent load (N)
$\quad$ C: Basic dynamic load rating (N)
$\quad$ p: Point contact $p = 3$, line contact $p = 10/3$

Accordingly, bearings such as deep groove ball bearings, angular contact ball bearings, and cylindrical roller

bearings have achieved actual lives that significantly exceed calculated values under ideal lubricating conditions.

In the case of spherical roller bearings, however, the improved cleanliness of bearing materials has not enhanced their life under ideal lubricating conditions to the same extent as with other types of bearings.

To address this situation, the authors studied the failure mechanism to discover why only spherical roller bearings tend to differ from other bearings and assessed specifications for longer life. In this article, we will discuss the failure mechanism of spherical roller bearings as Part I of our report.

2. Life Properties and Fatigue Pattern of Spherical Roller Bearings

Fig. 1 is a diagram showing the results of a life test performed with various bearings under ideal lubricating conditions. The figure indicates that other types of bearings achieved actual lives that significantly exceeded the calculated values based on the L-P theory, whereas the ratio of actual life against calculated values is smaller for spherical roller bearings.

In order to determine why the life of spherical roller bearings differs from other types of bearings, we compared bearing fatigue patterns after conducting a fatigue test using X-ray diffraction analysis. It is generally understood that when bearing material becomes fatigued, the half-value width of the martensitic structure in the material will decrease according to the degree of material fatigue.[6)-8)] For this test, the depth and degree of fatigue in various areas of different bearings, which were operated to their calculated lives in a fatigue test, was measured from the

raceway surface, assuming the decreased level in the half-value width as an indicator of the degree of fatigue.

Fig. 2 shows the test results of a spherical roller bearing, and shows the test results of a deep groove ball bearing as an example of another typical bearing. When comparing the inner rings of both bearings where the highest degree of fatigue was applied, the deep groove ball bearing had the greatest decrease in half-value width, which indicates the greatest amount of fatigue based on observations at a certain depth from the surface (near the point where maximum shear stress was applied), with less fatigue observed in the surface. Conversely, the greatest amount of fatigue in the spherical roller bearings was seen in the surface. Thus, the fatigue pattern of the spherical roller bearings was markedly different from other bearings. A fatigue pattern in which the surface shows the most surface fatigue, is typically observed in ball bearings and roller bearings operated under adverse lubrication conditions. Spherical roller bearings characteristically show this fatigue pattern regardless of the quality of lubricating conditions.

In addition, when comparing surface fatigue levels by areas of the inner ring, the outer ring, and the rolling elements of a deep groove ball bearing, there was little difference in fatigue levels (decrease in the half-value

width). In spherical roller bearings, however, an extremely large fatigue level was observed in the inner ring, followed by the outer ring and the rolling elements, with substantially different surface fatigue levels from area to area. Under actual life tests as well, fatigued areas in the spherical roller bearing were mostly observed on the inner ring.
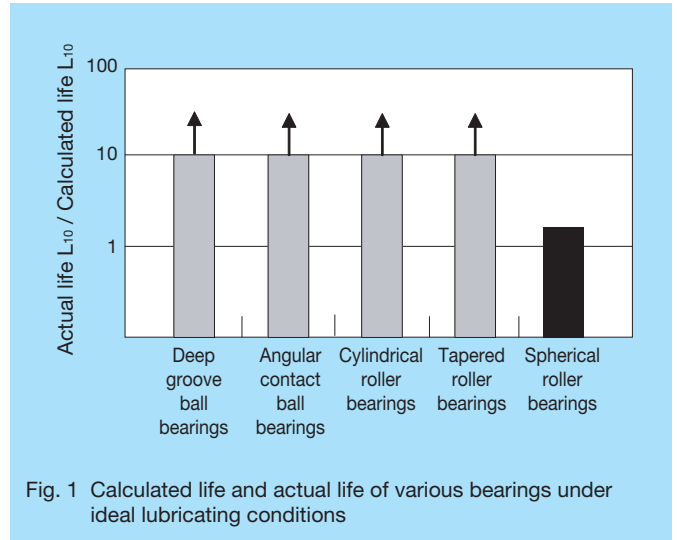
Fig. 1 Calculated life and actual life of various bearings under ideal lubricating conditions
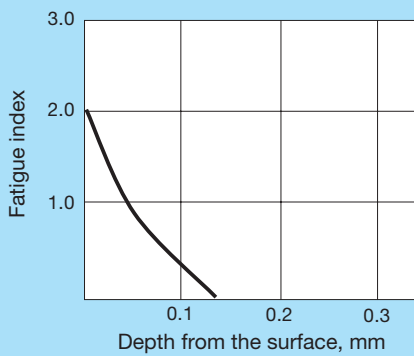
(a) In-depth fatigue index distribution of spherical roller bearing
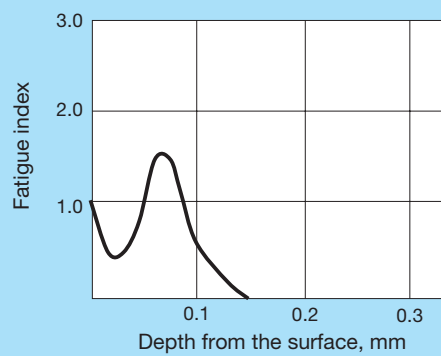
(b) In-depth fatigue index distribution of deep groove ball bearing
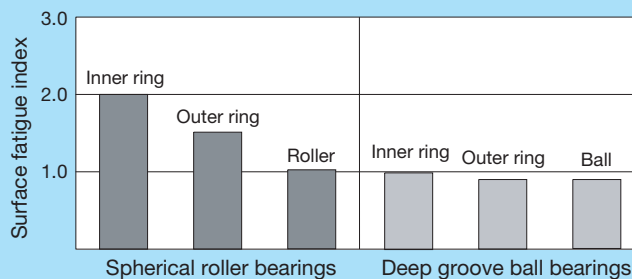
(c) Surface fatigue index in various parts of a spherical roller bearing and a deep groove ball bearing

Fig. 2 Fatigue index of spherical roller bearing and deep groove ball bearing under ideal lubricating conditions

3. Failure Pattern and Reproduction Test of Spherical Roller Bearings

As discussed thus far, spherical roller bearings display fatigue patterns different from other bearings. Due to this specific fatigue pattern, spherical roller bearings also express patterns of failure different from other bearings. Failure patterns specific to spherical roller bearings are discussed below based on results of surface observations performed until failure.

First, plastic flow appears in a minute region of the inner surface at the initial stage of the fatigue process (figure 3, a). The authors named the plastic flow regular ribbed markings or just ribbed markings. Fig. 4 shows the observation results of ribbed markings using an atomic force microscope (AFM). An AFM uses a microscopic probe that scans the surface of a sample at close proximity. Atomic forces between the probe tip and the specimen surface lead to deflections that are measured to create a three-dimensional surface profile. As shown in Fig. 4, the surface roughness in the area where ribbed markings developed was extremely milder than in other areas, and the surface condition was clearly different from other areas as well. However, due to the high hardness of the bearing material, the degree of plastic deformation in the bearings was too small to indicate that the area with ribbed markings was clearly a plastically flowed region. Afte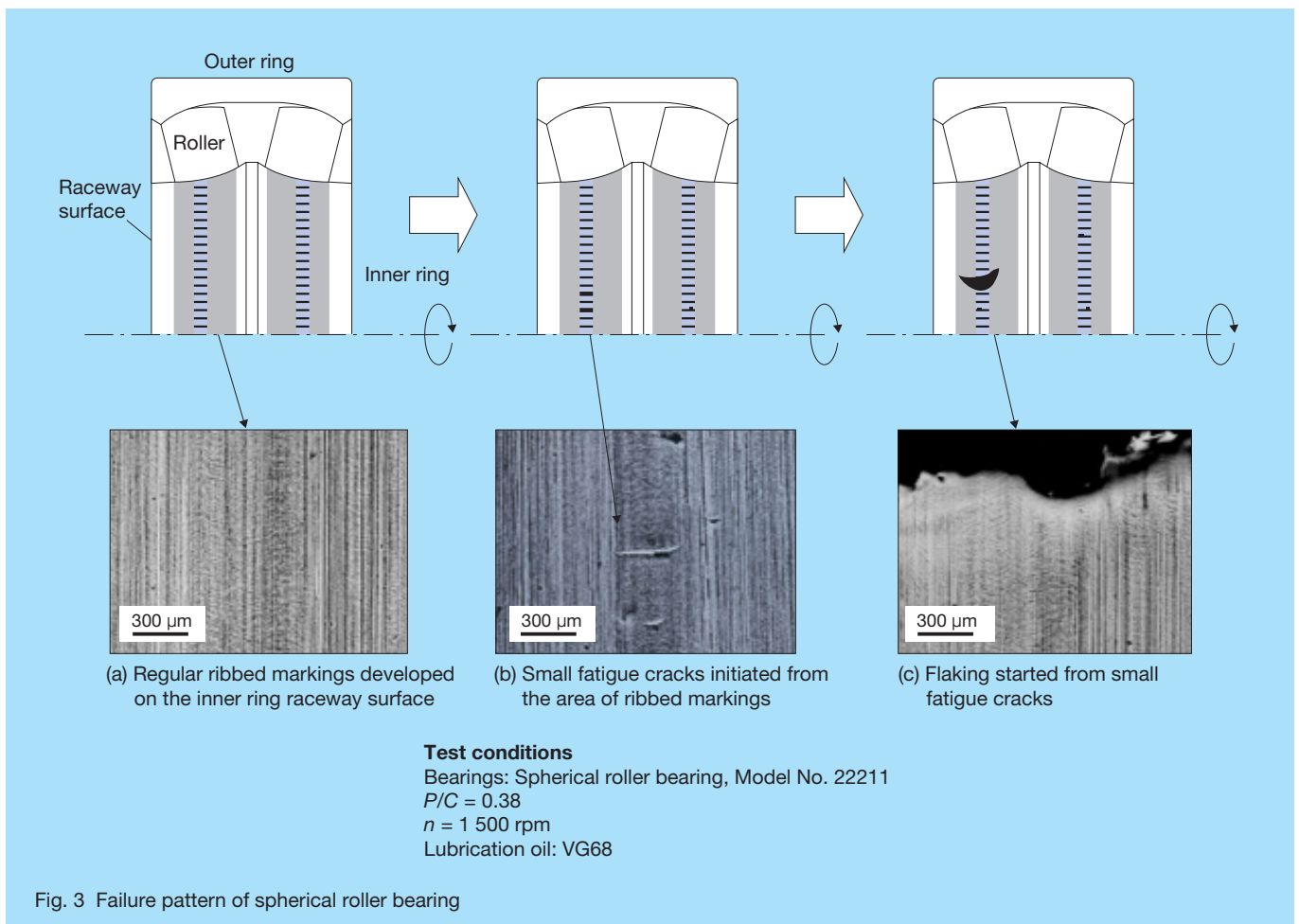r ribbed markings appeared, small fatigue cracks were generated (figure 3, b), and progressed until finally resulting in flaking (figure 3, c). Therefore, in order to fully explain the failure mechanism of spherical roller bearings, it is important to clarify the factors causing ribbed markings, which is the first stage of failure.

To this end, the authors used a twin-disk test machine to investigate the necessary conditions for causing ribbed markings. The investigation revealed that ribbed markings developed when bearings were subjected to sliding and contact pressure. Details of the ribbed-marking simulation test using the twin-disk machine are described below.

Fig. 5 shows the structure of the twin-disk machine. The driving member (with higher peripheral speed) is directly connected to a motor. The driven member (lower peripheral speed) is connected to a gear to reduce speed and to create sliding. Fig. 6 has illustrations of the test pieces. The outside diameter contact surface of the drive member (figure 6, b) has a rounded shape similar to that of a rolling element. Material of both the driving and driven members was hardened, tempered, bearing steel (JIS SUJ2). Testing was interrupted every two hours, and the contact surface areas were checked for any sign of regular ribbed markings.

(a) Regular ribbed markings developed on the inner ring raceway surface

(b) Small fatigue cracks initiated from the area of ribbed markings

(c) Flaking started from small fatigue cracks

Test conditions
Bearings: Spherical roller bearing, Model No. 22211
$P/C = 0.38$
$n = 1\ 500$ rpm
Lubrication oil: VG68

Fig. 3 Failure pattern of spherical roller bearing

As shown in Table 1, no regular ribbed markings were generated under conditions of a zero-percent or ten-percent slip rate and low contact pressure. However, ribbed markings (Fig. 7) were reproduced when the slip rate reached 10 % with contact pressure of more than 1.7 GPa. The regular ribbed markings were only observed on the driven member.

Tangential force, which acts between the two members, becomes greater with increased sliding and contact pressure (load).[9] The tangential force is exerted in the direction opposite to the rotating direction of the driving member, and it is exerted in the same direction as the rotating direction of the driven member. It is known that mechanical behaviors in the contact surface will vary according to the direction in which tangential force is applied and that pitching generally tends to occur more often in the driven member than in the driving member.[10)-12)] There are various theories for why pitching tends to occur more often with the driven member than with the driving member. One theory attributes the phenomenon to the fact that tensile stress is applied to the surface of the driven member immediately before it enters the contact surface, whereas compression stress is applied to the surface of the driving member immediately before it enters the contact surface,[10)] another theory, S. Way's theory,[12)] finds the

cause in the fact that lubricating oil intruding into surface cracks developed in the driven member will be confined to the cracks and cause tensile stress through hydraulic pressure. In this test, ribbed markings that were observed only on the driven member were considered to be associated with the difference in mechanical behaviors between the driving member and the driven member.

The above results obtained using a twin-disk test machine lead to the conclusion that ribbed markings occur when significant sliding is applied to bearings under high contact-pressure conditions on the driven member that is subject to dynamically harsh conditions.

Table 1 Twin-disk machine rolling-contact test results

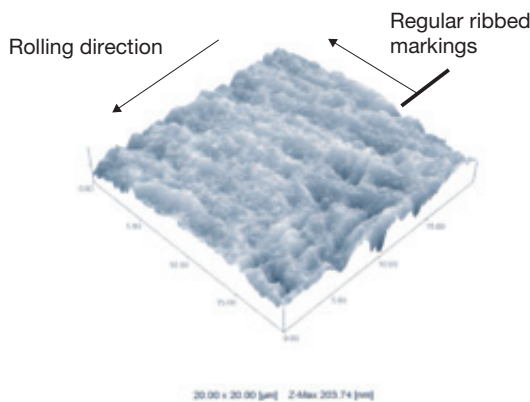| Pmax (GPa)	Slip ratio (%)	Test piece of driving member (rpm)	Time to development of ribbed markings (h)
3.2	10	500	2
2.5	10	500	10
1.7	10	500	24
1.2	10	500	No ribbed markings developed
3.2	0	500	No ribbed markings developed

Fig. 4 AFM observation of regular ribbed markings

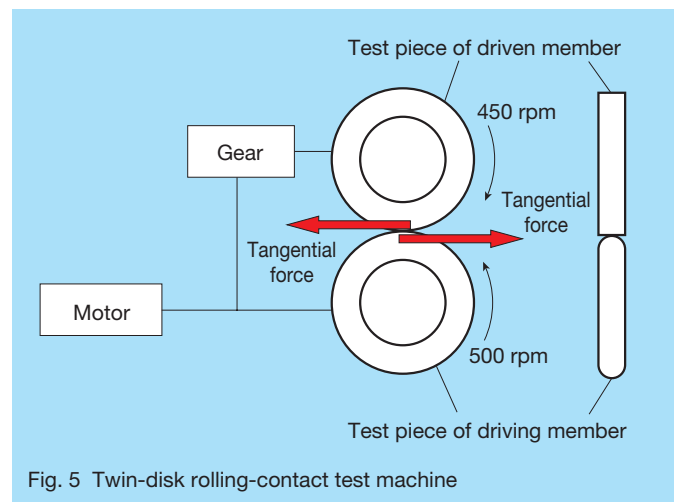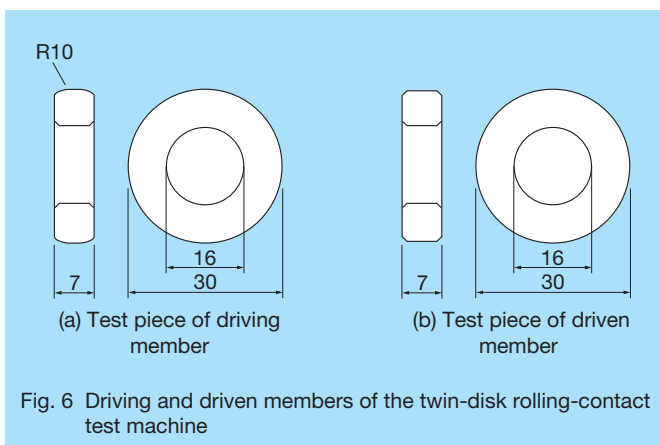Fig. 5 Twin-disk rolling-contact test machine

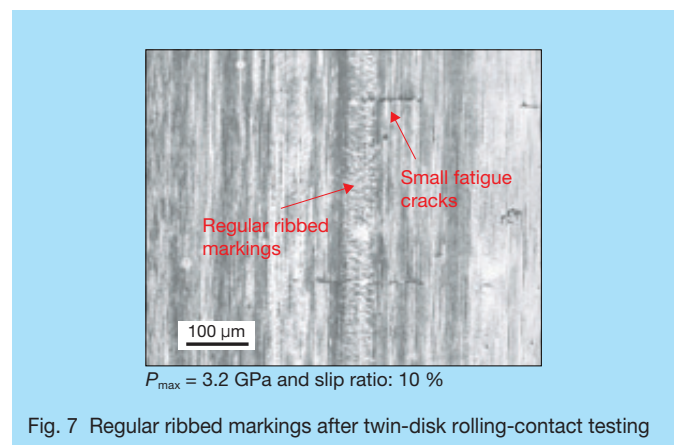Fig. 6 Driving and driven members of the twin-disk rolling-contact test machine

P_{max} = 3.2 GPa and slip ratio: 10 %

Fig. 7 Regular ribbed markings after twin-disk rolling-contact testing

4. Position of Sliding and Regular Ribbed Markings Occurring on Spherical Roller Bearings

The test results discussed in section 3 revealed that ribbed markings occur when significant sliding is applied to bearings under high contact-pressure conditions. Based on this finding, it is predicted that spherical roller bearings, which will fail as a result of the occurrence of ribbed markings, are operated under greater sliding and higher contact pressure compared to other types of bearings. In order to confirm this hypothesis, we studied the sliding exerted on spherical roller bearings.

There are two types of sliding that occur in spherical roller bearings, as shown in Fig. 8. One is spin slip that occurs when the rotating axis of the driving component (usually the inner ring) and the rotating axis of the rolling element are not parallel (figure 8, a). The other type of slip is differential slip that results from contact of the raceway and the rolling element along the curved contact surface (figure 8, b). Sliding that occurs in actual spherical roller bearings is a combination of these types of sliding with slip speeds distributed in the axial direction as shown in Fig. 8 (c). In other words, a spherical roller bearing generates sliding where the inner ring surface is a driven member at the contact point under high contact pressure.

With the objective of verifying the above results, the authors calculated the distribution of contact pressure and slip velocity, and compared them with the positions of actually developed ribbed markings. Fig. 9 shows the relationship between the contact pressure exerted on the inner ring, the outer ring, and the roller at the maximum load position, slip velocity, and the positions of ribbed markings occurring in a spherical roller bearing. Positions of ribbed markings occurring on a spherical roller bearing

were marked as shown in the photos of Fig. 9 and plotted in the diagram in the center of Fig. 9. The conditions under which contact pressures and slip velocity were calculated included bearing type 22211, P/C = 0.38, and the number of revolutions (n = 1 500 rpm). The slip velocity distribution is expressed by ▲ and △ in Fig. 9. In Fig. 9, the negative slip velocity area shows where the peripheral speed of the inner and outer rings is slower than the peripheral speed of the roller, that is, the area where the inner and outer rings act as a driven member. For this study, all calculations and experiments were performed with a rotating inner ring and a fixed outer ring. When the inner ring acts as a driven member, the peripheral speed of the inner ring is slower than that of the roller at the point where the inner ring contacts the roller, whereas when the outer ring acts as a driven member, the rotating speed of the roller is faster than the revolving speed of the roller at the point where the outer ring contacts the roller.

As shown in Fig. 9, ribbed markings occurred in the area where either the inner ring or the outer ring acts as a driven member. The figure also indicates that ribbed markings occurred more frequently in the inner ring than in the outer ring. This phenomenon can be attributed to the higher contact pressure applied to the inner ring than in the outer ring as indicated by ● and ○ in Fig. 9.

In addition, Fig. 9 indicates that the slip velocity is positive on the side closer to the roller end, or the area where the roller acts as a driven member (inner and outer rings act as a driving member). In this area, however, no ribbed markings were observed in the rolling member. The reason for this phenomenon is considered to be that lower contact pressure is exerted on the side closest to the end of the roller where it acts as a driven member.
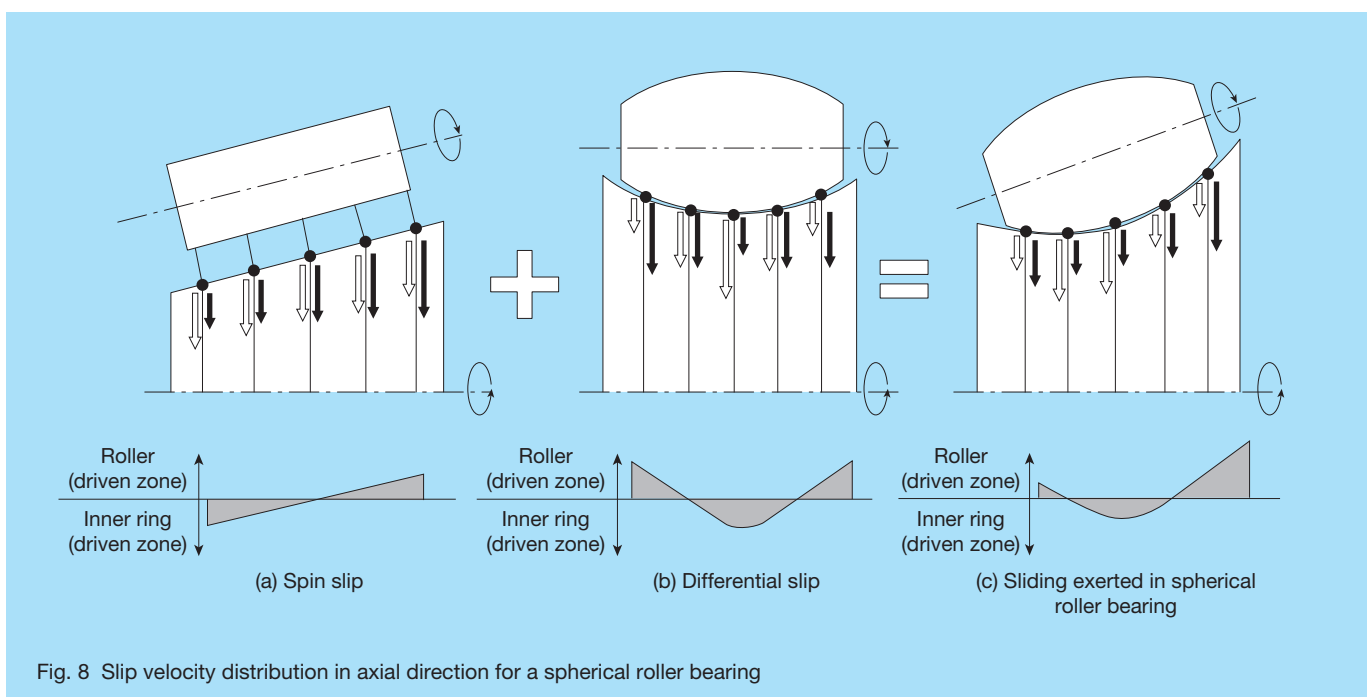
Fig. 8 Slip velocity distribution in axial direction for a spherical roller bearing

5. Occurrence of Regular Ribbed Markings

The results in sections 2, 3, and 4 revealed that the occurrence of ribbed markings that causes flaking of spherical roller bearings can be decisively associated with sliding and high contact pressure where the inner ring acts as a driven member.

Ribbed markings are a specific failure pattern that is observed only in spherical roller bearings and is typically not observed in ball bearings or cylindrical roller bearings. One conceivable reason is that the differential slip is smaller in cylindrical roller bearings with low contact pressure because the roller and rings come into line contact and with nearly negligible differential slip since it is basically free from curvature in the axial direction.

Conversely, ball bearings do not develop ribbed markings although they suffer high contact pressure resulting from the point contact structure and suffer differential slip. The authors believe this phenomenon is attributable to the following:

The failure pattern observed in spherical roller bearings is considered to be significantly associated with the tangential force applied between the rolling element and the raceway. Known factors that are associated with tangential force include surface roughness in addition to sliding and contact pressure (load) as described earlier.[13] In general, available surface roughness differs between a roller and a ball of a rolling element due to variation in surface polishing. As a ball does not have the same three-dimensional orientation of a roller, the ball finish can be achieved by grinding between two discs. However, in the

Conditions
Bearings: Spherical roller bearing, Model No. 22211
P/C = 0.38
n = 1 500 rpm
Roller position: Maximum load position

Fig. 9 Relation between slip velocity, contact pressure, and position of regular ribbed markings

case of a roller, since it has a three-dimensional orientation, only the rolling surface is finished using a different grinding method. In general, mean roughness achieved on a ball by the former polishing method is 0.01 μm (Ra) or less, whereas mean roughness on a roller by the latter method is 0.01 μm (Ra) or greater. For these reasons, it is considered that ball bearings are free from ribbed markings with small tangential force exerted on the rolling element and the raceway due to small surface roughness of the rolling element even with significant sliding or high contact pressure. The authors investigated the probability of the occurrence of ribbed markings on a ball bearing using a ball with a surface roughness equivalent to a roller incorporating a spherical roller bearing with the aim of demonstrating the effect of roughness of rolling members on the occurrence of ribbed markings. The result was the occurrence of ribbed markings on the ball bearing as shown in Fig. 10.

From those findings, ribbed markings that result from increased tangential force with high contact pressure, sliding, and roughness on the rolling element, can be considered a phenomenon specific to spherical roller bearings combining all the above conditions.
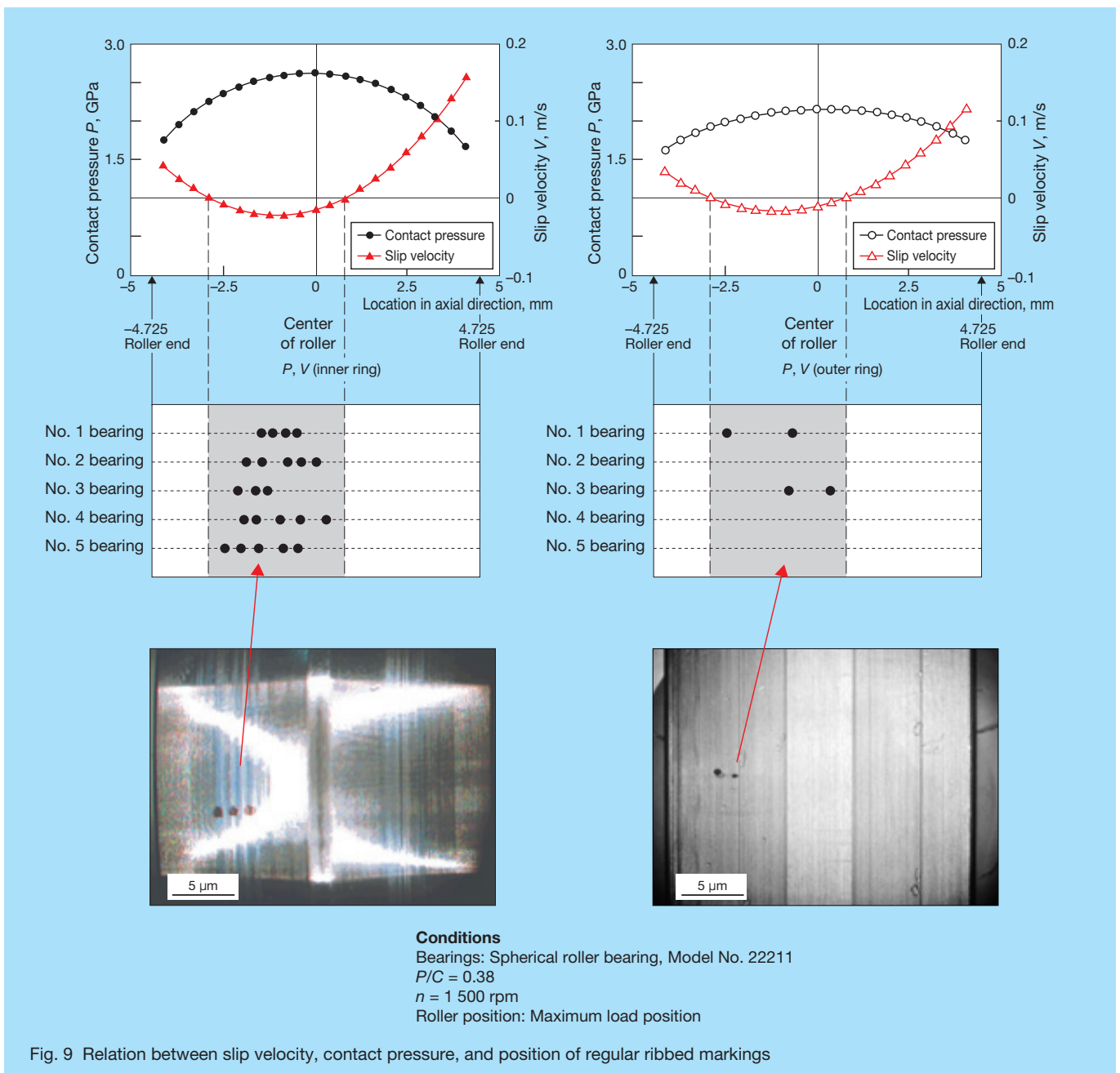
6. Conclusion

1. Spherical roller bearings develop a surface-originated fatigue pattern even under ideal lubricating conditions and flaking in the following process:
(1) Plastic flow (regular ribbed markings) occur;
(2) Small fatigue cracks initiate from regular ribbed markings; and
(3) Small fatigue cracks propagate, resulting in flaking.
2. Surface-originated flaking specific to spherical roller bearings arises from increased tangential force exerted on the rolling element and the race caused by the following factors:
(1) High contact pressure;
(2) Large sliding; and
(3) Significant roughness on the surface of the rolling element.
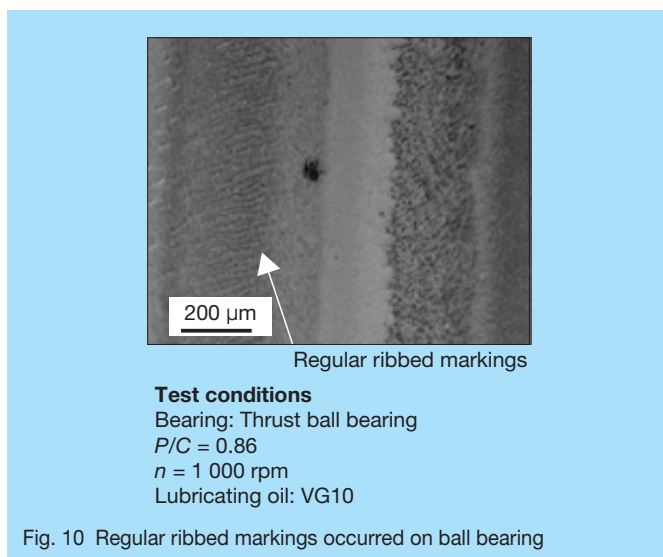
References

1) W. E. Littmann, R. L. Winder, J. O. Wolfe, J. D. Stover, "The Role of Lubrication in Propagation of Contact Fatigue Cracks " Trans. ASME, F, 90-1 (1968) 89-100.
2) K. Furumura, S. Shirota, K. Hirakawa, "Surface-Originated and Subsurface-Originated Rolling Fatigue" NSK Bearing Journal, 636 (1977) 1-10.
3) K. Furumura, Y. Murakami, C. Abe, "Development of Long-Life Bearings Materials under Clean Lubrication and Contaminated Lubrication Conditions" NSK Technical Journal, 656 (1993) 15-21.
4) G. Lundberg, A. Palmgren, "Dynamic Capacity of Rolling Bearings" IVA Handlingar, NR 196 (1947).
5) G. Lundberg, A. Palmgren, "Dynamic Capacity of Rolling Bearings" IVA Handlingar, NR 210 (1952).
6) K. Furumura, S. Shirota, A. Fujii, "Fatigue Analysis in Ball and Roller Bearings (Part 1) _Analysis of Surface Fatigue Failure (1)" NSK Bearing Journal, 643 (1982) 1-10.
7) K. Furumura, S. Shirota, A. Fujii, "Fatigue Analysis in Ball and Roller Bearings (Part 2) _Analysis of Surface Fatigue Failure (2)" NSK Bearing Journal, 644 (1984) 1-6.
8) K. Furumura, S. Shirota, A. Fujii, "Fatigue Analysis in Ball and Roller Bearings (Part 3) _Analysis of Internal Fatigue Failure" NSK Bearing Journal, 646 (1986) 18-25.
9) Y. Yamamoto, Y. Kaneda, "Tribology" (2001) Rikogakusha Publishing.
10) N. Soda, T. Yamashita, K. Ohzora, "Influence of Tangential Force Exerted on Rolling Fatigue" Lubrication, 16-8 (1971) 573-584.
11) Y. Murakami, C. Sakae, K. Ichimaru, "Application of Fracture Mechanics to Tribology Issues (Part 1, Analysis of Propagation of Three-Dimensional Curved Surface Cracks under Rolling Contact Load)" Kironshu A, 58-556, (1992) 2313-2320.
12) S. Way, "Pitting Due to Rolling Contact" J. Appl. Mech., 2-2 (1935) A49-A58.
13) N. Soda, R. Yamamoto, "Roles of Tangential Force in Development of Pitching in Gears" Lubrication, 20-4 (1975) 268-275.

Regular ribbed markings

200 μm

Test conditions
Bearing: Thrust ball bearing
P/C = 0.86
n = 1 000 rpm
Lubricating oil: VG10

Fig. 10 Regular ribbed markings occurred on ball bearing

Tohru Ueda

Kouji Ueda

Bearing Outer Ring Creep

Jianjun Zhan and Kinji Yukawa, Corporate Research & Development Center
Hiromichi Takemura, Automotive Bearing Technology Center

ABSTRACT

In recent years, advances in automobile and machine technology have led to an increase in the usage of rolling bearings in a compact space under conditions of high speed and heavy load. The result is a greater likelihood that outer ring creep may occur in certain applications. Conventionally, the phenomenon called outer ring creep was considered to be an effect of rotating load, where the outer ring slightly rotates in the opposite direction of the inner ring. However, there are many cases where outer ring creep has occurred even if the direction of load remained unchanged. Theories surrounding the mechanism of outer ring creep have proven inconclusive for conditions where the direction of load remained unchanged. NSK conducted tests and analyses to better understand the many factors related to outer ring creep. Our conclusion is that outer ring creep, which develops under conditions of nonrotating load, is a result of localized strain and rippling deformation that is generated with the passing of each rolling element. Our investigations, which are discussed below, further clarify how the amount of clearance, outer ring thickness, and the number of rolling elements influence outer ring creep.

1. Introduction

A slow relative rotation of an outer ring against the housing is sometimes encountered during the operation of a rolling bearing. This phenomenon, called outer ring creep, is a typical malfunction associated with rolling bearings. Outer ring creep may cause wear of the housing or outer ring, resulting in such problems as unusual noise and vibration. Outer ring creep may also allow the entry of abrasive particles into the bearing, resulting in bearing failure.

Creep has been generally considered an effect of rotating load. Given this concept, under conditions in which the inner ring rotates and the outer ring is fixed, the application of static load to the bearing may result in creep in the inner ring but not in the outer ring. The authors, however, have observed that, even in this case, creep occurs in the same direction of inner ring rotation under certain conditions. Few theories are available so far that explain the generation mechanism of this outer ring creep in the same direction of inner ring rotation.

In this article, we will clarify the mechanism of outer ring creep generated when bearing load is applied to the outer ring in a fixed direction--a phenomenon not explained by conventional creep theory. For the sake of convenience, our report focuses on outer ring creep under conditions in which the outer ring is fixed; however, the mechanism of outer ring creep generated when the outer ring is rotated can be similarly explained by movement relative to the outer ring.

2. Generation Mechanism

2.1 Generation mechanism of outer ring creep in the opposite direction of inner ring rotation

Outer ring creep in the opposite direction of inner ring rotation generally occurs when bearing load rotates along with the inner ring. Many reports have been previously published regarding this topic.[1-4]

As shown in Fig. 1, when there is clearance between the housing and the outer ring of a bearing, the application of bearing load Fr will force the outer ring against the housing bore in the same direction as the load (in a direction that is perpendicular to the axis of rotation). The contact region between the outer ring and the housing, then, will also move in the same direction according to the rotation of bearing load Fr, resulting in rotational movement of the outside surface of the outer ring against the housing bore.

Given c as the difference between the inner diameter of the housing and the outer diameter of the outer ring, the difference in the circumferences of the two circles will be πc. Accordingly, for each rotation cycle of the inner ring, the movement of the outer ring will be delayed by length πc on the circumference relative to the housing, causing the outer ring to rotate in the opposite direction of the inner ring (Fig. 1).

2.2 Outer ring creep in the same direction of inner ring rotation

Conversely, for outer ring creep that occurs when bearing load is applied in a fixed direction, the outer ring

Fig. 1 Generation of outer ring creep (slight rotation) in the opposite direction of inner ring rotation
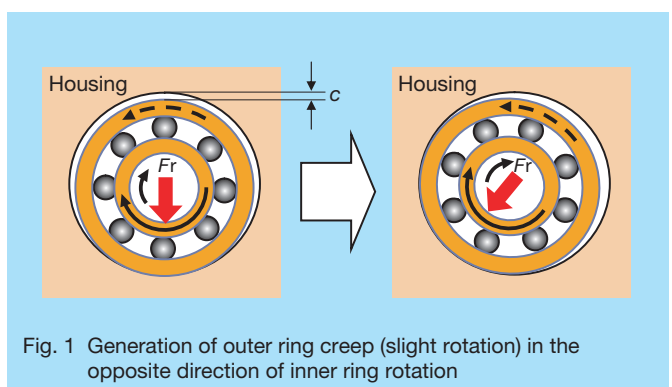
of the bearing will move in the same direction as the inner ring while sliding as shown in Fig. 2. In order to quantitatively study this creeping phenomenon, the authors reproduced outer ring creep in an experiment using the method shown in Fig. 3 and recorded with a video camera the behavior of the outer ring under various conditions.

Main experimental conditions:
· Type of bearing: Deep groove ball bearing (6207)
· Lubricant: Grease
· Rotational speed: 0 to 5 000 rpm
· Bearing load ratio (Fr/Cr): 0 to 0.4
      Fr: Bearing load
      Cr: Basic dynamic radial load rating of bearings

We evaluated the relationships among bearing load ratio, rotational speed, and creep speed based on experimental data.

Fig. 4 shows the relationship between outer ring creep speed and bearing load, indicating that outer ring creep speed increases along with the increase in bearing load. No outer ring creep was generated at a relatively low bearing load ratio ($Fr/Cr<0.05$), even at faster inner ring rotational speeds.

Fig. 5 shows the relationship between outer ring creep speed and the rotational speed of the bearing inner ring. This figure indicates that once outer ring creep has been generated, creep speed is almost proportional to the rotational speed of the inner ring.

2.3 Generation mechanism of outer ring creep in the same direction of inner ring rotation

One probable cause for outer ring creep is the dynamic torque of the bearing. From this perspective, the authors conducted experiments to study the relationship between torque that causes the generation of outer ring creep (creep torque) and dynamic torque.

Creep torque was measured with a torque arm mounted to the outer ring and connected to a load cell with a wire (Fig. 6). Meanwhile, dynamic torque of the driving element was measured as torque was applied to the axis of

rotation. Fig. 7 shows the results of measurements that were taken under the same experimental conditions as in the previous section. These results indicate that creep torque was approximately 50 times greater than dynamic torque. It is therefore evident that dynamic torque was not a cause for the generation of creep.

Next, we observed changes in the deformation of the outer ring associated with passage of the rolling element as a possible cause for generating outer ring creep. In order to obtain data on changes in deformation of the outer ring, we performed static FEM analysis with the two-dimensional model shown in figure 8, under the same conditions as the previous creep experiment. Fig. 9 (a) shows the distribution of circumferential strain (ε_θ) and radial strain (ε_r) at the outer ring region where maximum rolling element load was applied to the contact region with the bore housing. The solid line in the graph indicates deformation distribution relative to the present position of the rolling element, and the dotted line indicates deformation distribution relative to the position where the rolling element will reach as it moves in the next moment. In terms of static distribution at each moment, distribution of ε_θ and ε_r is symmetric with respect to the center of the contact region surface between the outer ring and the rolling element.

Now, Fig. 9 (b) shows the calculated distribution of deformation variations associated with movement of the
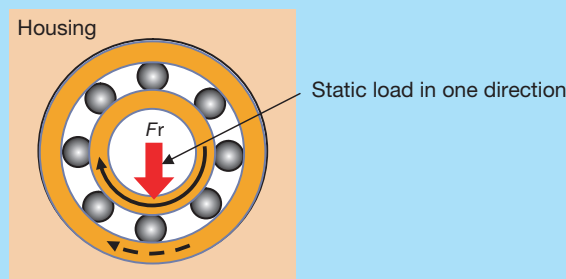
Fig. 2 Generation of outer ring creep (slight rotation) in the same direction of inner ring rotation
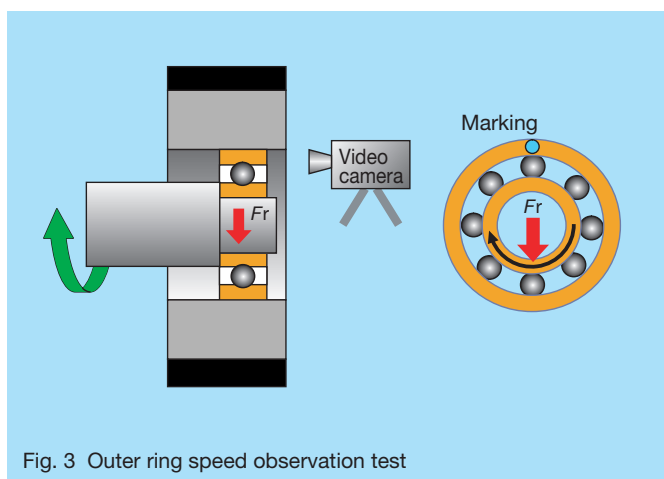
Fig. 3 Outer ring speed observation test
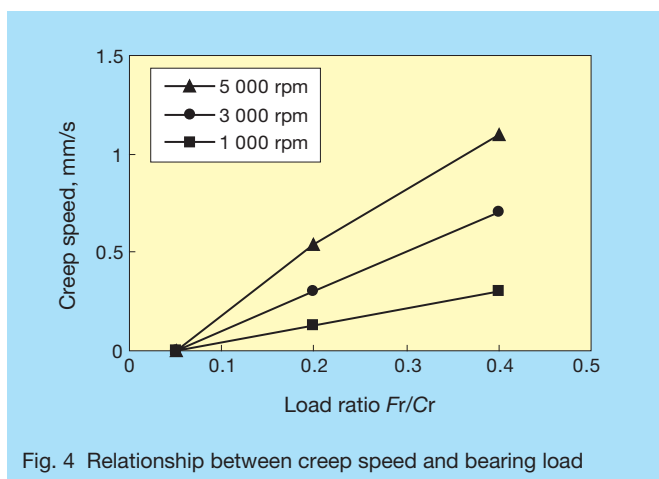
Fig. 4 Relationship between creep speed and bearing load

rolling element: $\varDelta\varepsilon_\theta$ and $\varDelta\varepsilon_r$. According to Fig. 9 (b), deformation variations are distributed differently with the passing of each rolling element at the contact points located just in front of and right behind the roller. Because contraction on the front side occurs gradually, $\varDelta\varepsilon_r$ will take a negative value. At the same time, because expansion occurs gradually, $\varDelta\varepsilon_\theta$ will take a positive value. Meanwhile, as the rolling element continues rolling motion, the outer ring will contract in the circumferential direction and expand in the radial direction right after the roller. In addition, severe surface pressure will immediately arise between the outer ring under the rolling element and the housing, which will cause temporary sticking. The area just before the loaded zone will expand outwards in the same direction of roller motion; and simultaneously, the area right after the loaded zone will contract in the same direction of rolling element motion. From these findings, it can be seen that every deformation change that arises with each passage of a rolling element generates a force that rotates the outer ring circumferentially, which causes the outer ring to rotate in the house ever so slightly, thus resulting in creep.

3. Examination by FEM Analysis

With regard to the experimental device in the previous section, we made an FEM model that had a fixed housing with stiff body and used an outer ring with an elastic body using bearing steel (SAE 52100) (Fig. 8). We performed a two-dimensional FEM analysis with rolling element loading applied to the model as a boundary condition. Outer ring deformation and movement were calculated for rolling element load rotated gradually at a coefficient of friction, which varied significantly depending on surface conditions under normal operation, which was set at 0.2 in this experiment.

Analysis was performed under the following conditions as a basic model. Calculated results were used as reference values. Results of calculations performed under changing conditions are shown as ratios in relation to reference values.

· Number of rolling elements: 9
· Ratio of outer ring thickness to rolling element diameter: 0.33
· Clearance between outer ring and housing: 30 µm
· Bearing load ratio (Fr/Cr):   0.2

Fig. 5   Relationship between outer ring creep speed and inner ring speed

Fig. 6   Outer ring creep torque test
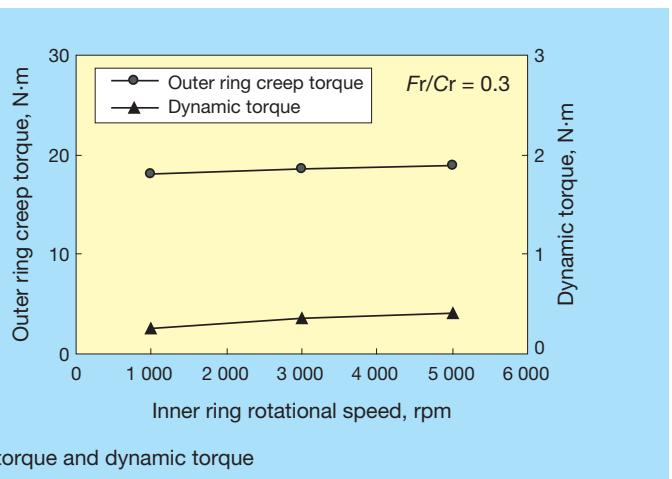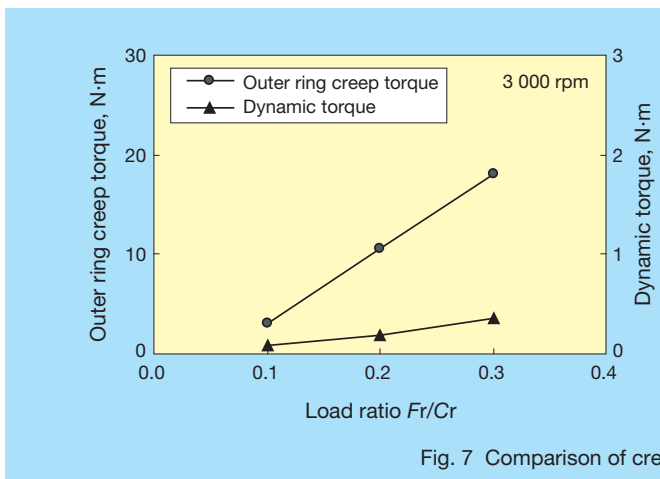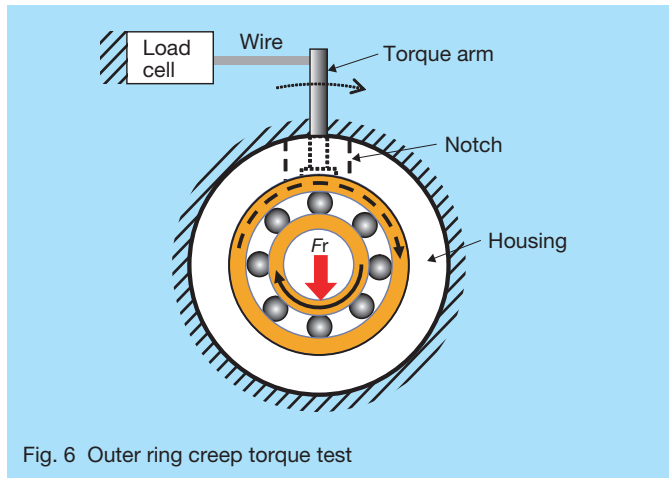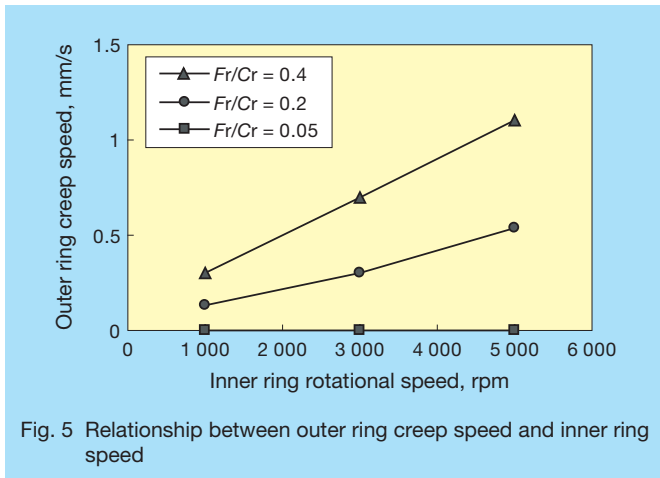
Fig. 7   Comparison of creep torque and dynamic torque

3.1 Relationship between outer ring creep speed and bearing load

First, we calculated the circumferential displacement of reference point P on the outer diameter of the outer ring with the inner ring rotated a little at a time, given that the rolling element moved by one pitch (the distance between neighboring rolling elements). We took into consideration changes in the size of rolling element load associated with rotation.

We calculated creep speed by multiplying the displacement for one pitch rotation of the rolling element load by the number of revolutions and the number of rolling elements. Fig. 10 shows the relationship between creep speed and bearing load. Fig. 10 indicates that creep speed increased with the increase in bearing load. This tendency agreed with experimental results shown in Fig. 4.
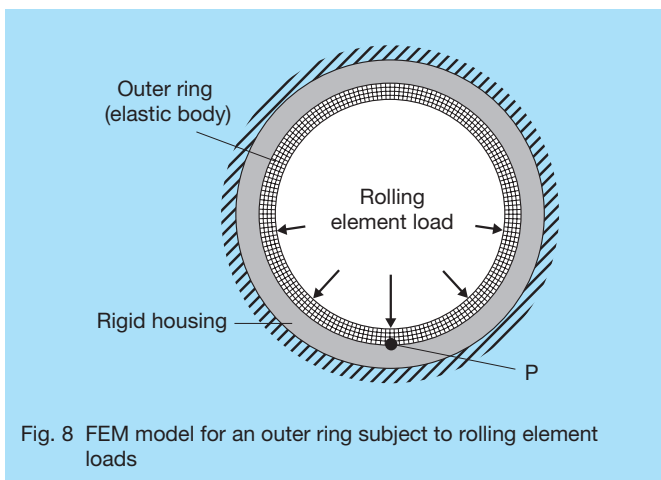
Fig. 8 FEM model for an outer ring subject to rolling element loads

3.2 Relationship between outer ring creep torque and bearing load

Creep torque can be also calculated from the reaction force at point P, given that rolling element load is similarly rotated with reference point P on the outer ring fixed in the circumferential direction. Fig. 11 shows the relationship between creep torque and bearing load. The findings from Fig. 11, which indicate that outer ring creep torque increases with increased bearing load, essentially agree with the measured results of outer ring creep torque as shown in Fig. 7 (a).

4. Factors Affecting Likelihood of Outer Ring Creep

4.1 Influence of the amount of clearance

Fig. 12 shows the result of calculation performed assuming that clearance changed in the range from -30 µm to +30 µm. Fig. 12 indicates that creep torque changes in proportion to the increase or decrease in clearance within the range of -30 µm to +30 µm. When clearance is negative, creep torque becomes smaller and creep is less likely to occur.

4.2 Influence of the number of rolling elements

Fig. 13 shows the result of calculation regarding the influence of the number of rolling elements. Fig. 13 indicates that creep torque becomes smaller with a greater number of rolling elements. This is because the rolling element load will become smaller with the higher number of rolling elements and, as a result, local deformation of the outer ring will be curbed.
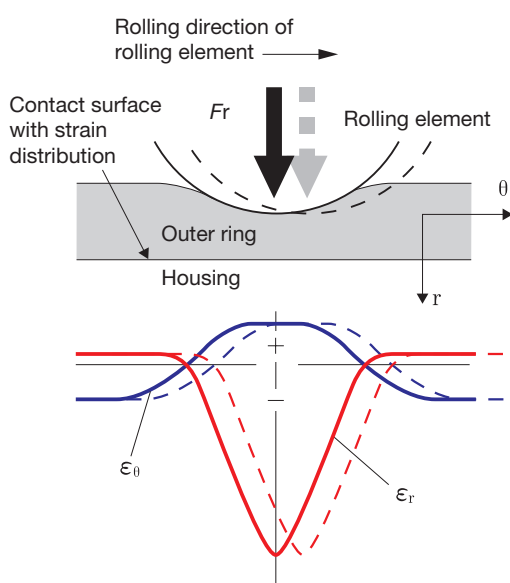
(a) Strain distribution induced by contact surface pressure from rolling element load
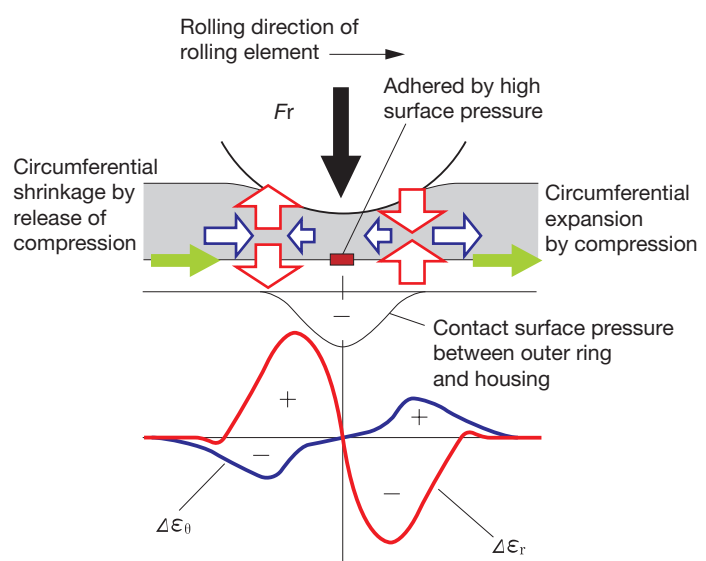
(b) Variations of distribution of contact surface strain of the outer ring during passage of the rolling element

Fig. 9 Outer ring creep resulting from local deformation

4.3 Influence of the outer ring thickness

In light of the fact that the cause of creep is changes in deformation of the outer ring, it can be seen that increasing the stiffness of the outer ring will prevent outer ring creep. Fig. 14 shows changes in creep torque for given outer ring thickness in relation to rolling element diameter. Fig. 14 indicates that as creep torque becomes smaller with increased outer ring thickness, the occurrence of creep is less likely to occur.

5. Postscript

Based on experimental findings and analyses, we have verified that outer ring creep results from changes in local deformation of the outer ring caused by the movement of rolling elements. In addition, we have demonstrated that a simple two-dimensional FEM model is effective in verifying outer ring creep. Furthermore, we introduced study results relating to several factors that affect the occurrence of outer ring creep as references for prediction and prevention of creep.

It has been shown that outer ring creep may occur under conditions of static load as well as when bearing load rotates. In particular, with the trend toward an increase in the usage of bearings that are operating at higher speeds under heavy loads, bearings associated with recent advances in automotive and machine technology are more likely to suffer from outer ring creep. Under these circumstances, predicting or restricting creep phenomena will become more important in bearing applications in the future.
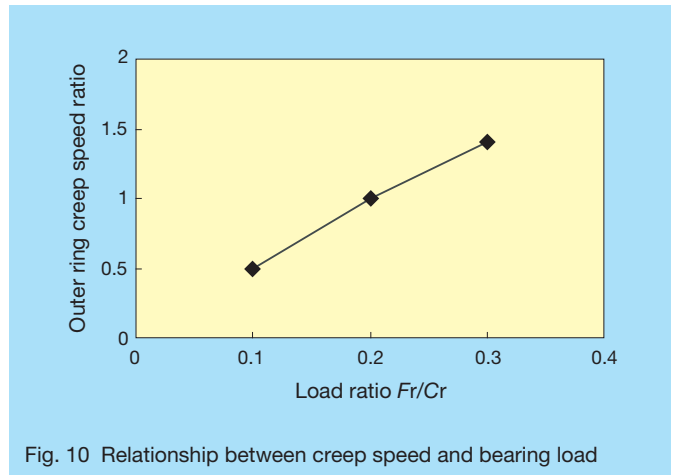
Fig. 10 Relationship between creep speed and bearing load
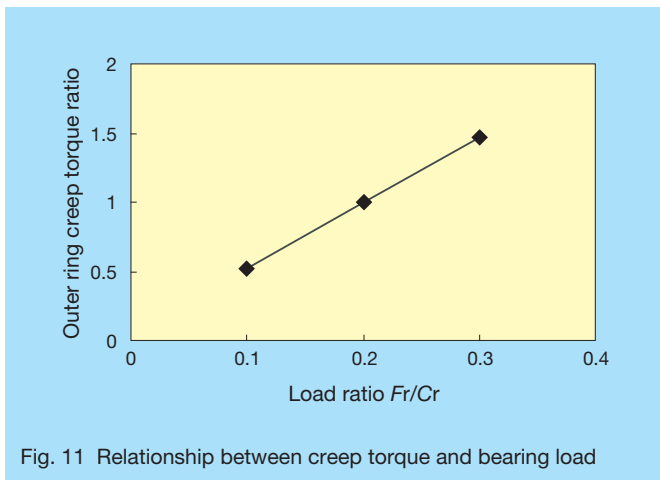
Fig. 11 Relationship between creep torque and bearing load
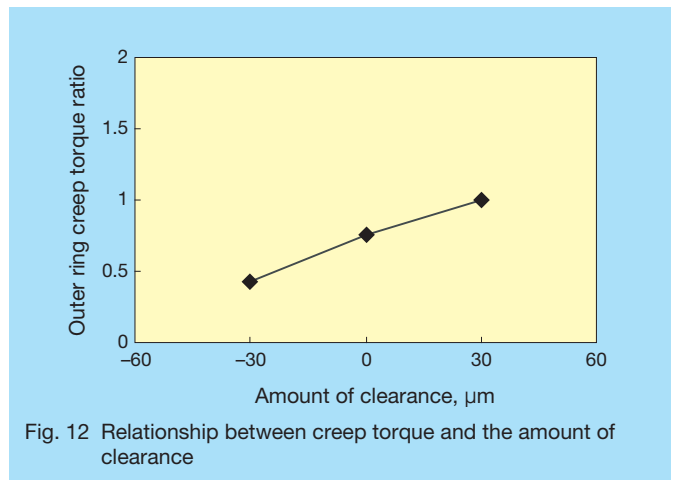
Fig. 12 Relationship between creep torque and the amount of clearance
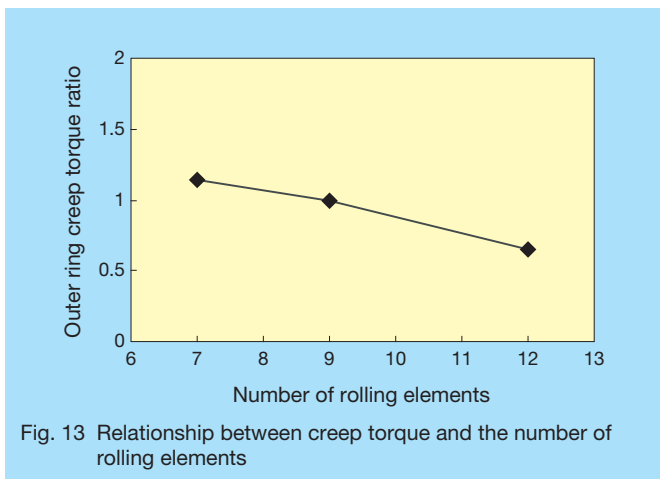
Fig. 13 Relationship between creep torque and the number of rolling elements
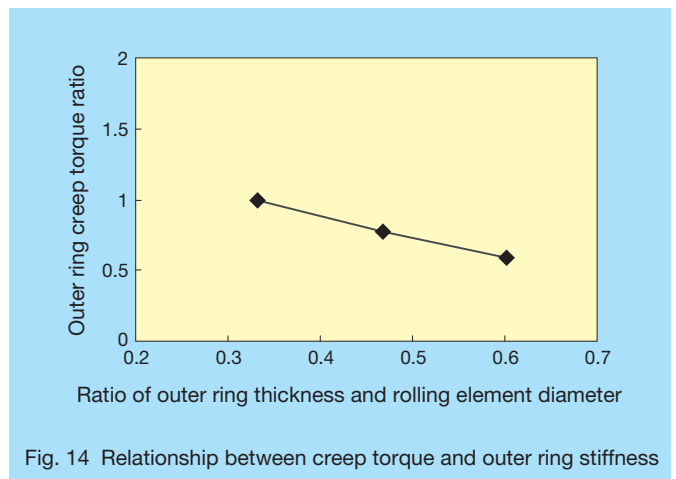
Fig. 14 Relationship between creep torque and outer ring stiffness

References

1) N. Soda, "Bearings" Iwanami Shoten (1964) 196-203.
2) J. Okamoto, K. Kakuta, "Rolling Bearings—Characteristics and Practical Design" Saiwai Shobo (1981) 131-132.
3) E. Watabayashi, "Rolling Bearing Manual" Japanese Standards Association (1999) 111-113.
4) E. Watabayashi, H. Tawara, "Knowledge about Bearings" Japanese Standards Association (1987) 123.
5) Y. Sakajiri, H. Takemura, "Behaviors of Outer Ring Wavy Deformation Creep in Rolling Bearings" Proceedings for tribology meeting, Japanese Society of Tribologists (2003) 103-104.

Jianjun Zhan

Hiromichi Takemura

Kinji Yukawa

Latest Developments in Thin-Film Lubrication Technology for Vacuum and Clean Environments

Dai Kinno
Corporate Research & Development Center

ABSTRACT

In this report, we will discuss the latest developments in thin-film lubrication technology for vacuum and clean environments. Specifically, we will focus on the structure and characteristics of NSK's newly developed lubricant-film treatment called E-DFO, which takes advantage of DFO thin-film lubrication technology. We will present evaluations and test results of E-DFO treated ball screws and linear guides that revealed a twentyfold increase in durability and a nearly 50 % cut in outgassing and contamination in comparison with conventional DFO treated applications.

1. Introduction

Mechanical components of equipment used to manufacture liquid crystal display panels or semiconductors are increasingly being called upon to reduce particle emissions and outgassing associated with the effects of contamination by organic matter. It is difficult, however, for conventional technology that typically uses grease and solid lubricants to completely meet these requirements. Given this background and observing that thin-film lubrication produces less organic matter contamination, NSK successfully developed a new thin-film lubrication technology called durable film outer (DFO) coating process. This technology was applied to linear guides, ball screws, and bearings that were introduced into the market in 2001 as the V-DFO series, which provided the least tolerance for organic matter contamination. Recently, however, high durability with less frequent maintenance intervals has also been highly sought in addition to reduced contamination by organic matter, as mentioned above. In response to this need, NSK successfully developed E-DFO, which is superior to V-DFO in terms of both reducing organic matter contamination and extending product operating life.

This paper explains the technical details of E-DFO and presents the results of evaluation tests on ball screws and linear guides treated with E-DFO.

2. Thin-Film Lubrication Technology for Vacuum and Clean Environments

Fig. 1 summarizes NSK's lubrication technologies for special environments. Lubrication technologies for vacuum and clean environments, categorized as special environments, include grease lubrication, solid lubrication, and DFO thin-film lubrication. DFO is a lubricant-film treatment that leaves a baked-on finish to form a thin film that serves as a lubricant on component surfaces. The DFO treatment is applied to both E-DFO products (Fig. 2), and V-DFO products, which have already been commercialized and are utilized in the market.

Lubrication for special environments
└─ Lubrication for vacuum and clean environments
   ├─ Grease lubrication
   ├─ Solid lubrication
   └─ DFO (thin-film lubrication)
      ├─ V-DFO (thin-film lubrication for vacuum environments)
      └─ E-DFO (long-life, thin-film lubrication for vacuum environments)
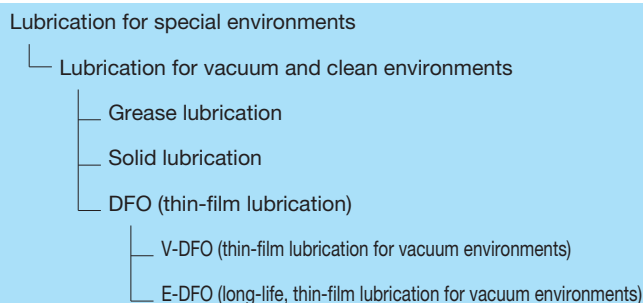
Fig. 1 Progress of NSK's thin-film lubrication technologies

3. Characteristics of E-DFO

3.1 Thin-film structure

Fig. 3 illustrates the thin-film structures of V-DFO and E-DFO. In the thin-film structure of V-DFO, perfluoropolyether (PFPE), a kind of fluorine oil, is baked onto the surface to form a uniform, free-flowing PFPE layer (Fig. 3; left). Conversely, the thin-film structure of E-DFO consists of multiply-alkylated cyclopentanes (MACs), which have a lower vapor pressure than other types of synthetic hydrocarbon oil.

Furthermore, PTFE powder is applied to the E-DFO thin film to improve the retention of MACs, lubrication oil, and reduce particle emissions.[3]

3.2 Characteristics of thin film

The concept behind the development of E-DFO is to extend product life and decrease organic matter contamination by reducing the outgassing rate (evaporation rate) of the lubrication oil that constitutes the thin film.

Evaporation rate refers to the amount of lubrication oil that evaporates per unit area and indicates how quickly the lubrication oil is diminished. E-DFO is designed to reduce the evaporation rate by employing lubrication oil with low vapor pressure. MACs used for E-DFO exhibit very low saturation vapor pressure as a result of being

refined at least twice to remove ingredients with high vapor pressure due to low boiling points.

Fig. 4 shows the relation between saturation vapor pressure and evaporation rates of MACs and PFPE at 20 °C and 100 °C. The saturation vapor pressure of MACs is lower than that of PFPE by on a double-digit scale or more while the saturation vapor pressure of MACs at 100 °C is nearly the same as that of PFPE at 20 °C,[4), 5)] which also applies to evaporation rates. MACs exhibit a very low evaporation rate, at least 1/100 of PFPE, demonstrating that MACs have a small evaporation rate and high retaining capacity.

The outgassing rate represents the amount of gas released from lubricant per unit of time and indicates the volume organic contaminants produced in a vacuum-environment device. E-DFO is intended to slow down the outgassing rate by applying powder to the thin film in addition to using MACs.

PTFE powder applied to the E-DFO's thin film has a molecular weight as low as 5 000 or less and has a variable flake form with a large surface area. Because of these properties, the powder can easily retain oil. E-DFO, therefore, further reduces the outgassing rate compared with the use of MACs alone and improves the retention of

lubrication oil, thus achieving longer product life and reduced organic matter contamination.

Furthermore, MAC polycyclic structure yields the advantage of higher viscosity due to the interaction of an isotropically arranged alkyl group, leading to the ready formation of an oil film. Constituent tests have also established that MACs are superior to PFPE in load capacity and is suitable for rolling contact under high surface pressure conditions.

3.3 Outgassing

Evaluation of outgassing (rates and gas constituents) was carried out using a vacuum-heating device equipped with quadrupole ion trap mass spectrometry (Fig. 5). Tests were conducted on E-DFO treated bearings, V-DFO treated ball bearings, and ball bearings filled with fluorine grease in amounts equivalent to 10 % of the spatial volume of the ball bearing. Outgassing rates up to 200 °C and gas constituents at 200 °C were measured for each ball bearing. Outgassing rates were measured up to 170 °C and gas constituents were measured at 170 °C for ball bearings with fluorine grease.

Fig. 6 shows outgassing rate measurements. The outgassing rate of an E-DFO treated ball bearing is about

Fig. 2 E-DFO treated products available from NSK for vacuum and clean environments
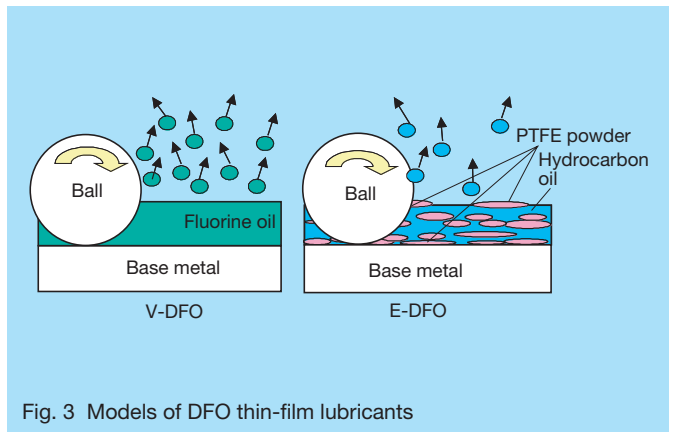
Fig. 3 Models of DFO thin-film lubricants
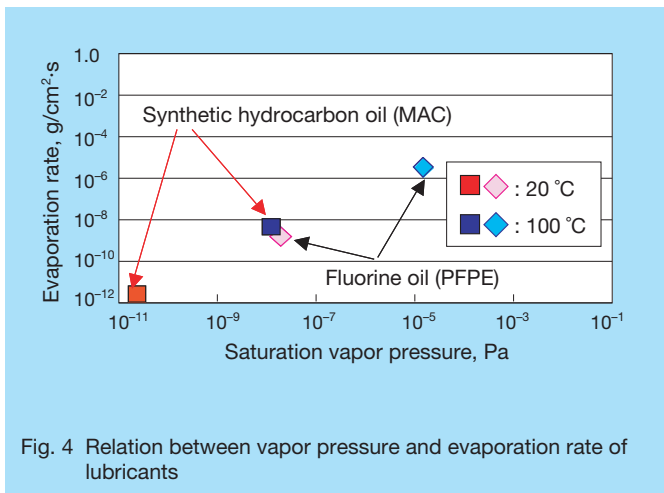
Fig. 4 Relation between vapor pressure and evaporation rate of lubricants
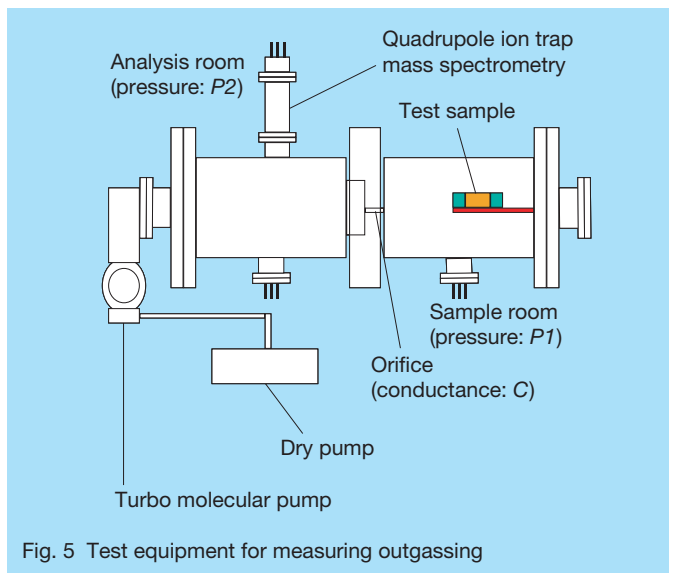
Fig. 5 Test equipment for measuring outgassing

half of a V-DFO treated ball bearing and 1/10 of a ball bearing with fluorine grease under high-temperature conditions of 100 °C or higher.

Fig. 7 shows gas constituents released when heated at 200 °C (170 °C for ball bearings with fluorine grease). An E-DFO treated ball bearing produced fewer gas constituents, including organic contaminants, than a V-DFO treated bearing and a bearing with fluorine grease. The small outgassing rate of the E-DFO treated ball bearing shown in Fig. 6 is dependent upon the volume of gas constituents shown in Fig. 7.

These test results indicate that E-DFO makes it possible to reduce organic matter contamination. It can be assumed that properties of MACs that constitute the E-DFO thin film and PTFE powder applied to the thin film produce the required effects.

3.4 Durability

Durability tests were conducted on E-DFO treated linear guides and ball screws and V-DFO treated linear guides and ball screws.

Fig. 8 shows the results of lifetime tests conducted on linear guides. The lifetime of a linear guide was deemed to end at the driven distance at which the friction power of its bearing (slider) was at least three times higher than its initial value.

While a V-DFO treated linear guide showed a lifetime of 4 600 km under a surface pressure condition of 1 GPa, an E-DFO treated linear guide lasted 9 000 km under the same conditions. At surface pressures of 1 GPa or more, durability of the V-DFO linear guide sharply decreased, while the E-DFO linear guide showed a high durability of 3 200 km even under 1.5 GPa although its durability decreased as surface pressure increased, indicating that, unlike the V-DFO treated linear guide, the E-DFO treated guide can endure high surface pressures.

Fig. 9 shows the results of ball screw durability tests. Due to the large slippage between a rolling element and the raceway, combinations of a diamond-like carbon (DLC) coating and E-DFO or V-DFO were used (table 1). The lifetime of a ball screw was deemed to end at the driven distance at which torque reached at least three times its initial value.

While the torque of a V-DFO treated ball screw increased and the lifetime of the ball screw ended within about 1 000 km under a surface pressure of 1 GPa, the E-DFO treated ball screw showed outstanding durability under the same conditions without showing increased torque even at 4 500 km.

Fig. 6 Relation between temperature and outgassing rate
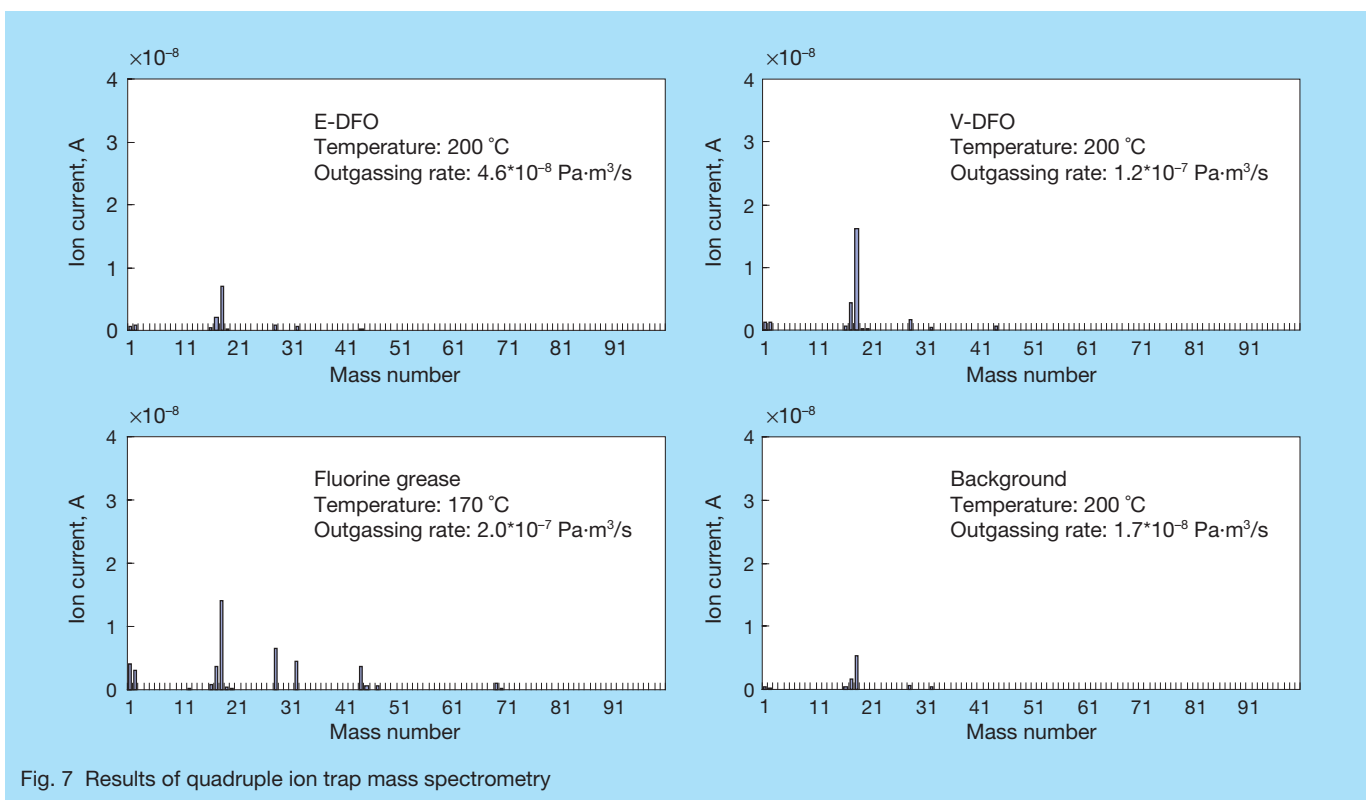
Fig. 7 Results of quadruple ion trap mass spectrometry

It can be assumed that E-DFO's ability to retain lubrication oil in the form of a thin film for a long time can improve the lifetime of an E-DFO treated product. In a vacuum environment where heat is not dissipated well, the track surface of a ball screw or linear guide is exposed to an environment in which lubrication oil easily evaporates with rising temperatures. Even under these conditions, E-DFO decreases the evaporation of lubrication oil through the synergistic effect of MACs and PTFE powder applied to the thin film, thereby simultaneously achieving reduced outgassing and improved product life. It is also conceivable that lubrication performance improves due to MACs' advantage of easily forming an oil film; thereby increasing the lifetime of E-DFO treated products.

4. Postscript

In this article, we introduced NSK's newly developed E-DFO, which further improves the performance of V-DFO thin-film lubrication technology for vacuum environments. Lubrication technology applied to mechanical elements used in vacuum environments needs to be developed further since the level of market demand is expected to steadily rise. Efforts will be made to respond to these market needs by incorporating customer feedback into new development efforts.

References

1) T. Saito, "Vacuum Clean Lubricant Film V-DFO" NSK Technical Journal 673 (2002) 22-25.
2) T. Saito, "Lubrication Characteristics of PFPE Based Thin-Film Lubrication Treated Ball Screws under a Vacuum Environment" Preparatory Manuscripts for a Tribology Conference.
3) T. Saito, "Study of Long Life V-DFO under Severe Conditions" ITC Kobe Synopses, (2005) 186.
4) William R. Jones, Jr. Mark J. Jansen, "Lubrication for Space Applications" NASA/CR-2005-213424.
5) Robert L. Fusaro, Michael M. Khonsari, "Liquid Lubrication for Space Applications" NASA/TM-213424 (1992).
6) M. Masuko, I. Fujinami, H. Okabe, "Lubrication Performance of Perfluoropolyalkylethers under Hight Vacuum" Wear,159 (1992) 249-256.
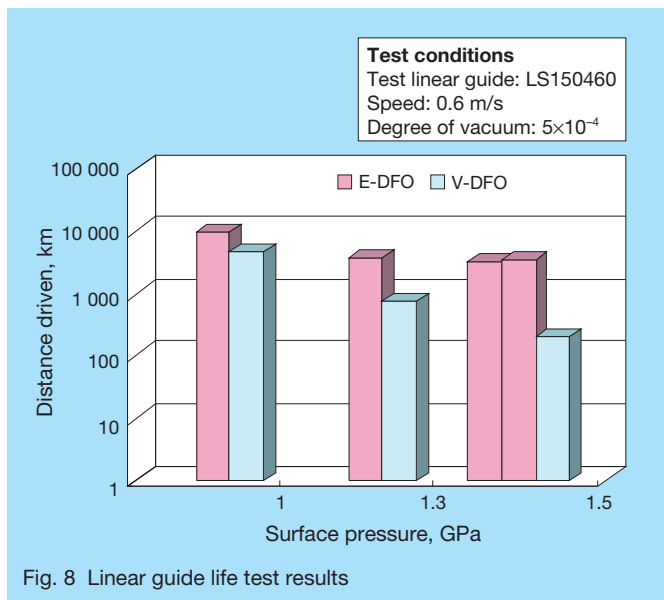
Fig. 8 Linear guide life test results

Test conditions
Test linear guide: LS150460
Speed: 0.6 m/s
Degree of vacuum: 5×10^{-4}
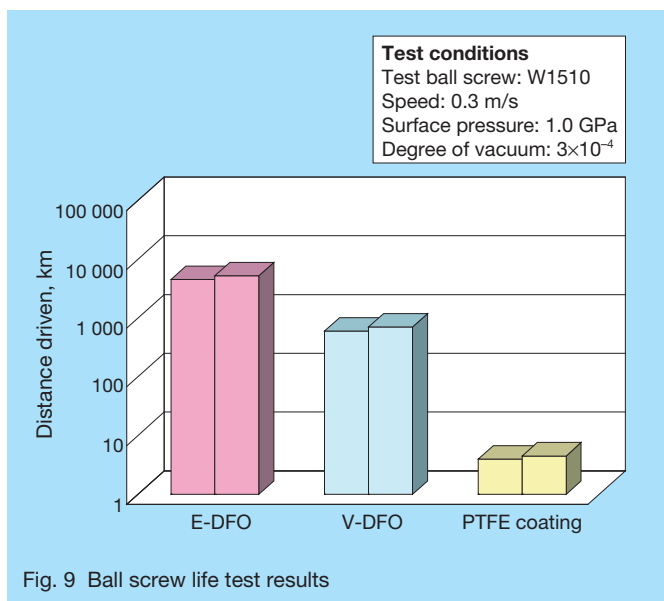
Fig. 9 Ball screw life test results

Test conditions
Test ball screw: W1510
Speed: 0.3 m/s
Surface pressure: 1.0 GPa
Degree of vacuum: 3×10^{-4}

Table 1 Specifications of DLC coated ball screws

	DLC	DFO treatment
Screw shaft	Coated	Treated
Ball screw nut	Not coated	Treated
Ball	Not coated	Treated
Circulating tube	Not coated	Treated

Dai Kinno

Development of Nanopositioner

Nobuaki Tanaka
Mechatronics Technology Development Center

ABSTRACT

NSK has developed a Nanopositioner that incorporates a specially designed ball screw fixed-end bearing unit, which provides mechanical rigidity, and integrates it with a piezoelectric element, which provides ultra-fine positioning. In this paper, we describe the structure and operational characteristics of the NSK Nanopositioner. The Nanopositioner combines a ball screw and stepping motor for coarse-motion control, and a piezoelectric element for fine-motion control. NSK's Nanopositioner is capable of a maximum speed of 72 mm/s and a resolution of 5 nm. NSK's combination of these capabilities achieves step positioning on a 5 nm scale and positioning accuracy within a range of ±15 nm in 3σ.

1. Introduction

Demand for positioning mechanisms with nanometer accuracy continues to grow in a number of industries, including semiconductor manufacturing equipment, optical communications devices, biotechnology, microelectromechanical systems (MEMS), etc.

Coarse/fine positioning stages intended to meet these requirements have been available. Coarse positioning typically involves a ball screw and stepping motor, and a piezoelectric element for fine positioning. The stiffness of these conventional devices, however, is generally low; and fails to deliver high resolution at high speeds.

NSK devised a unique ball screw fixed-end bearing unit incorporating a piezoelectric element (patent pending) as a fine positioning control device and has successfully developed Nanopositioner that provides fine positioning at nanometer accuracy and at high speeds without sacrificing mechanical rigidity.

This article discusses the configuration and operational characteristics of NSK's Nanopositioner.

2. Problems of Conventional Devices

To date, several types of coarse/fine positioning stages equipped with ball screws and piezoelectric elements have been released into the market.

These conventional positioners either involve a piezoelectric actuator directly mounted between the table and the ball screw nut (Fig. 1) or have a fine-motion table incorporating a piezoelectric element mounted to a coarse positioning stage.[1] These types of positioners use a stacked piezoelectric element as a piezoelectric actuator. A stacked piezoelectric element, however, is vulnerable to tension, moment, and radial forces. Consequently, the structure must be reinforced so as to provide compression force using a spring or similar means to prevent tension force from acting on the piezoelectric element (Fig. 2) or provide pin support between the moving element and the driven object to prevent moment force from acting on the piezoelectric element.[2]

Rigidity of the compression springs is, in general, not adequate for this purpose, and the installation of springs in the feeding process hampers high-speed operation. Furthermore, high accuracy is required when a piezoelectric actuator is mounted between a table and the ball screw nut. In addition, insufficient accuracy allows radial and moment forces to act on the piezoelectric element, thereby decreasing the durability of the device.

3. Device Configuration

3.1 Fine positioning system structure

Fig. 3 and 4 show the structure of the newly developed fine positioning system developed by NSK. The fine positioning system incorporates a piezoelectric element
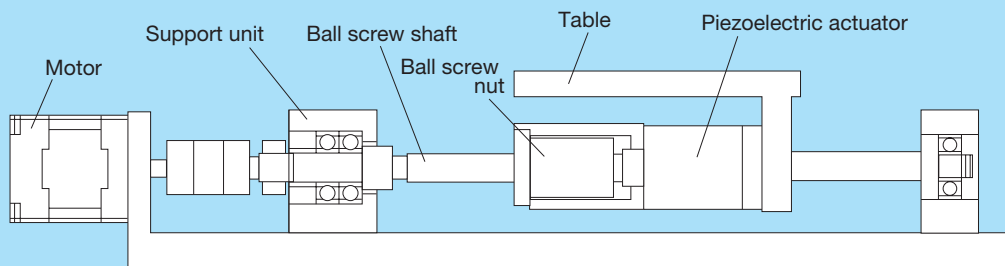
Fig. 1 Basic structure of a typical Nanopositioner

into a ball screw fixed-end bearing unit. Figure 3 shows an application that incorporates a cylindrical piezoelectric element while figure 4 displays the use of a rectangular parallelepiped piezoelectric element. Both have the same basic structure.

A spacer is installed between the inner rings of two support bearings and space is provided between the outer rings. The inner rings are mounted to a screw shaft with a lock nut, and the outer rings are contained in a housing along with a piezoelectric element and a spacer collar. The bearing is preloaded by adjusting the width of the spacer collar, and a compressed preload is simultaneously applied to the piezoelectric element.

As the piezoelectric element is displaced, the outer ring on one side is moved by the spacer collar. The movement is made so as to bring into balance the forces of the bearings on both sides, with the inner rings and fixed screw shaft moving slightly by a distance equivalent to about one-half the displacement of the piezoelectric element. This is the principle behind the fine positioning system developed by NSK.

The newly developed fine positioning system has the following advantages:

• A piezoelectric element and preloaded bearings are mounted on the same shaft, preventing the application of moment or radical forces on the piezoelectric element.
• Bearing preload is always provided to the piezoelectric element as compression force, preventing the application of tension force on the piezoelectric element.
• Incorporation of a piezoelectric element causes virtually no loss of rigidity.
• Use of the mechanism requires only a structural change in the support unit.

3.2 Positioner structure

Fig. 5 displays the structure of the new Nanopositioner. The above-described fine positioning system is incorporated into a ball screw fixed-end bearing unit. Table 1 summarizes the main specifications of the new Nanopositioner. Two types are available: the M series featuring a single-axis unit and the CD series with a dual-

axis XY table. A feedback linear scale is positioned on one side of the table; and a 5 nm resolution is standard.

3.3 System configuration

Fig. 6 shows the system configuration of the new Nanopositioner. Controllers for coarse/fine positioning are off-the-shelf stepping motor control boards and servomotor control boards (for piezoelectric-element control), which users can select according to the required function. However, since the same position information is input, the feedback scale used to control the unit of the coarse/fine-positioning controller, the input frequency of the controller boards must be compatible with a high-speed frequency of about 20 MHz to for maximum operational speed.

The driver unit housing, which contains a motor driver, an amplifier for driving the piezoelectric element, terminal blocks, and other components, is mounted between the Nanopositioner main unit and the controller.

Since the driver unit contains a voltage conversion unit which supports input to and output from commercially available controller units, the user can easily design controllers without having to consider this issue.
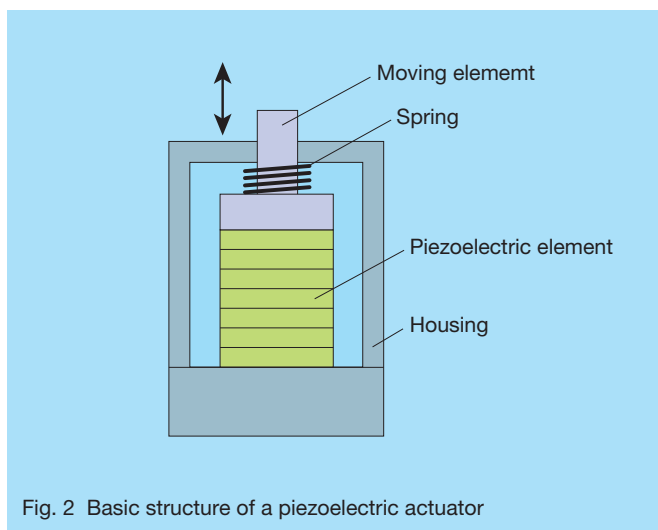
Fig. 2 Basic structure of a piezoelectric actuator
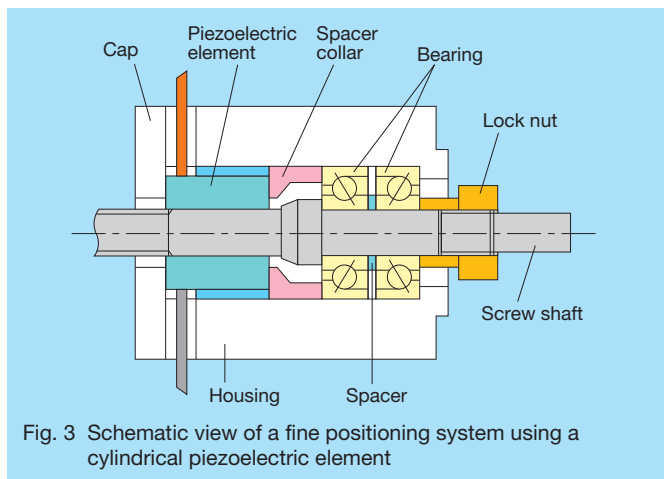
Fig. 3 Schematic view of a fine positioning system using a cylindrical piezoelectric element
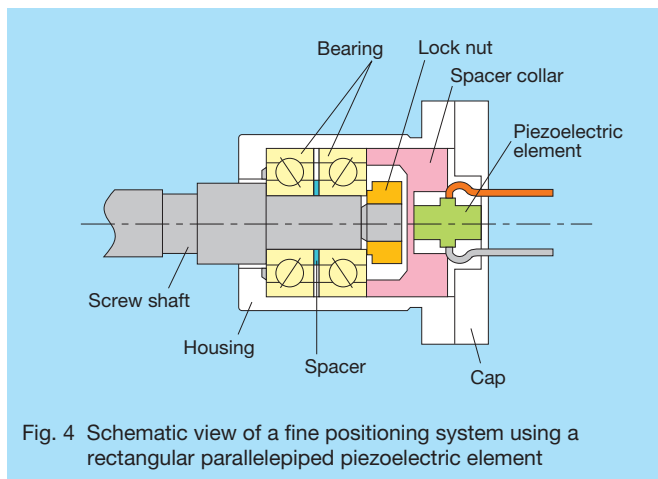
Fig. 4 Schematic view of a fine positioning system using a rectangular parallelepiped piezoelectric element

4. Operational Characteristics of Fine Positioning System

Fig. 7 and 8 show examples of voltage and the amount of fine motion of the screw shaft measured as DC voltage applied to the piezoelectric element. Fig. 7 displays the results of a fine positioning system using an M series Nanopositioner while figure 8 shows the results using a CD series Nanopositioner.

It can be seen that the screw shaft was displaced 6 μm in Fig. 7 and 4 μm in Fig. 8 by the application of 150 V. Since the piezoelectric elements used in the fine positioning systems were displaced 12 μm and 9 μm, respectively, the displacement of each screw shaft was roughly half the displacements of piezoelectric elements, as indicated by the principle described in paragraph 3.1.

Apparent positive and negative operations are needed for fine-motion positioning to correct error that occurs during coarse-motion positioning. For this purpose, the M series Nanopositioner and the CD series Nanopositioner have fine-motion strokes of ±3 μm and ±2 μm respectively. Positioning error during coarse-motion positioning is about 0.5 μm because the Nanopositioner uses a linear scale to perform feedback control even during coarse-motion positioning. Therefore, the fine-motion strokes described above are sufficient.

Fig. 9 and 10 show results of rigidity measurements made on a support bearing unit incorporating a fine positioning system. The rigidity of the M series Nanopositioner was 25 to 28 N/μm regardless of load direction (Fig. 9) while that of the CD series Nanopositioner was 50 to 54 N/μm (Fig. 10). Both series fell within predicted ranges.
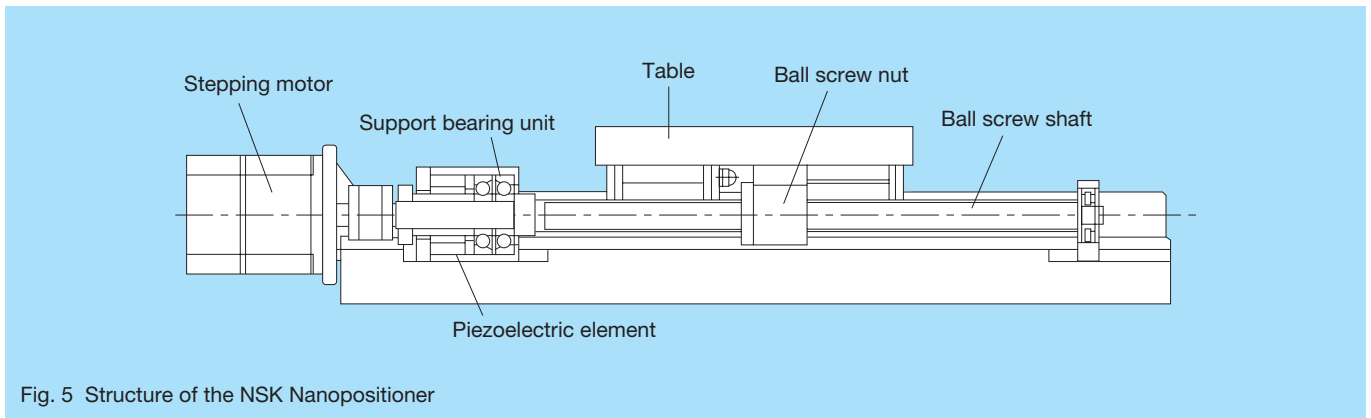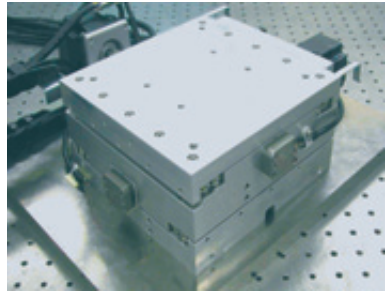
Fig. 5 Structure of the NSK Nanopositioner

Table 1 Specifications of the Nanopositioner

Type	M-series, compact, single axis stage		CD-series XY table	
Effective stroke	50 mm	100 mm	50 mm × 50 mm	100 mm × 100 mm
Table size	32 mm × 46 mm		125 mm × 125 mm	200 mm × 200 mm
Minimum resolution	5 nm			
Maximum speed	72 mm/s			
Horizontal transportable mass	2 kg		10 kg	
Driving method	Coarse-motion: stepping motor + ball screw Fine-motion: piezoelectric element			
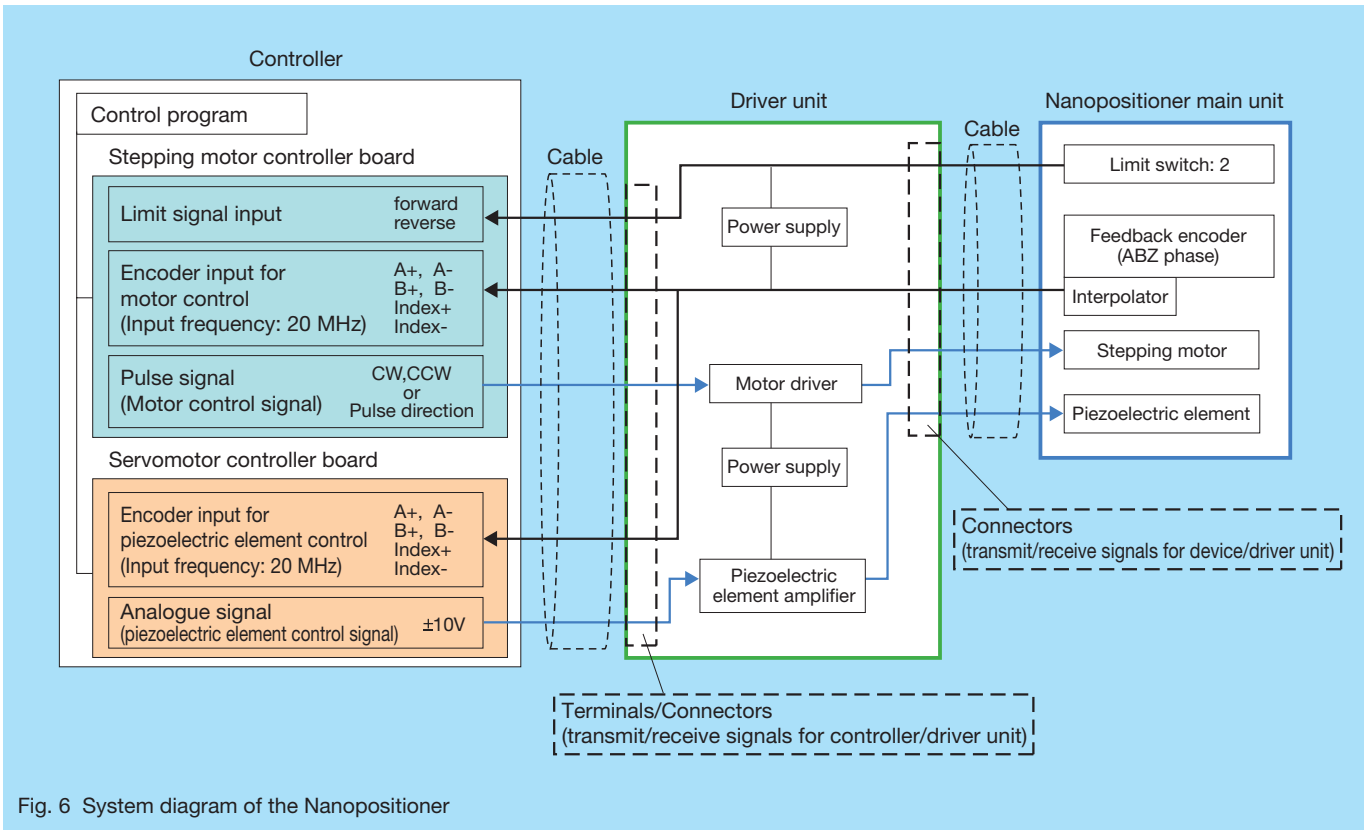
Fig. 6 System diagram of the Nanopositioner
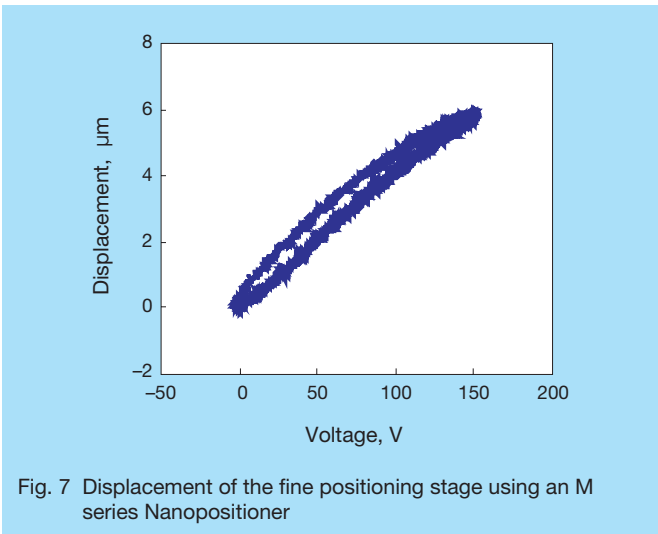
Fig. 7 Displacement of the fine positioning stage using an M series Nanopositioner
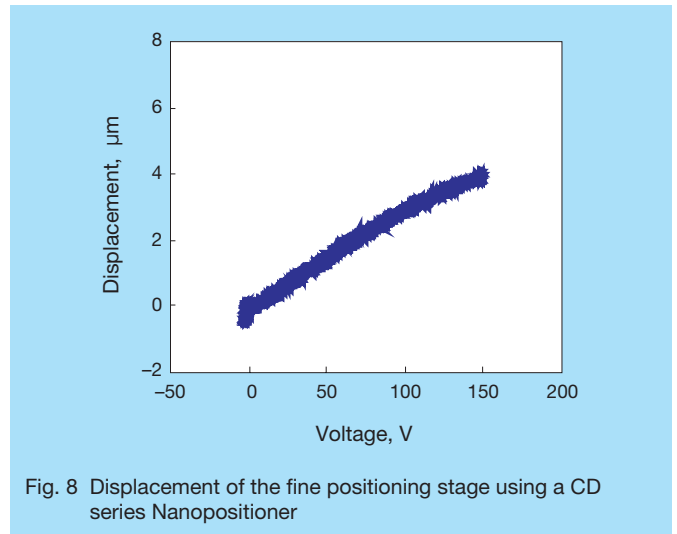
Fig. 8 Displacement of the fine positioning stage using a CD series Nanopositioner

5. Results of Performance Evaluation

5.1 Fine-motion positioning characteristics

Fig. 11 to 14 show measurement results of fine-motion positioning operations. Measurements were made using a high-precision laser scale (resolution: 0.14 nm) separately installed on a table.

Fig. 11 shows the results of fine-motion positioning operation of 2 μm using an M series Nanopositioner. It can be seen from the figure that a precise fine-motion positioning operation of 2 μm was implemented while requiring a time of 50 ms or less.

Fig. 12 shows results of 50 nm step positioning and Fig. 13 shows results of 5 nm (minimum resolution) step positioning. These figures indicate that precise operations were made in both cases. In the case of 5 nm step positioning, flutters of about 5 nm occurred at the time of stopping. The flutters were caused by the fact that the feedback resolution of the linear scale was 5 nm.

Fig. 14 shows the result of 5 nm step positioning using a CD series Nanopositioner. Just as in the case of an M series Nanopositioner, the figures indicate that precise operation was implemented.

Results shown in the figures are based on

measurements made by a high-precision laser scale. Similar results were attained using a volume displacement gauge to confirm measurements.

It is understood from the results described above that the newly developed fine positioning system is capable of precise fine positioning on the order of micrometer and nanometer levels.

The new Nanopositioner uses a feedback linear scale with a resolution of 5 nm. It has been confirmed, however, that precise operation can be made even for 1 nm step positioning if a feedback scale with a higher resolution is used.

5.2 Accuracy in coarse- and fine-motion positioning

Fig. 15 and 16 show results of the tests in which coarse-motion positioning operations were completed over full strokes, and accuracy in each positioning operation was checked. In one positioning operation, 6.25 mm positioning was repeated at a maximum speed of 72 mm/s to make 30 reciprocation motions over the full stroke. Measurements were made using a linear scale for feedback. It was found that using both an M series Nanopositioner and a CD series Nanopositioner, the average positioning error, or lost motion, was a few nm. Furthermore, it is clear from the frequency of the occurrence of positioning errors indicated in the figures that all errors in 60 positioning operations fell within a range of ±10 nm. It can also be observed that it is possible to implement high-precision positioning of about ±15 nm in 3σ.

Space does not permit a more detailed explanation, although resonance frequency in a feeding process was also measured. Consider, for example, measurement results of a CD series Nanopositioner. Under no-load conditions, resonance frequency was 250 Hz in the X axis direction and 460 Hz in the Y axis direction, and even when carrying a load of 10 kg, the resonance frequency was 150 Hz in the X axis direction and 200 Hz in the Y axis direction; sufficient characteristics for such a small table.
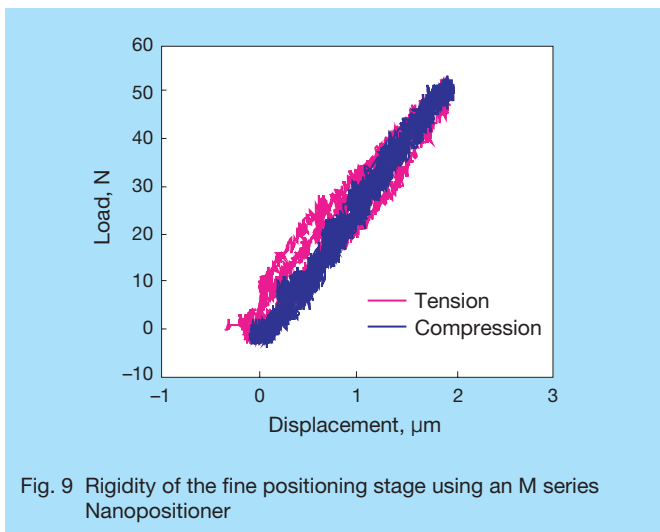
Fig. 9 Rigidity of the fine positioning stage using an M series Nanopositioner
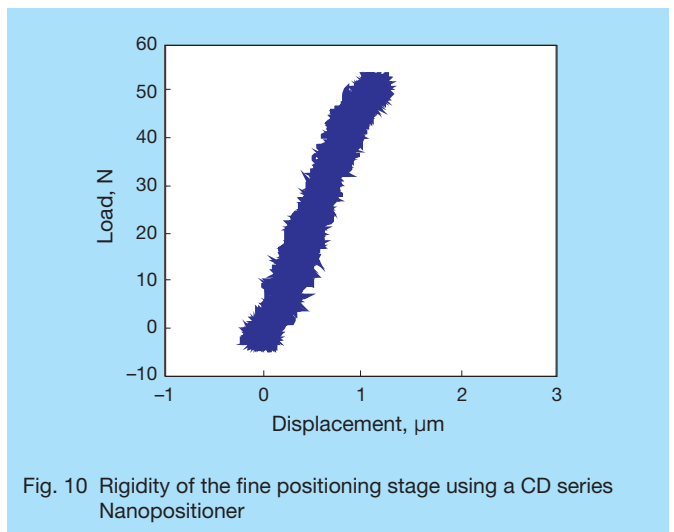
Fig. 10 Rigidity of the fine positioning stage using a CD series Nanopositioner
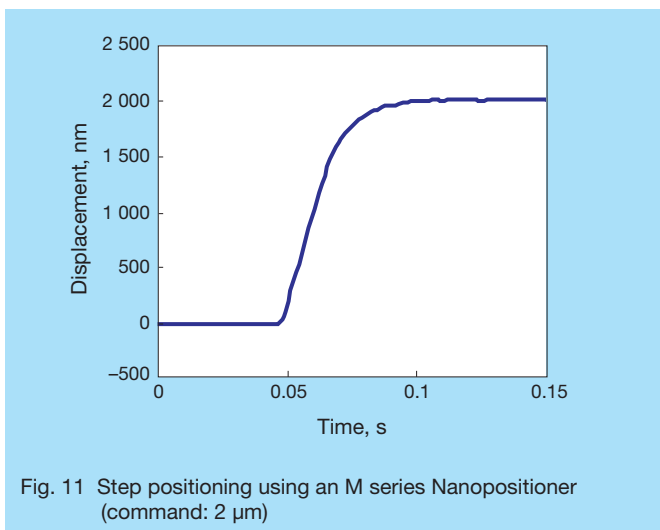
Fig. 11 Step positioning using an M series Nanopositioner (command: 2 μm)
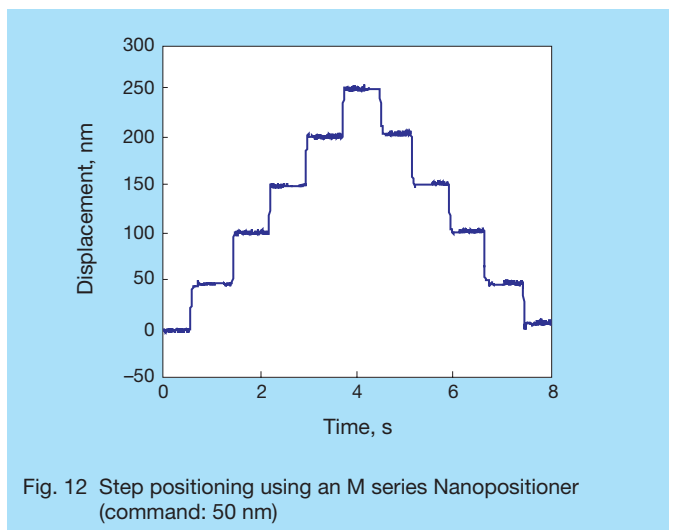
Fig. 12 Step positioning using an M series Nanopositioner (command: 50 nm)

6. Postscript

The newly developed Nanopositioner achieves fine positioning operation without impairing the rigidity of mechanical elements by devising and employing a unique fine positioning system that is different from those employed by conventional course/fine positioning stages. This fine positioning system can be easily applied to an existing XY table.

NSK, as a leading company with specialized expertise in manufacturing XY tables, has developed many devices ahead of the other manufacturers, including ultraprecision tables and mirror projection aligners, while predicting future market demand. NSK will continue to develop nanotechnologies to support clients by combining our accumulated technologies with the constituent technologies of the new Nanopositioner to contribute to future advances.

References

1) J. Otsuka, K. Sakato, "High-Precision Positioning Mechanism, 2nd Edition" Kogyo Chousakai Publishing Co. Ltd.
2) Physik Instruments Catalogue, "Micro Positioning, Nano Positioning, Nano Automation Solution for Cutting-Edge Technologies" (2001) 1-7.

Fig. 13 Step positioning using an M series Nanopositioner (command: 5 nm)

Fig. 14 Step positioning using a CD series Nanopositioner (command: 5 nm)

Fig. 15 Positioning accuracy of an M series Nanopositioner (forward & back)
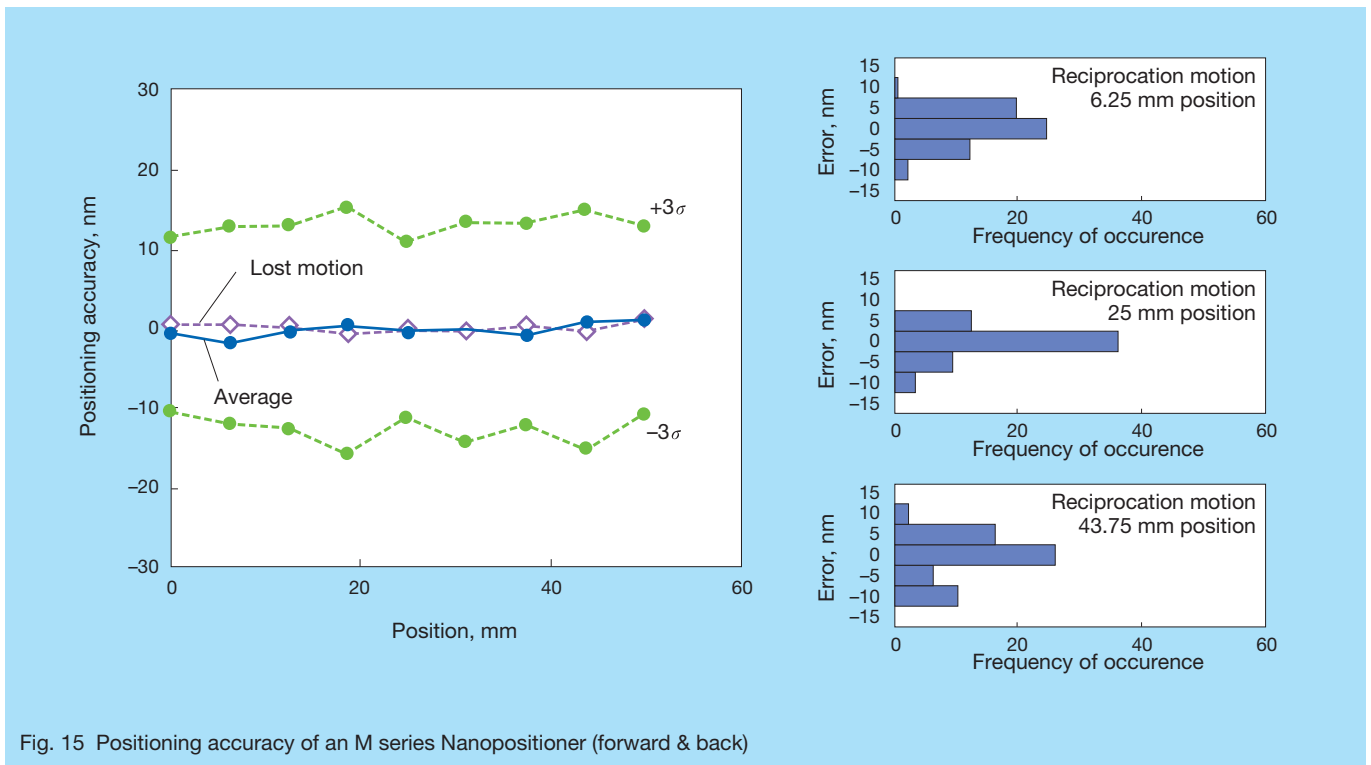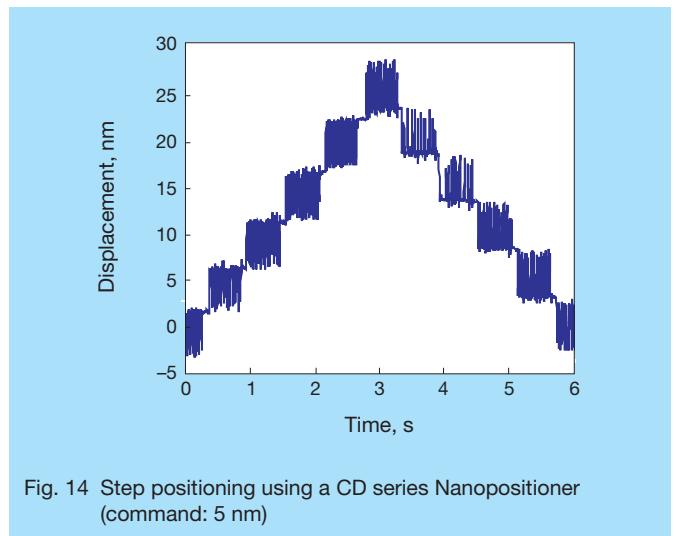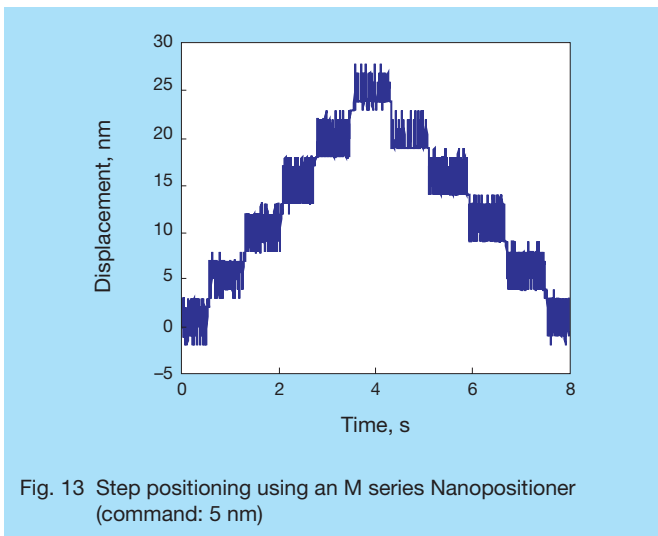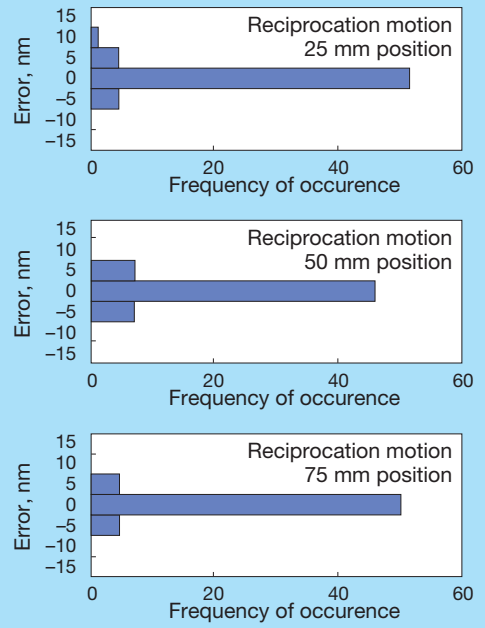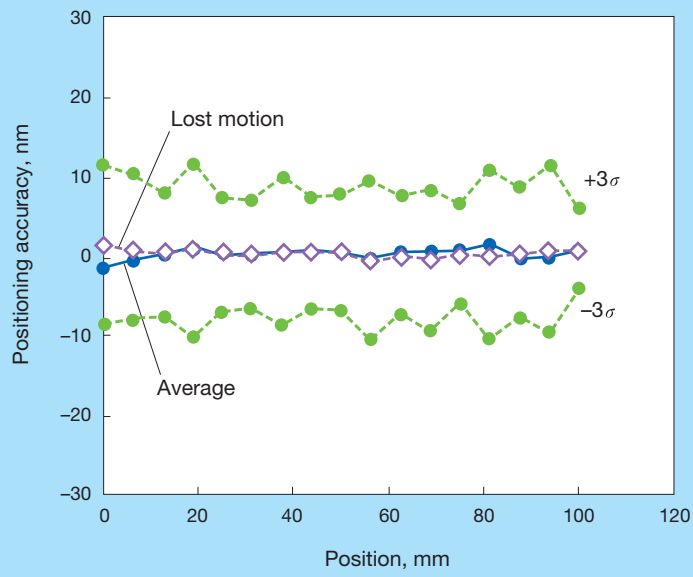
Fig. 16 Positioning accuracy of a CD series Nanopositioner (forward & back)

Nobuaki Tanaka

Development of Ultrahigh-Speed Planetary Needle Roller Bearings

Seigo Urakami, Automotive Bearing Technology Center
Jun Liu, Yoichi Matsumoto,   Corporate Research & Development Center

ABSTRACT

Planetary pinion needle roller bearings for automatic transmissions are apt to generate high stress and frictional heat due to not only rotational motion around the shaft but also orbital motion around the sun gear. Caged needle roller bearings, which provide superior rotating and revolving performance in comparison to full complement needle roller bearings, have been adopted in recent years for their low-torque and high-speed capabilities. In recent years, the number of gears in automatic transmissions has increased, which means that demand for higher rotating-speed capability of the needle roller cage and pinion shaft has also increased. To meet this demand, NSK conducted various analyses and extensive testing in order to develop an ultrahigh-speed planetary needle bearing. In this paper, we present our latest technologies that have resulted in the development of ultrahigh-speed planetary needle roller bearings.

1. Introduction

Several to tens of pinion gears are used in planetary mechanisms, which are a type of change-speed gearbox used in automatic transmissions (ATs) for use in automobiles. Needle roller bearings are used between a pinion gear and a pinion shaft. These planetary needle roller bearings support loads that are generated by the transmission of torque from the engine to the tires. The bearings also promote smooth rotation of the pinion gear and pinion shaft. The motion of this bearing is not only rotational motion around the shaft, but also orbital motion around the sun gear. Due to rotational motion, orbital motion, and the load described above, high levels of stress and heat are apt to be generated inside the bearing, such that designing the bearing requires advanced technologies. Due to the improved fuel economy and acceleration performance of newer vehicles, typical ATs have evolved from conventional four-speed transmissions to six-, seven-, and even eight-speed transmissions. With this increase of gear ratios, the maximum speed of rotation and revolution required of the planetary needle roller bearing is also escalating. Conventionally, full complement planetary needle roller bearings with no cage were mainstream, but with the requirement of higher rotational speed, the use of a needle roller assembly that is equipped with a cage to prevent friction between rollers has gradually increased. However, this rise in required speed revealed a problem of insufficient durability of the cage and shaft. NSK addressed this issue by conducting several types of experiments and analyses, and developed planetary needle roller bearings that are capable of responding to ultrahigh-speed operations. The results of our efforts are discussed in this paper.

2. Structure of Planetary Needle Roller Bearings and Required Performance

There are two types of planetary gear mechanisms used in ATs: a simple planetary gear mechanism and a compound planetary gear mechanism. The change-speed gearbox of an AT is composed of both types. There are two types of simple planetary gear mechanisms: the single pinion-type planetary gear, which consists of a pinion gear, carrier, sun gear, and ring gear (Fig. 1); and a double pinion type planetary gear mechanism, which has double pinion gears (Fig. 2).

Additionally, there is the Ravigneaux gear set, which is a type of compound planetary gear mechanism. The Ravigneaux gear set is a combination of a single pinion–type planetary gear mechanism and a double pinion–type planetary gear mechanism. Since this gear set can be reduced in size and weight, it is has been adopted for use in six-speed ATs and other multi-gear ATs.

Fig. 3 shows an illustration of a Ravigneaux gear set. This mechanism has long pinion gears, which engage with two gears in the axial direction, and short pinion gears, which engage with one gear. Due to its unique structure, it is difficult to ensure the rigidity of the carrier. Also, since it has long pinion gears, the operating environment of the bearing is severe. The planetary pinion consists of a pinion gear, a shaft fixed to the carrier, and a planetary gear needle roller bearing. The rotational motion around the shaft and orbital motion around the sun gear with the carrier are complex motions in the gear set that work to transmit torque. The planetary needle roller bearings consist of a full complement-type without a cage (photo 1) and a needle roller assembly with cage (photo 2). These bearings consist of a pinion gear that acts as an outer ring (rotating ring) and a shaft that acts as an inner ring (stationary ring). They support the load and rotate. A helical gear is the main application of a planetary gear mechanism. As shown in Fig. 4, the engaging force among the gears that transmits torque (figure P: tangential force; S: radial force, and T: thrust force), acts on the bearing as load. Similarly, the centrifugal force of the pinion gear and the bearing, which is generated by orbital motion around

sun gear, acts on the bearing, too.

In Fig. 4, the single pinion type planetary gear mechanism is shown. As for the Ravigneaux planetary gear mechanism, there is a mode where the long pinion gear engages at a different position in the axial direction. The load condition for the bearing is more complicated under this situation. Typical radial needle roller bearings usually consist of a stationary outer ring and a rotating inner ring where contact stress of the inner ring is higher than that of the outer ring because of curvature, but the number of stress cycles of the outer ring, which is the stationary ring, is larger than that of the inner ring. Therefore, from viewpoint of durability, there is no large difference between the load that is acting on the inner and outer rings.

Meanwhile, when the planetary needle roller bearing is operated under conditions where the pinion gear (outer ring) is rotating, and the shaft (inner ring) is stationary, the shaft is exposed to not only high contact stress, but also a high number of stress cycles, and loading acting on the shaft is the severest. Conventionally, high-capacity full complement needle roller bearings are mainly used in the planetary needle roller bearings. However, in this type of bearing, the adjacent rollers repeatedly collide and slide resulting in increased friction torque, or even seizure if rotated at high-speed. In comparison to a full complement needle roller bearing, a cage and needle roller assembly can rotate at high speed because the rollers do not contact each other directly. However, load capacity is reduced due to the fewer number of rollers than a full complement needle roller bearing.

Therefore, NSK improved durability by applying a special heat treatment (carbonitriding) to the shaft, which is made of bearing steel. As a result, the application of cage and needle roller assemblies has increased recently. However, if advances in newer multi-speed ATs require higher rotating speed of the pinion gear, there is a possibility that the following issues could become arise in current planetary needle roller bearings.

a. Stress and heat generated in the cage increases and cage durability is weakened.
b. Centrifugal force increases and load acting on the shaft increases.
c. The long pinion shaft used in the Ravigneaux gear set is easily bent and durability deteriorates.

Consequently, it is necessary to ensure sufficient shaft and cage durability for ultrahigh-speed operating conditions. In order to achieve the required levels of performance, NSK has developed a planetary needle roller bearing that meets the performance demands of ultrahigh-speed rotation and revolution.

3. Damage Mechanism

Fig. 5 illustrates cage and needle roller bearing behavior in a planetary pinion gear. Due to centrifugal force caused by orbital motion, the roller collides with the cage bar
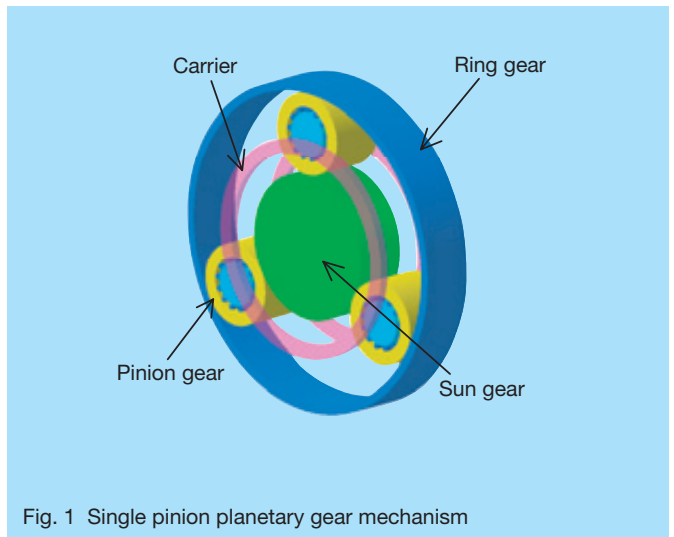
Fig. 1 Single pinion planetary gear mechanism
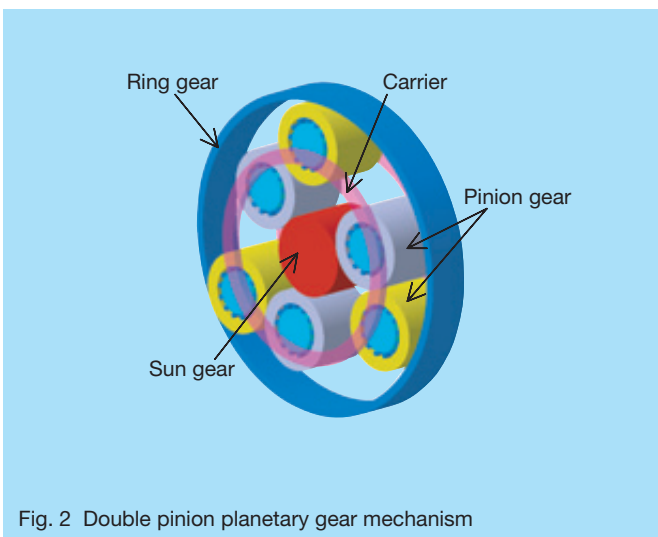
Fig. 2 Double pinion planetary gear mechanism
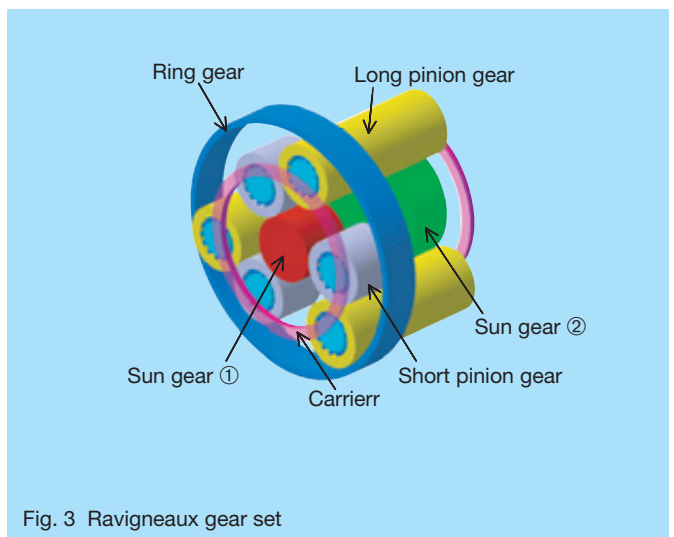
Fig. 3 Ravigneaux gear set

Photo 1 Full-complement needle roller bearing

Photo 2 Cage and needle roller assembly
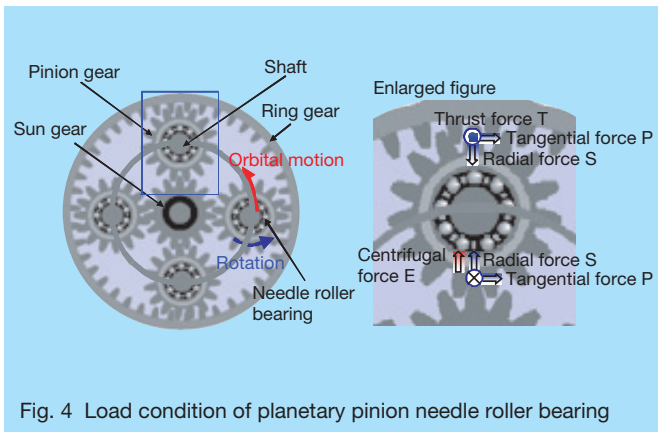
Fig. 4 Load condition of planetary pinion needle roller bearing

when it passes through the loaded zone, and collides with the cage bar on the opposite side when it enters the loaded zone. As a result, the pocket surfaces suffer from repeated stress on both sides.

In addition, centrifugal force presses the cage against the bore surface of the pinion gear. Since the pinion gear is rotating at a speed different from that of the cage, the cage rubs against the bore surface and generates frictional heat.

Consequently, under ultrahigh-speed rotation and revolution, the cage might suffer from fatigue cracks (photo 3) originating at the core of the cage bar, or suffer from cage damage (photo 4) due to excessive frictional heat. When the cage is damaged, the normal rolling motion of the roller is disturbed. As a result, the inner rings, outer rings, and rollers may suffer from flaking or seizure, or lead to a frozen pinion gear. The shaft also bears loads such as that of the gear engaging through the rollers, and the centrifugal force of the pinion gear and the bearing itself.

As shown in Fig. 6, elastic bending and plastic bending increase under ultrahigh-speed rotation and revolution. In other words, as centrifugal force of gear and engaging force increase under ultrahigh-speed rotation and revolution, elastic bending of the shaft also increases. Furthermore, as shaft temperature increases with bearing temperature under ultrahigh-speed rotation and revolution, plastic bending of the shaft also increases due to the decomposition of retained austenite, which further promotes cubical expansion. This situation is especially

true for the long pinion of a Ravigneaux gear set because the pinion gear is heavy and the shaft is long, thus, the amount of bending described above increases significantly. Therefore, contact stress between the bearing and the edge of the shaft increases and the durability of the shaft deteriorates.

4. Ultrahigh-Speed Technologies

The following measures were taken to alleviate the effects of ultrahigh-speed operating conditions:

(1) Strengthening cage structure
Fig. 7 shows flanges that strengthen the cage structure and reduce cage weight. The thinner cross-section minimizes the effects of centrifugal force. Additionally, a double row design has been adopted to further reduce collision force of each roller and centrifugal force of the cage itself.

(2) Optimal cage configuration
When a roller collides with a cage bar, the cage pocket corners suffer from stress concentrations. Fig. 8 shows a new cage configuration that employed FEM analysis to reduce stress concentrations in the new cage pockets.

(3) Highly durable cage material
Although carbon steel was conventionally used for cage material, the strength of cage material was improved by
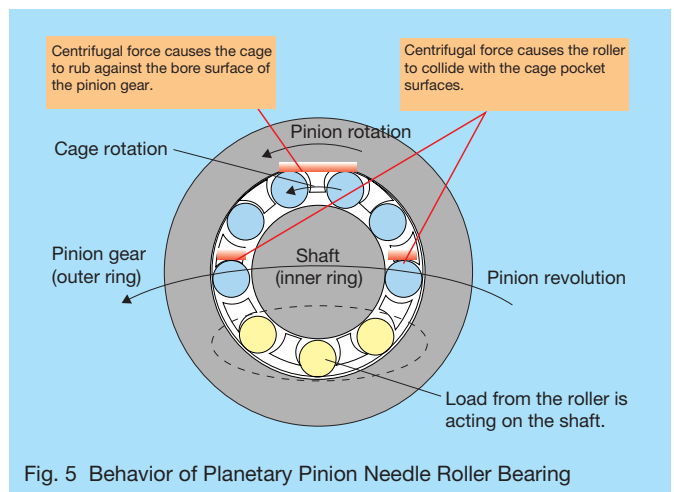
Fig. 5 Behavior of Planetary Pinion Needle Roller Bearing

adopting high-strength chrome molybdenum steel (casehardened steel).

(4) Improved seizure resistance

Chemical coating was implemented on the surface of the cage (photo 5) with the shape of the cage designed to reduce sliding friction index PV value, which is the product of contact stress P between the bore surface of the pinion gear and the outside surface of the cage, and sliding speed V. As a result, direct contact between the cage and the pinion gear, which are sliding against each other, is restricted and further high-speed rotation was achieved.

(5) Life enhancement of shaft and measures against deformation

Special induction heat treatment, which is NSK's original heat treatment process, is adopted for the shaft. The features of this heat treatment are shown in Fig. 9. Life enhancement (Fig. 10) was achieved by separating out retained austenite on the surface layer, which affects rolling fatigue life. Additionally, eliminating retained austenite at the core significantly reduced plastic bending of the shaft. Furthermore, the effective load center was moved to the carrier wall side by optimizing the number of rows and the width of the bearings, and by positioning a spacer at the center of the bearing. This has resulted in

Fig. 6 Negative impact of shaft deformation on durability

further restricting elastic bending (Fig. 11).

(6) Further life enhancement of shaft

In order to enhance service life of the shaft, which must meet the demands of higher rotational speeds, NSK established a life enhancement technology that optimally balances life characteristics using a surface strengthening method called shot peening (Fig. 12), and by adding retained austenite to the surface of the shaft using a special induction heat treatment process.

By incorporating the technologies described above, NSK achieved development of planetary needle roller bearings that maintain sufficient durability under ultrahigh-speed operating conditions.

Photo 3 Cage damage due to fatigue
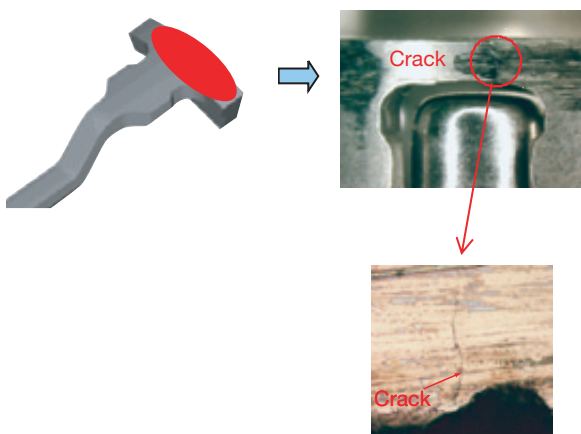
Photo 4 Cage damage due to frictional heat
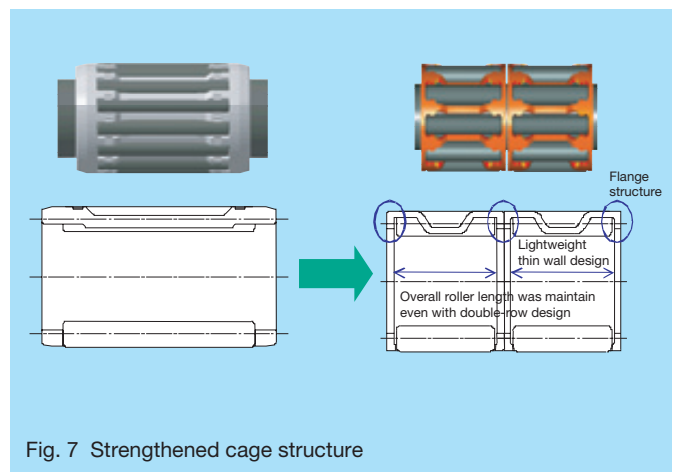
Fig. 7 Strengthened cage structure

Fig. 8 Optimized cage structure

5. Postscript

In this paper, we introduced ultrahigh-speed technology for planetary needle roller bearings. Depending on the planetary gear mechanism, the type of pinion, the operating conditions and so on, it is necessary to combine various technologies. In the future, advancements in multi-speed ATs will required that AT components be more compact, have higher capacity, and function with lower friction. NSK is actively working to further promote the advancement of ultrahigh-speed technologies for use in AT components.

Photo 5 Chemical coating

Separating out more retained austenite by increasing carbon and nitrogen at the surface area to improve life and durability.

Eliminating retained austenite at the core to 0 %.
↓
Reducing retained austenite throughout the whole shaft to restrict thermal deformation
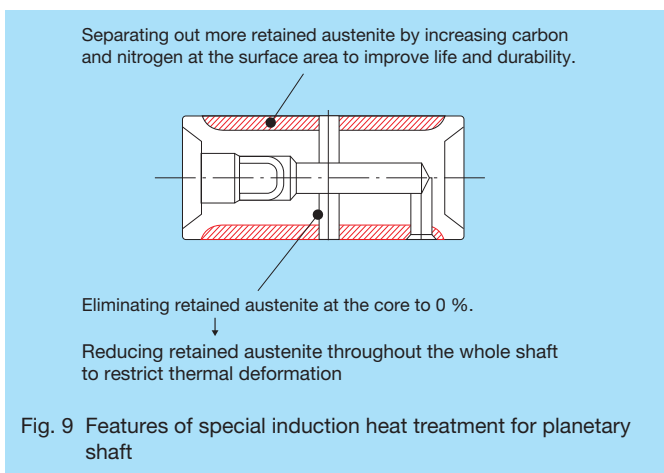
Fig. 9 Features of special induction heat treatment for planetary shaft
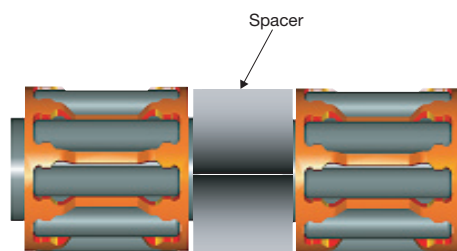
Spacer

Fig. 11 Spacer is used to reduce shaft deformation
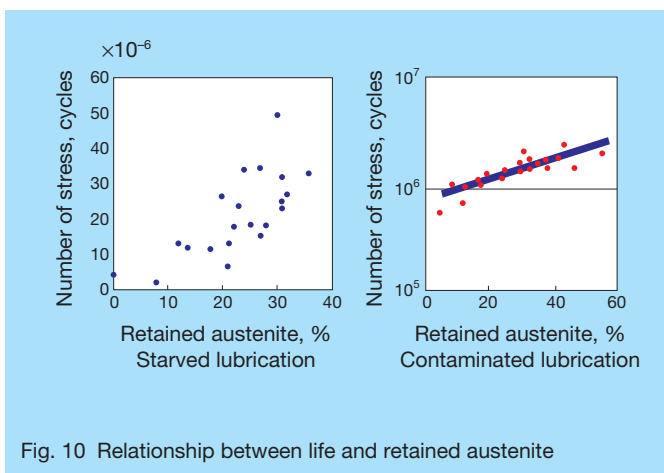
Fig. 10 Relationship between life and retained austenite
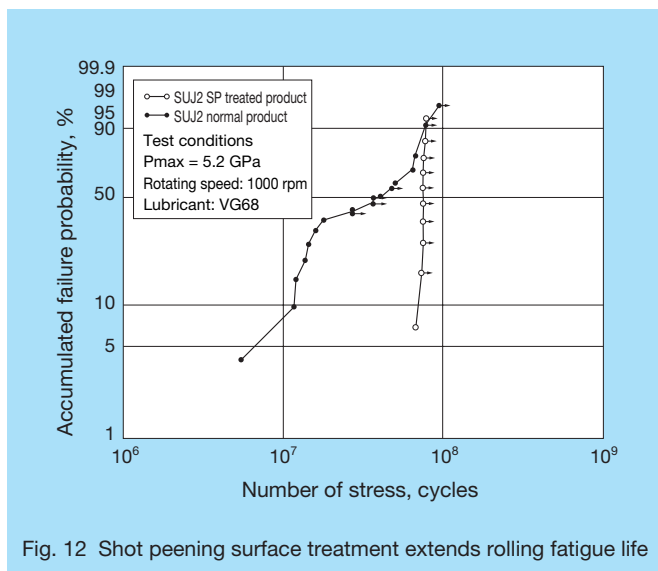
Fig. 12 Shot peening surface treatment extends rolling fatigue life

Seigo Urakami

Jun Liu

Yoichi Matsumoto

Development of Thrust Needle Roller Bearing with Wear-Resistant & High-Strength Cage

Satoshi Masuda and Hiromichi Takemura
Automotive Bearing Technology Center
Yasuyuki Shimizu
Corporate Research & Development Center

ABSTRACT

Thrust needle roller bearings are often found in gearsets mounted between gears, and the housing and the rotating shafts in an automatic transmission. The location of where a bearing is to be mounted largely determines what type of bearing will be used. Customers also prefer bearings in a unitized design, which facilitates greater ease of handling and installation. However, unitized bearing assemblies must allow for some eccentricity during operation, such as that which is found in a torque converter. Here, challenges exist in regards to preventing excessive wear and fatigue of the cage. To resolve such issues, we applied two measures: 1. Improve wear-resistance and fatigue-strength using a special heat treatment process applied to the cage; and 2. Expand bearing internal clearance of thrust needle roller bearings fitted with a raceway ring that has a curved lip along the entire outer circumference. This report introduces NSK's thrust needle roller bearing matched to a wear-resistant and high-strength cage (NSK HYTEC Bearing) for use in eccentric (off-centering) applications.

1. Introduction

An automatic transmission (AT) is a system that is in charge of an important role of automatically determining and manipulating shift changes and disengagement of the clutch depending on driving conditions for transmitting optimal torque to the tires. A rolling bearing, which is one of many AT components, performs an important role of supporting smooth rotation of each component in the unit. Among the many bearings used in an AT, the bearing used most is the thrust needle roller bearing, which numbers about ten pieces.[1] Thrust needle roller bearings are mounted between gears, or gears and housing, and sustain axial loads generated by gear engagement. In general, thrust needle roller bearings with raceways that are formed by pressing a steel plate and cage and roller assembly into a unitized design, are widely used because of greater ease of handling and installation.

However, if there is some eccentricity due to misalignment of shaft centerlines of the engine and AT axes, an excessive load is imposed on the cage of the thrust needle roller bearing, and the flange area of the raceway washer interferes with the side face of the cage resulting in cage wear or fatigue damage.[2] This paper discusses the NSK HYTEC thrust needle roller bearing with inner and outer raceway washers that was developed for use under conditions of substantial eccentricity.

2. Current Problems and Concept of Development

2.1 Current problems

Operating conditions of transmission bearings have become increasingly severe due to higher rotational speed, higher torque output, and demand for further weight reductions of automatic transmissions found in newer automobiles. Table 1 lists the various performances requirements of thrust needle roller bearings for ATs.

If thrust needle roller bearings with unitized inner and outer raceway washers are employed in a torque converter, which facilitate easier handling and mounting, the durability of the bearings under conditions eccentricity becomes a major technical issue since the bearings employed in a torque converter are easily affected by the influence of the eccentricity between the engine and the transmission. Primarily, excess load is not imposed on the cage in a typical bearing application. However, if a thrust needle roller bearing with inner and outer raceway washers is used in an application under conditions of large

Gear train

Torque converter
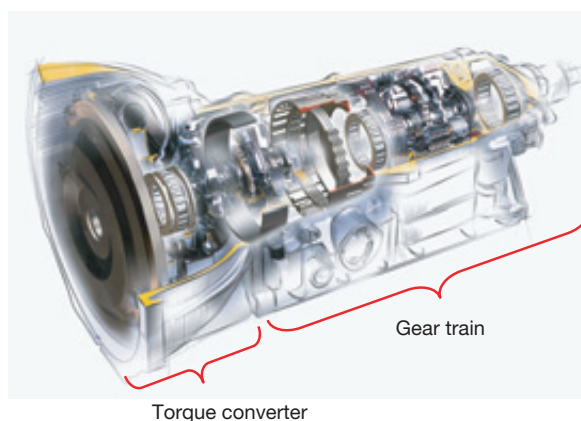
Fig. 1 Automatic transmission

eccentricity, the flange area of the raceway ring interferes with the side face of the cage in the radial direction, causing the cage to bear excessive loads.

Fig. 4 illustrates how the flange area of the raceway interferes with the cage.

If internal clearance of the bearing (C: outside diameter side clearance, C1 + bore diameter side clearance, C2) is smaller than the eccentricity between the left and right supporting parts (E), this eccentricity is not absorbed by the internal clearance of the bearing(C), causing excessive loading on the side face of the cage. As a result, wear or fatigue fractures generate in the cage material and the bearing eventually suffers from premature failure. In order to prevent the flange area of the raceway ring from interfering with the side face of the cage, a separate-type bearing that combines a thrust needle roller bearing with one raceway and a flat raceway could be adopted.

Unfortunately, this design defeats the customer's need for a unitized design that facilitates easier handling and mounting.

2.2 Concept of development

In order to respond to customer requirements for durability under eccentric operating conditions and requirements for ease of handling and installation, NSK focused on the following concepts:

1) Improve cage durability: The cage must have sufficiently proven strength even under conditions of eccentricity where the cage is pinched by the flange section of the raceways in the radial direction (E (eccentricity) > C/2 (bearing internal clearance)).

2) Bearing internal clearance that is larger than the eccentricity (E (eccentricity) ≤ C/2 (bearing internal clearance)): Bearing internal clearance absorbs eccentricity so that the flange section of the raceways in the radial direction does not pinch the cage.

3. Features of Developed Product

3.1 Wear-resistant and high-strength cage (NSK HYTEC)

A special heat treatment process, which is superior to NSK's conventional nitriding treatment, is applied to the cage for dramatically improved wear resistance and fatigue strength. Fig. 6 illustrates a nitrided layer of the conventional heat treatment process and that of the special heat treatment process.

Table 1 List of requirements for thrust needle roller bearings

Life	· Improved durability under high-speed operations · Improved durability when gear ratio changes
	· Improved durability under fluctuating loads · Improved durability under misalignment (eccentricity)
Mounting surface	· Accommodate insufficient rigidity of supporting surface · Maintain supporting surface accuracy
	· Accommodate a diversity of housing specifications and mounting methods
Handling	· Ease of mounting
	· Prevent improper mounting
Improved fuel economy	· Reduce bearing weight
	· Reduce bearing torque (friction)
High-temperature conditions	· Improved heat resistance
Lubrication	· Increase the amount of oil that flows through the bearing interior
	· Control of lubricant path around the bearing · Accommodate starved lubricating conditions

Fig. 2 Thrust needle roller bearing with inner and outer raceway washers

Outer flange
Roller
Cage
Inner flange

Fig. 3 NSK HYTEC Bearing
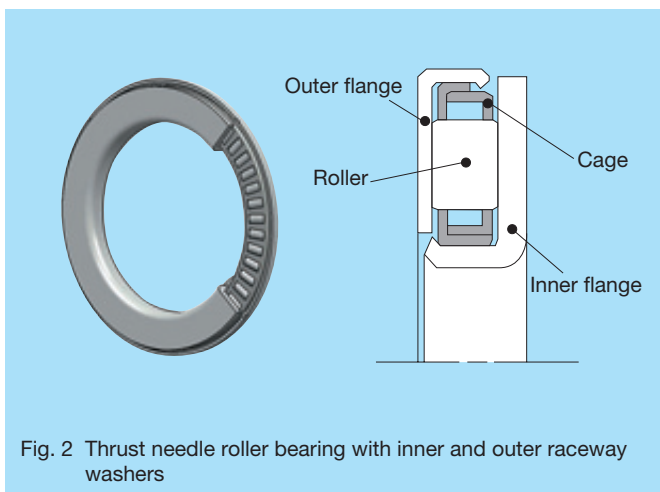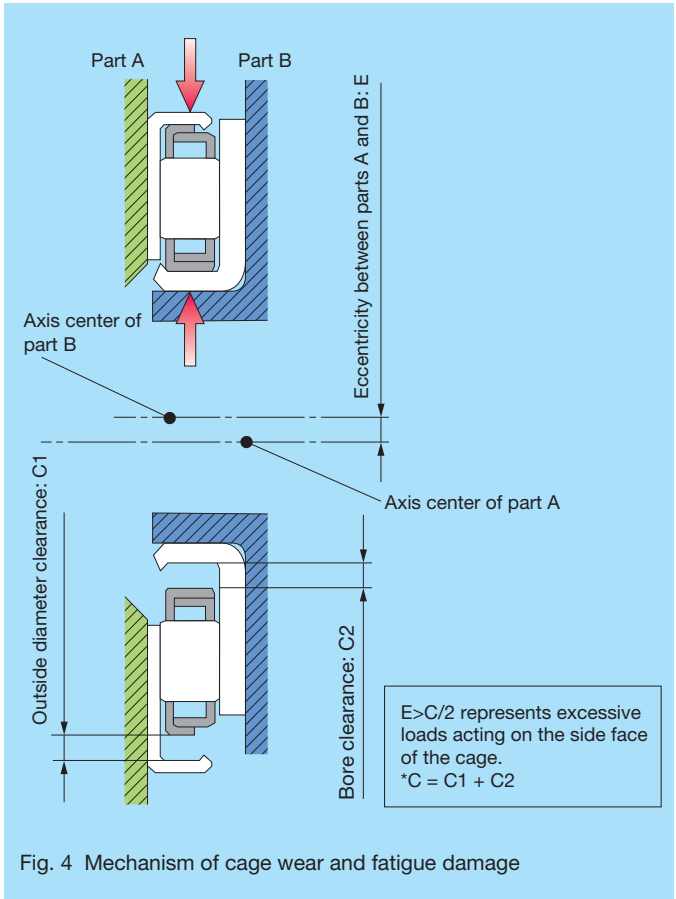
Fig. 4 Mechanism of cage wear and fatigue damage

Part A   Part B

Axis center of part B

Axis center of part A

Eccentricity between parts A and B: E

Outside diameter clearance: C1

Bore clearance: C2

E>C/2 represents excessive loads acting on the side face of the cage.
*C = C1 + C2
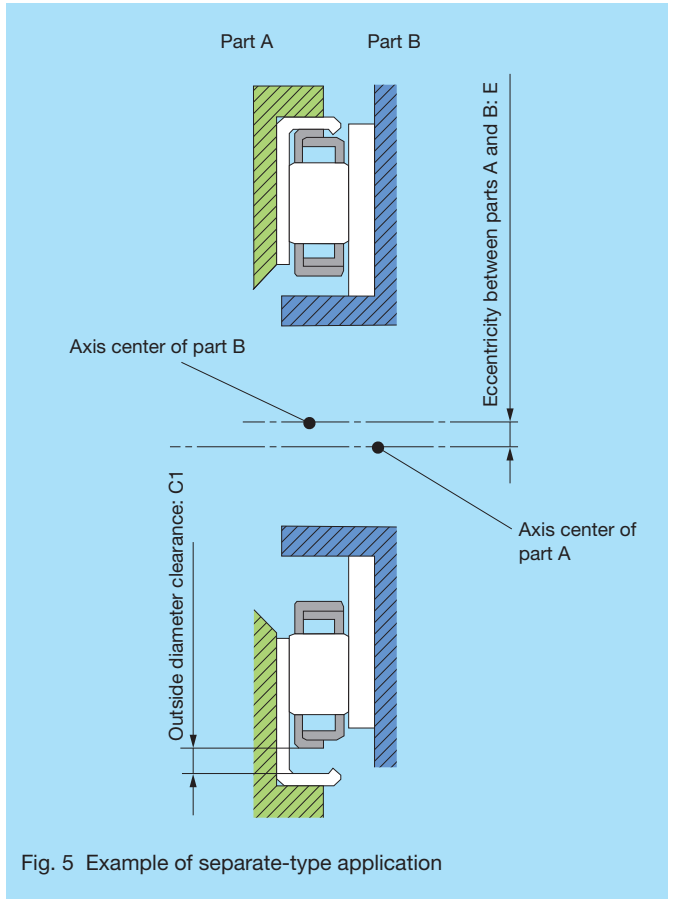
Fig. 5 Example of separate-type application

Part A   Part B

Axis center of part B

Axis center of part A

Eccentricity between parts A and B: E

Outside diameter clearance: C1

【Cross-sectional views of surface layer (see position ①)】

Porous nitrided layer

5 µm

(Conventional nitriding treatment)

Oxide layer

Fine nitrided layer

5 µm

(Special heat treatment)

②

①

【Diagrammatic and cross-sectional sketches of the pressed curved lip section (see position ②)】

(Conventional nitriding treatment)

(Special heat treatment)

Fig. 6 Cross-section view of nitrided film

The nitrided layer of the conventional nitriding treatment process has a porous (low density) surface that has low resistance to sliding wear. NSK developed a unique special heat treatment process that produces a nitrided layer and an oxide layer on the cage surface. This two-layer structure dramatically improves wear resistance and fatigue strength. Also, it was difficult to form a uniformly thick nitrided layer on the bent surface areas using a conventional nitriding treatment process. The special heat treatment process, however, forms a uniformly thick layer on all of the cage surface areas. The results of various comparison tests between the conventional nitriding treatment and the special heat treatment are shown in Fig. 7 and 8. Surface-wear test results shows that the special heat treatment process offers three times greater wear-resistance than that of the conventional nitriding treatment process. Drop-impact test results also confirmed that the special heat treatment process provides more than three times the fatigue strength of the conventional nitriding treatment process.

3.2 Raceway ring with a curved lip along the entire outer circumference

Conventionally, outer ring raceways had curved lip sections as a means to unitize the bearing raceways and cage & roller assembly. The curved lip sections were positioned at intervals along the circumference of the raceway flanges by press forming, and served to unitize the whole bearing assembly. Using a bending process for the HYTEC series bearing, a curved lip is formed along the entire outer circumference of the raceway ring to unitize the bearing assembly (Fig. 9). Conventionally, processing limitations of the curved lip section method did not allow for expansion of bearing internal clearance while simultaneously ensuring a unitized and secure assembly. The new curved lip along the entire outer circumference enables expansion of the bearing's internal clearance while simultaneously ensuring an inseparable design. By adopting a curved lip along the entire outer circumference instead of curved lip sections at intervals, bearing internal clearance was increase by approximately twofold.

4. Effectiveness of Developed Product

The following durability tests were conducted under conditions of excessive eccentricity in order to compare cage durability of the newly developed product and the conventional product.

4.1 Impact test under excessive eccentricity

Impact load testing under excessive eccentricity was used to compare durability of bearings with cages that had undergone different heat treatment processes: conventional nitriding treatment and special heat treatment.

The tested bearings used outer ring raceways with curved lip sections with an internal clearance of 0.45 mm. Fig. 10 shows test results for each type of heat treatment. A comparison of test results revealed that cage strength of the special heat-treated product showed an improvement of more than six times that of the conventional nitrided product.

Although there were no obvious differences in wear on the side face of the cage, further observations of both specifications revealed cracking that progressed from the inner side of the bent area of the pressed cage to a fracture on the side face of the conventional nitrided product. Conversely, the special heat-treated product was free of any crack generation throughout the entire surface area of the cage. These observations confirm that the special heat treatment process produces a uniform and highly dense nitrided and oxidized layer that contribute towards improving fatigue strength of the cage.

4.2 Interference durability testing under excessive eccentricity

This test was conducted to verify the durability of outer raceway washers with curved lip sections and outer raceway washers with a curved lip along the entire outer circumference. Testing was conducted under conditions of excessive eccentricity and cage interference. The tested bearings had conventional nitrided cages.

Fig. 11 shows the test results for each outer raceway.

Fig. 7 Surface-wear test result

Fig. 8 Drop-impact test results

Raceway waster with curved lip sections (conventional)

Raceway washer with curved lip along the entire circumference
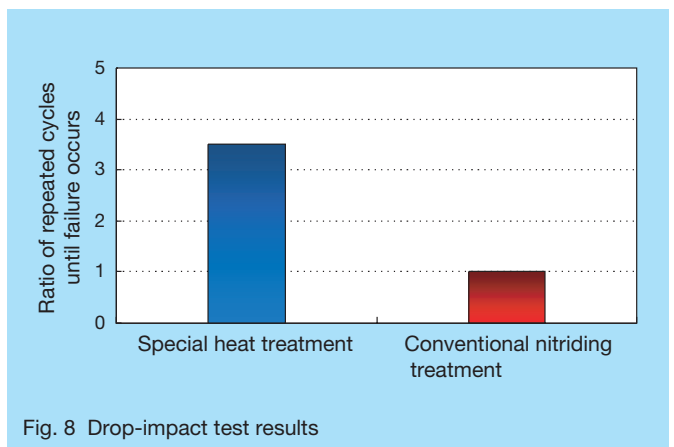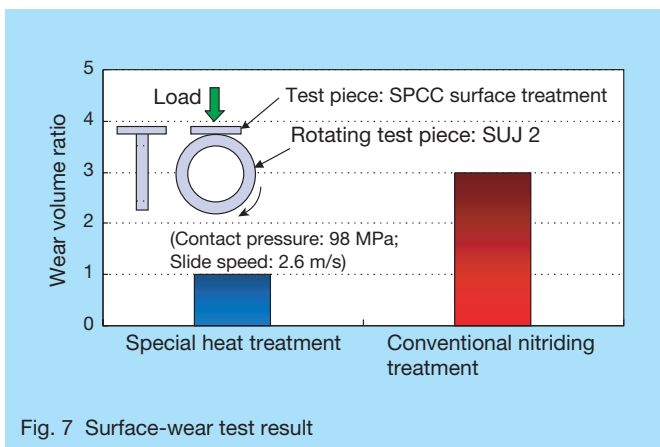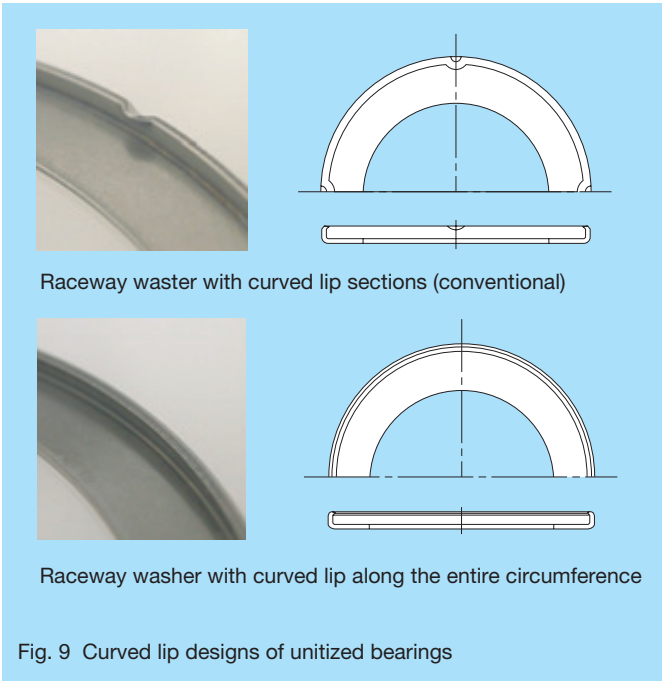
Fig. 9 Curved lip designs of unitized bearings

(Bearing rotating speed: 3000 rpm; bearing internal clearance: 0.45 mm; lubrication: ATF·oil bath)

【View of cage side face】

No abnormality

Generation of crack

(NSK HYTEC)

(Conventional nitriding treatment)

【Cross sectional view of pressed curved lip】

Pressed curved lip

Direction of crack progression

(Crack generation in conventional nitrided product)

Fig. 10 Lip designs of unitized bearings

A comparison of test results revealed that strength of the cage of the newly developed bearing showed an improvement of more than four times that of the cage of the conventional bearing. The newly developed bearing had an internal clearance of about 1.0 mm—nearly twice that of the conventional bearing (0.45 mm).

In other words, it is clear that the newly developed bearing, having sufficient bearing internal clearance to accommodate eccentricity on the order of 0.5 mm, has sufficient proven cage strength in comparison with the conventional bearing where compression force applies to the side face of the cage.

5. Postscript

In this paper, we have discussed development of the NSK HYTEC thrust needle roller bearing with inner and outer raceway washers, and have shown that this product performs well under conditions of excessive eccentricity. This bearing promotes greater efficiency of assembly line operations by reducing the number of component parts that need to be mounted to an AT unit, in addition to meeting the demands for high tolerance in relation to interacting with other component parts.

We are confident that the newly developed bearing will also meet the various needs of our customers in other applications. NSK will continue to further develop products and applications that meet or favorably exceed the needs of our customers.

(Bearing rotating speed: 3 000 rpm; cage: conventional nitriding treatment; lubrication: ATF·oil bath)

【View of thrust needle roller bearing cage】

No abnormality

Generation of crack

(Bearing with curved lip along the entire circumference)
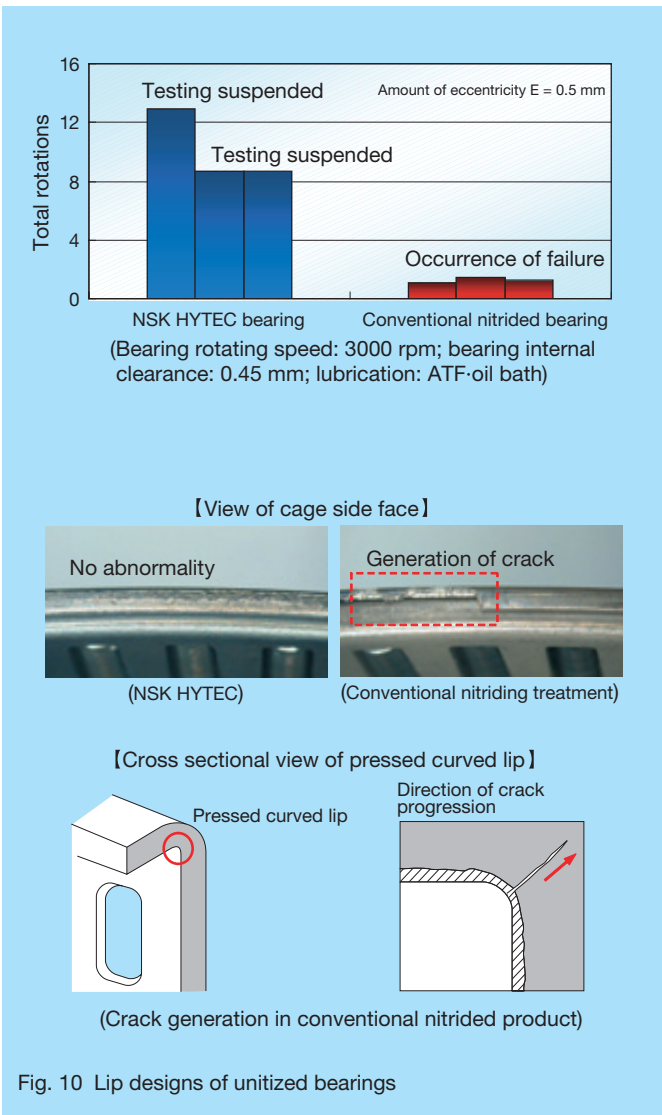
(Conventional bearing with curved lip sections)
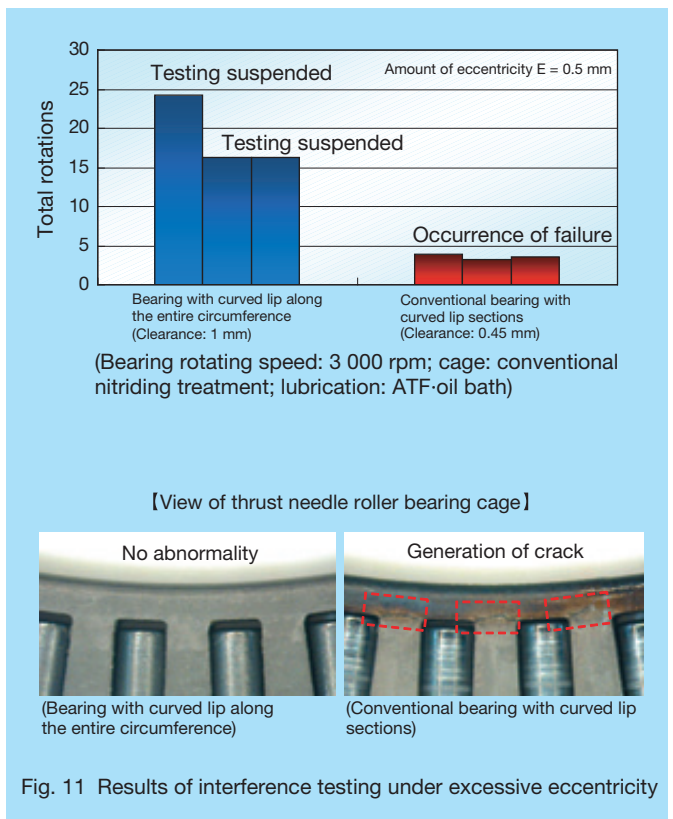
Fig. 11 Results of interference testing under excessive eccentricity

References

1) T. Otsubo, S. Kadokawa "Trends and New Technologies of Automatic Transmission Bearings" NSK Technical J. Motion & Control, No. 17 (2005) 39-47.
2) S. Chiba "Thrust Needle Roller Bearings for Automatic Transmission" NSK Technical J., No. 662 (1996)16-24.

Satoshi Masuda

Hiromichi Takemura

Yasuyuki Shimizu

Newly Developed Series of Electrically Conductive Bearings for Office Equipment

Bearings used in office equipment, such as plain paper copiers (PPCs) and laser printers, can be classified into two types according to their operating temperatures. Bearings for normal temperature applications are used in the photoreceptor drum assembly, the photosensitive unit, and the paper feed and discharge rollers. Bearings for high-temperature applications are used in the fuser/pressure rollers. Bearings that are prelubricated with electrically conductive grease are used in paper transport assembly and photoreceptor drum assembly rollers to eliminate electrical charge buildup, which can cause copiers and laser printers to suffer from poor image quality.

In order to produce high-quality images in newer PPCs and laser printers, bearings are required to ensure stable electrical conductivity for a longer length of time. This situation has placed greater demand on bearings for increased electrically conductive performance.

In response, NSK has developed two grease products, ECZ grease for normal temperature applications and ECF grease for high-temperature applications, that offer enhanced performance over that of conventional electrically conductive grease. These grease products are packed in bearings for use in our new series of electrically conductive bearings for office equipment components operating under normal-temperature and high-temperature conditions.

1. Specification of Electrically Conductive Grease

An optimum combination of carbon-black particles of different sizes were mixed with grease. The quantity of carbon-black particles mixed with grease was substantially increased for both the ECE grease and the ECH grease in comparison with conventional grease products. Since carbon-black particles approaching the nanometer-scale serve not only a conductive function, but also serve as a thickening agent, we were able to further thicken the grease by increasing the amount of carbon-black particles. Also, by using different sizes of carbon-black particles, the network structure of carbon-black was enhanced. As a result, separation of base oil in the grease was restricted, and the formation of a fine oxide film on the inner and outer ring raceways and ball surface was prevented. After long-term, extensive use, the electrical conductivity of these bearings remained stable.

Fig. 1 Newly developed series of electrically conductive bearings for office equipment

100 nm
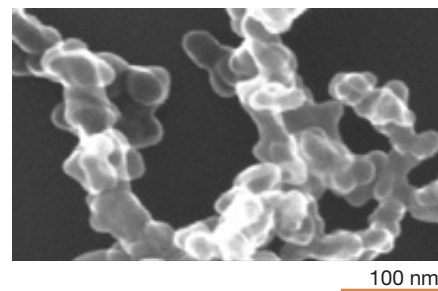
Fig. 2 SEM micrograph of carbon-black particles

Table 1 Newly developed series of electrically conductive bearings for office equipment

	Electrically conductive bearings		
	Normal-temperature ECE grease		High-temperature ECH grease
Operating temperature	Up to 60 ℃	Up to 100 ℃	Up to 230 ℃
Applications	ATMs, cash dispensers	Copiers, printers	Copiers, printers
Location	Paper transport assembly rollers	Photoreceptor drum, transfer roller, developer unit cylinder, paper feed and discharge rollers	Fuser/pressure roller

2. Features

The features of electrically conductive bearings for office equipment components operating under normal-temperature and high-temperature conditions are described below.

2.1 Electrically conductive bearings for normal temperatures

(1) Conductivity is eight times better than that of conventional bearings.
Formation of a fine oxide film is prevented by the use of a proprietary grease additive.
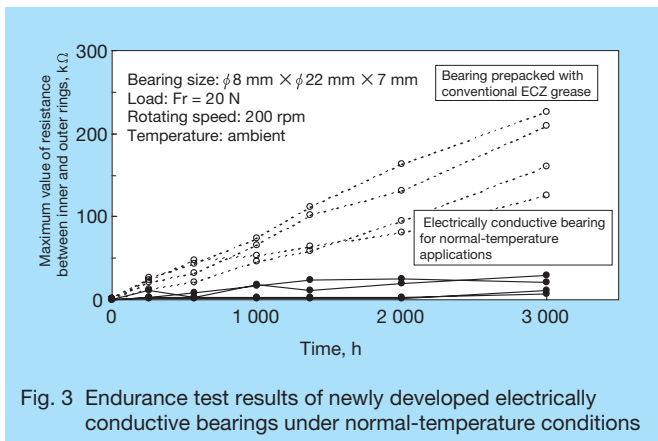
Fig. 3 Endurance test results of newly developed electrically conductive bearings under normal-temperature conditions
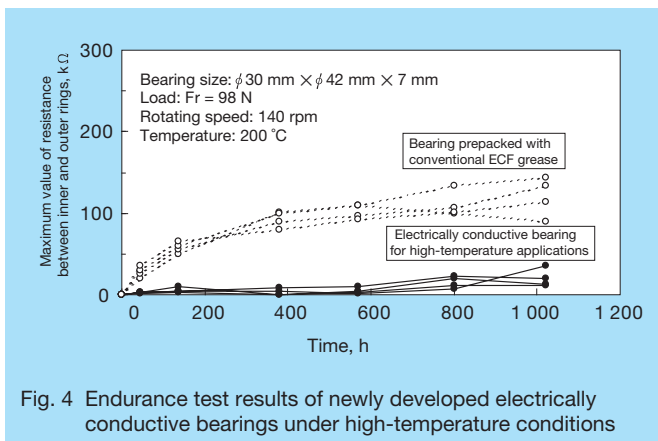
Fig. 4 Endurance test results of newly developed electrically conductive bearings under high-temperature conditions
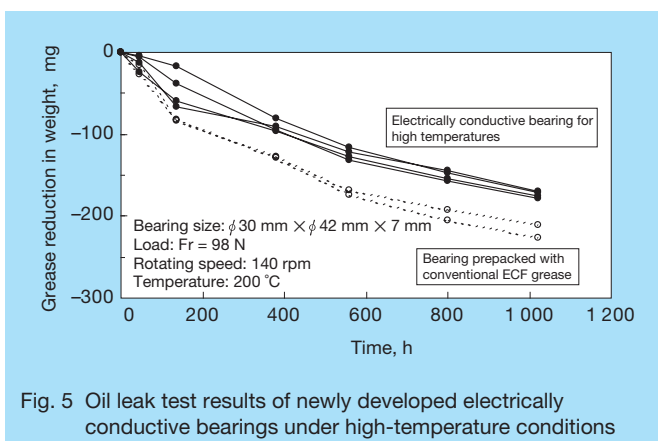
Fig. 5 Oil leak test results of newly developed electrically conductive bearings under high-temperature conditions

(2) Synthetic carbon hydride oil, which is suitable for normal operating temperatures, is used for the base oil of grease. Additional benefits include minimal friction loss, compatibility with peripheral resin material, and good resistance against exposure to chemicals.

2.2 Electrically conductive bearings for high temperatures

(1) Conductivity is three times better than that of conventional bearings.
(2) Fluorine oil, which is suitable for high operating temperatures, is used for the base oil of grease. Additional benefits include a maximum operating temperature of nearly 230 ºC, compatibility with peripheral resin material, and good resistance against exposure to chemicals.
(3) The leakage of base oil, which becomes a problem at high temperatures, is less than that of conventional grease by as much as 20 %, which helps to prevent contamination of the working environment immediately surrounding the bearing.

3. Application

Electrically conductive bearings are perfect for the photoreceptor drum assembly, the photosensitive unit, and the paper feed and discharge rollers of PPCs and laser printers. These bearings contribute towards better image quality and act as a measure against interference caused by electromagnetic waves. Furthermore, these bearings are an effective measure against the buildup of static electricity generated in cash dispensers and ATMs. NSK's latest series of electrically conductive bearings meets the needs of long-life conductivity and the need for stable performance for applications operating under conditions of normal temperatures and high temperatures not exceeding 230 ºC.

4. Summary

In the past, office equipment makers ensured electrical conductivity by mounting a grounding mechanism, such as a plate spring or brush, to the rollers. NSK recognized the need to eliminate such a complicated grounding mechanism and developed bearings that facilitate the flow of electricity between the inner and outer rings of the bearings used in the rollers. The electrically conductive bearings introduced in this article offer substantially improved conductivity, thus improving the reliability of the grounding mechanism of bearings used in office equipment. NSK's electrically conductive bearings contribute towards greater simplification and downscaling of office equipment components by enhancing bearing life and eliminating mechanical grounding mechanisms.

High-Temperature Long-Life Engine Accessory Bearings

In response to the growing need for lightweight, low-cost, and high-speed bearings used in engine-driven accessories of modern automobiles, conventional pulley bearing materials have been replaced with resin material. This change in material has resulted in a pulley bearing that is somewhat poor at heat dissipation while generating larger amounts of heat due to higher rotational speeds. The result is an operating environment that has become hotter than ever before. For example, the maximum operating temperature used to be around 150 ºC to 160 ºC, but in newer automobiles, pulley bearing must operate in temperatures reaching as high as 180 ºC. Needless to say, development of a bearing that can maintain sufficient reliability at such high temperatures has become an urgent issue that must be addressed.

NSK has responded accordingly with a newly developed automotive engine accessory bearing that is able to meet the severe demands of high-temperature operating conditions (photo 1).

1. Bearing Specifications

1.1 Grease

We have developed a new grease that substantially improves the seizure life of bearings operating under high-temperature conditions (Fig. 1).
- An optimum grease was developed by blending oil that is superior in heat resistance with oil of good lubricating qualities.
- A thickener was developed that generates less heat during bearing rotation while maintaining excellent oil retention.

- An additive that prevents oxidization under high-temperature conditions was blended with the grease mixture.

1.2 Cage and seal

Improvements were made to the cage's internal geometry and seal design to take fuller advantage of the lubricating qualities of the grease (Fig. 2 and 3).
- The newly improved internal geometry of the cage pocket ensures a stable supply of grease on the rolling surface areas.
- The newly optimized rubber seal design is configured to prevent grease leakage, and works to promote lubricant circulation inside the bearing.
- Both cage and seal materials were specially selected for their high-temperature endurance for temperatures as high as 180 ºC.

Thickener — Less heat generation and excellent oil retention

Base oil — Superior heat resistance and good lubricating qualities

Additive — Antioxidant performance

Fig.1 Illustration of grease composition
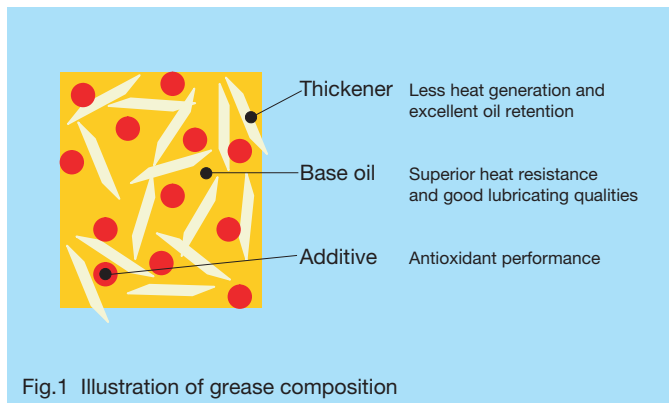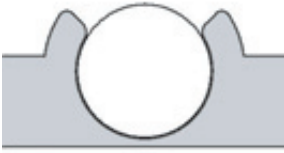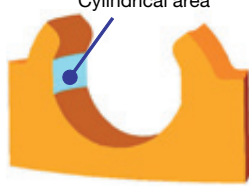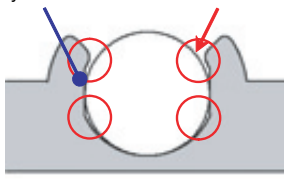
Photo 1 High-temperature long-life engine accessory bearings

Pocket configuration	3-D view	Cross-section view	Condition after rotation
Single spherical surface (conventional)			
Axial cylindrical surface (newly developed)	Cylindrical area	Cylindrical area Grease reservoir	

Note: Operating conditions: bearing size: bore diameter 15 mm × outer diameter 35 mm × width 13 mm; room temperature; inner ring rotation 1 800 rpm × 2 minutes

Fig. 2 Axial cylindrical pocket cage

Outer ring

Grease

Restricts grease leakage and promotes grease circulation inside bearing

Grease lip was added.

Inner ring
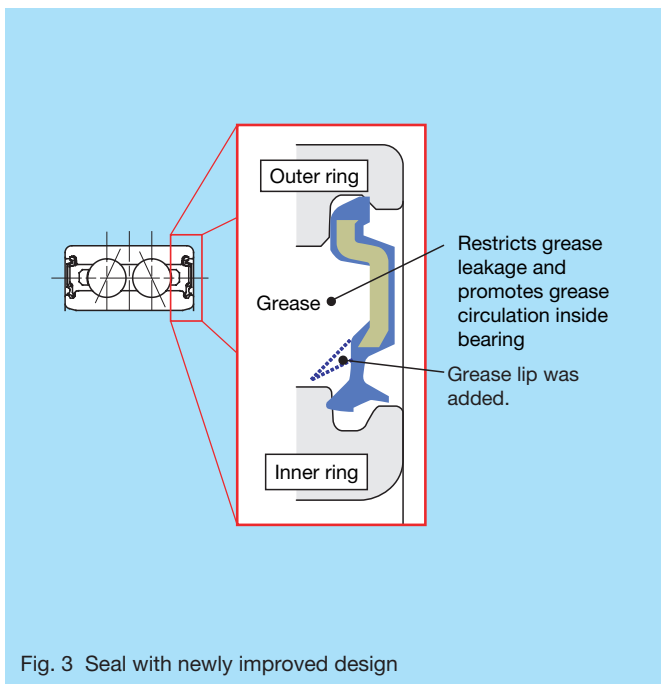
Fig. 3 Seal with newly improved design

Test conditions
Tested bearing: deep groove ball bearing
(Bore diameter 17 mm × outer
diameter 40 mm × width 12 mm)
Outer ring rotating speed: 12 000 rpm
Bearing inner ring temperature: 150 to 180 ℃
Test load: 2 000 N

The number 1 indicates the seizure life ratio of a conventional bearing at 160 ℃.

Long life

Seizure life ratio

Newly developed bearing
Conventional bearing

Test temperature, ℃

Fig. 4 High-temperature seizure-life test results

2. Features

As a result of the newly developed grease and significant improvements made to bearing components, bearing seizure life for high-temperature conditions reaching 180 ℃ was more than doubled. Not only do these developments provide more than enough reliability for high-temperature long-life engine accessory bearings operating in a high-temperature environment of 180 ℃, but they also provide sufficient reliability for applications operating in temperatures exceeding conventional temperatures by as much as 20 ℃ (Fig. 4).

3. Summary

NSK has achieved the successful development of a high-temperature long-life engine accessory bearing that offers significant improvements to bearing life under high-temperature operating conditions. NSK will continue efforts further improve bearing performance and reliability for high-temperature applications that meet or exceed market demands.

High-Capacity Angular Contact Water Pump Bearings

The automotive industry is placing greater importance on fuel economy and high reliability at lower costs for newer automobiles. Such requirements extend to many engine components, including water pump bearings. Historically, NSK water pump bearings have incorporated a highly water-resistant triple-lip seal with high-performance WPH grease as measures against water intrusion while offering high reliability. In order to provide greater flexibility for a variety of operating conditions, NSK has developed new type of high-capacity angular contact water pump bearing (photo 1), which is introduced in this paper.

1. Structure and Specifications

A water pump bearing is a double-row type of bearing with an integral shaft. In the past, a ball/roller configuration (photo 2) was used in applications requiring higher load capacity, and a ball/ball configuration (photo 3) was used under lighter loads. Our newly developed high-capacity angular contact water pump bearing, which is of the same ball/ball configuration used conventionally, has been designed to provide higher capacity by increasing the number of balls in the front row, where relatively larger loads apply. Both rows of consist of angular contact balls for reduced play and increased rigidity under moment load.

In order to ensure sufficient reliability, this bearing takes advantage of NSK's highly water-resistant triple-lip seal for the rear side and uses high-performance WPH grease.

Photo 1 Newly developed high-capacity angular contact water pump bearing (ball/ball unit)

Photo 2 Current water pump bearing (ball/roller unit)

Photo 3 Current water pump bearing (ball/ball unit)

Table 1 Comparison between current and newly developed bearings

Configuration		High-capacity angular contact (BWFH35)	Ball/roller (RWF35)	Ball/ball (BWF35)
Number of balls	Front	8	10 (Roller)	6
	Rear	5	6	6
Load rating (N)	Front	11 200	21 800	8 150
	Rear	8 200	8 150	8 150
Weight ratio		0.9	1	0.95
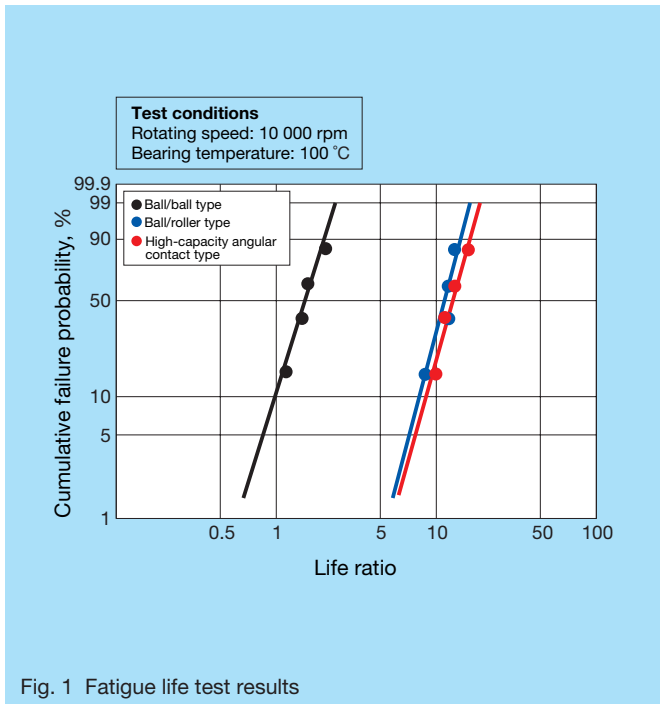
Fig. 1 Fatigue life test results
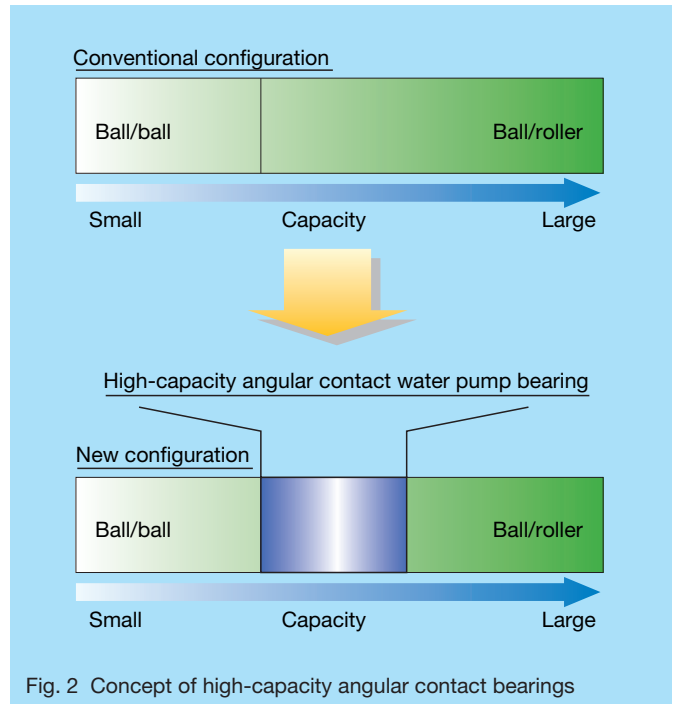
Fig. 2 Concept of high-capacity angular contact bearings
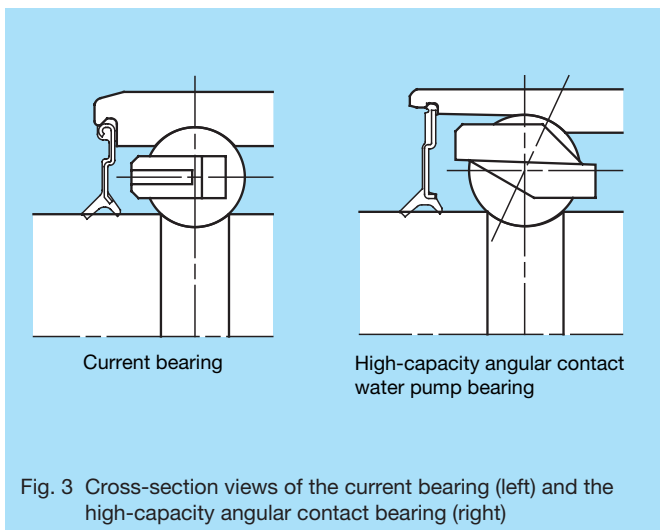
Fig. 3 Cross-section views of the current bearing (left) and the high-capacity angular contact bearing (right)

2. Features

(1) Higher capacity

The increased number of balls in the front row ensures sufficiently high capacity (table 1). Internal comparisons (Fig. 1) reveal that this new bearing achieves nine times longer life than that of current ball/ball configurations, thus making it possible to replace the current ball/roller configuration (Fig. 2) with the newly developed ball-ball type.

(2) Improved sealing capability and rigidity

Using angular contact bearings reduces axial play, which supports the mechanical seal in preventing water leakage from the impeller side of the pump. Whereas issues related to reliability and water leakage are basically eliminated, water pumps can be expected to run with substantially greater degrees of reliability. Furthermore, rigidity under moment load is much higher in comparison with current ball/ball configurations thanks in part to the expanded distance between effective load centers.

(3) Lightweight

Another advantage of using an angular contact ball bearing is having a counterbore formed on the outer ring (Fig. 3), which facilitates a more lightweight design (table 1).

3. Summary

Replacing ball/roller configured bearings in an automotive water pump with NSK's newly developed angular contact water pump bearing not only meets the high-capacity and lightweight requirements of such an application, but also provides the pump with improved seal performance and higher rigidity.

Eccentric Bearings

Conventional antilock braking systems (ABS) have a motor and piston-reciprocating pump assembly. Mounted to the motor's output eccentric shaft is a ball or needle bearing assembly. The outside surface of the bearing's outer ring functions as an eccentric cam, where piston plungers ride the outside surface of the outer ring and reciprocate when the eccentric shaft is running. With each stroke of the piston plunger, the pump boosts brake fluid pressure in the ABS. However, since the manufacturing process of an eccentric shaft is considerably complicated, NSK endeavored to develop a more improved and cost-effective structure for the pump assembly.

The result of our efforts was a newly developed eccentric bearing that performs the same function of a conventional rotating shaft. This paper provides an outline of this newly developed bearing (see photo 1).

1. Structure and Specifications

The bore of this newly developed eccentric bearing is mounted off center on the motor output shaft (Fig. 1). Use of this bearing eliminates the need for an eccentric shaft while providing a means for converting rotational motion to reciprocating motion, thus driving the pistons in a reciprocating motion (Fig. 2 and 3).

2. Features

(1) Metallic shield

Normally, the metallic shield used in this bearing would be notched along the outer circumference to create small tabs that facilitate crimping of the shield into a groove in the outer ring. However, since the inner ring bore is off center in an eccentric bearing, the bearing becomes susceptible to partial cyclic loads. Due to this load, the outer ring slightly deforms and stress is generated along the tabs formed on the shield. In this particular bearing, the notches have been eliminated to improve bearing strength.

(2) Inner ring

Conventionally, it has been difficult to manufacture an eccentric bearing with an off center inner ring bore. NSK resolved this issue by developing a proprietary tooling machine process specifically for the off center inner ring

Eccentric bearing   Standard bearing
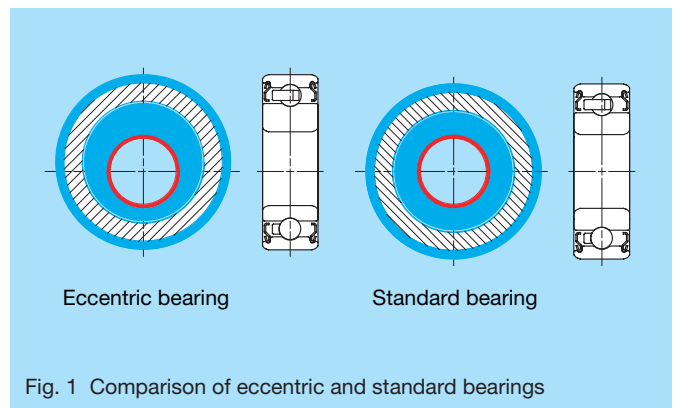
Fig. 1 Comparison of eccentric and standard bearings
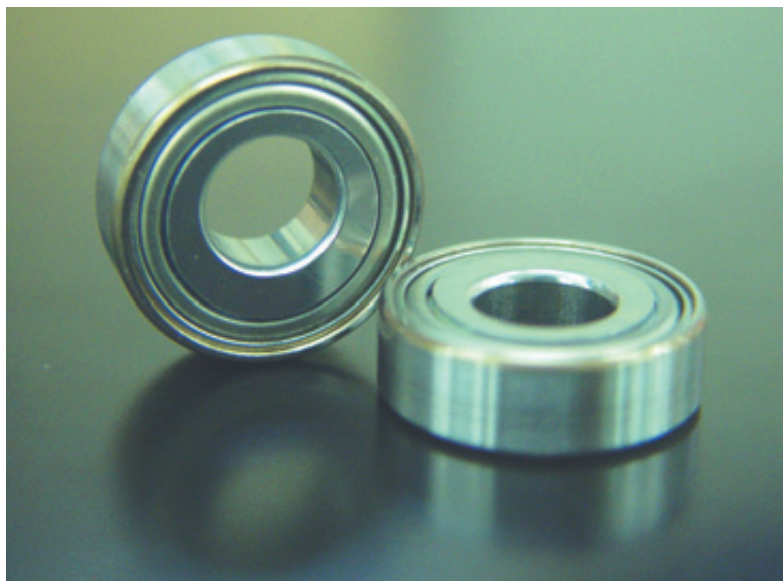
Photo 1 Eccentric bearings

bore, which has enable NSK to more efficiently mass-produce eccentric bearings. At the same time, NSK developed an inspection machine specifically the eccentric bearing's inner ring bore surface to ensure stable quality of the product.

3. Summary

In addition to performing a conventional rotating function, NSK's newly developed eccentric bearing functions as a cam mechanism. This newly developed bearing eliminates the need for an eccentric shaft, which helps to lower production costs while performing the same function of conventional products.

In the future, NSK will continue working on technologies that meet the requirements of various modules involving bearings, and work to enhance the added value of other applications where this bearing can be used.
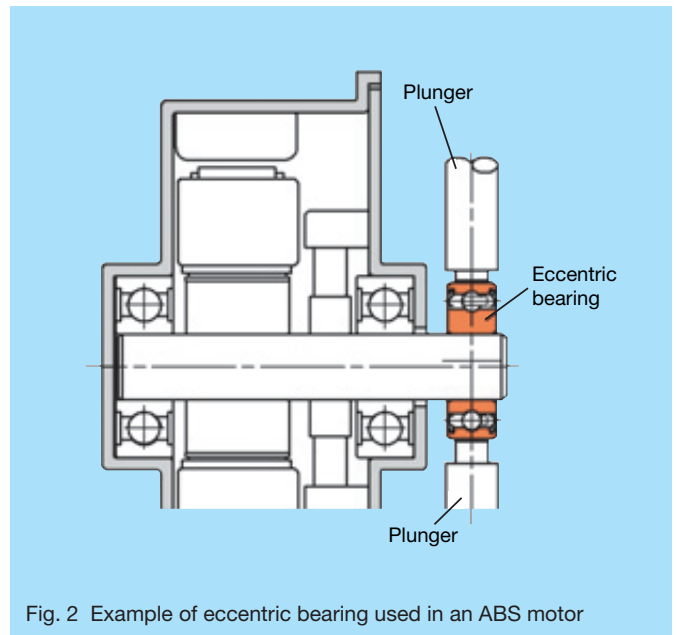
Fig. 2 Example of eccentric bearing used in an ABS motor
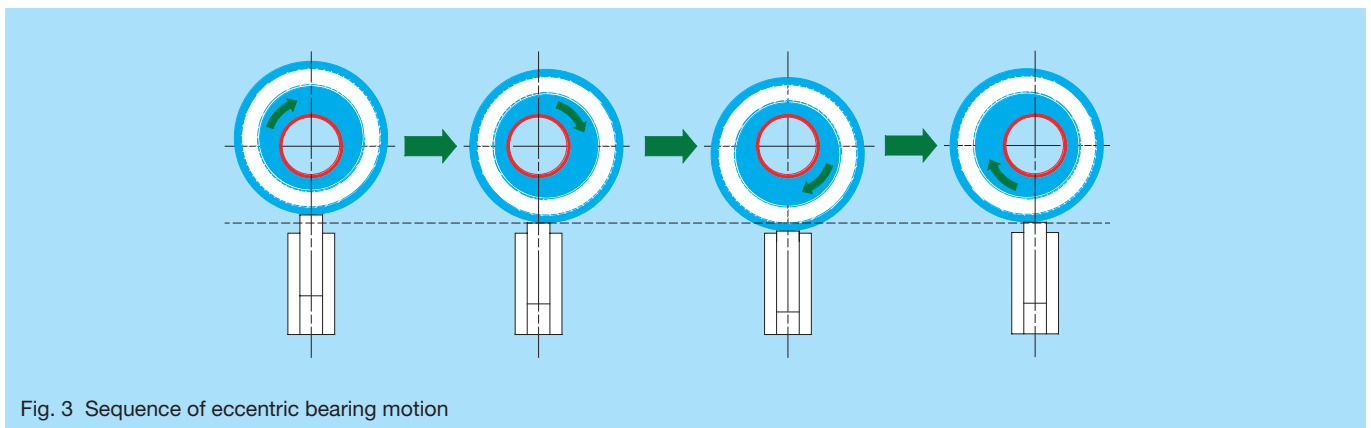
Fig. 3 Sequence of eccentric bearing motion

V1 Series of Highly Dust-Resistant NSK Linear Guides

Suitable for a wide range of applications, linear guides are sometimes used in severely contaminated environments where they are exposed to foreign matter of various types and sizes. Under these conditions, foreign matter may invade the linear guide interior and cause abnormal wear of the rolling surface or rolling elements (balls), which would hamper smooth ball movement in the recirculation circuit, thus leading to early failure of the linear guide.

A cover, such as a bellows, is typically used to prevent foreign matter from directly adhering to the linear guide. This measure alone, however, is inefffective against very minute particles. Moreover, not all applications are compatible with the installation of a bellows cover due to equipment configuration or space limitations.

NSK addressed this issue by developing and marketing the V1 series of NSK linear guides (photo 1), which features significantly higher dust-resistance than conventional linear guides and ensures long operating life even in a contaminated environment. This article discusses the details of this new series.

1. Features and Specifications

One of the most striking features of the V1 series linear guide is its long operating life under contaminated operating conditions.

As shown in Fig. 1 and 2, durability tests indicate that the V1 series achieves better than a fivefold increase in operating life under rubber particle contaminated conditions in comparison with the standard series, and achieves more than twice the life under fine sawdust contaminated conditions.

Longer operating life under contaminated conditions was achieved by implementing the specifications listed below.

(1) Highly dust-resistant end seal

The highly dust-resistant design of the triple-lip end seal (Fig. 3) reduces ingress of foreign particles by more than 90 %, compared with conventional seals. Dustproofing test results are shown in Fig. 4.

(2) NSK K1™ lubrication unit

The NSK K1 lubrication unit, which is equipped as a standard specification, improves lubricating performance of the ball race, enhances sealing capability of the end seals, and boosts the durability of the related parts.

(3) Caps for rail mounting holes

The counterbored rail mounting holes have caps that prevent debris from accumulating in the holes from where contaminants could invade the linear guide interior if left uncapped.

(4) Tapped holes on rail bottom face

The V1 series is available with tapped mounting holes from the bottom of the rail to prevent contamination build-
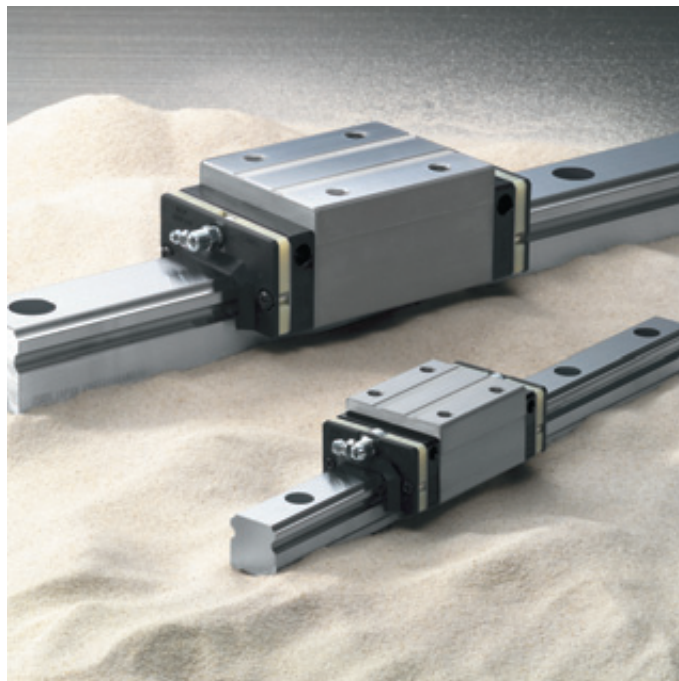
Photo 1 V1 series of highly dust-resistant NSK linear guides

Test conditions

Specimen	VH30
Rail orientation	Horizontal (wall mounted)
Speed	500 mm/s
Lubricant	Grease (packed only at the beginning)
Foreign matter	Rubber particles
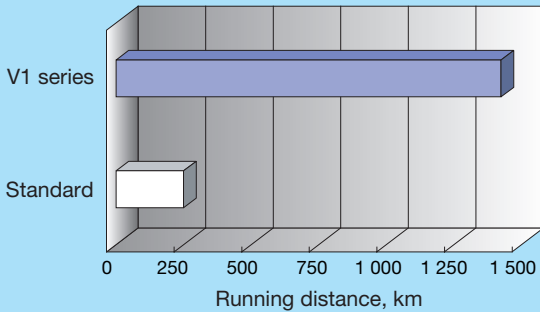
Fig. 1 Durability test results under rubber particle contaminated conditions

Test conditions

Specimen	VH30
Rail orientation	Horizontal (wall mount)
Speed	400 mm/s
Lubricant	Grease (packed only at the beginning)
Foreign matter	Fine sawdust
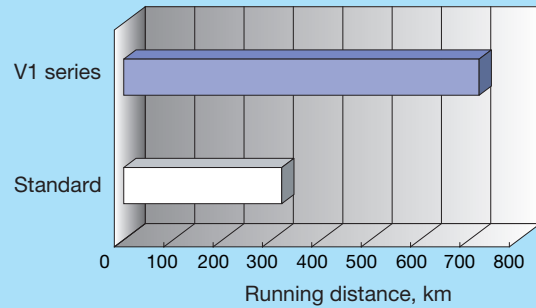
Fig. 2 Durability test results under fine sawdust contaminated conditions
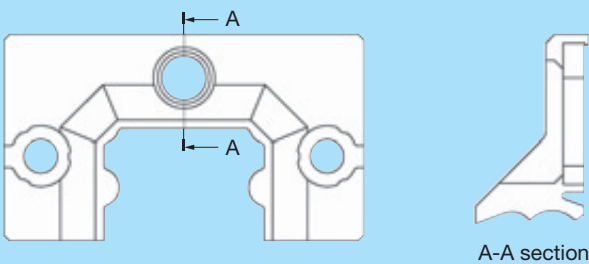
Fig. 3 Cross-section view of triple-lip wiper seal

Test conditions

Specimen	VH30
Speed	16.7 mm/s
Foreign matter	Graphite (average grain size: 0.037 mm) and grease
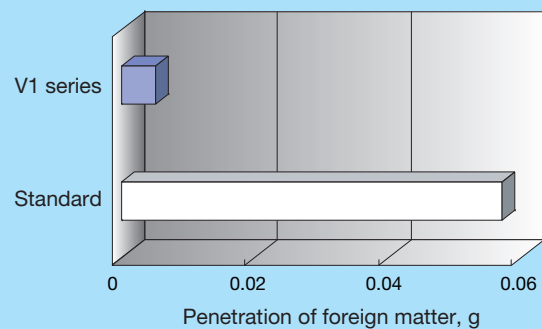
Fig. 4 Dustproofing performance test results

up. This optional specification of the V1 series is in addition to the standard counterbored mounting holes on the top face of the rail.

2. Type and Dimensions

Table 1 summarizes the types and major dimensions of the V1 series.

3. Applications

The V1 series is most suitable for woodworking machinery, graphite processing machines, tire buffers, laser processing machines, welding lines, transfer equipment, and more.

Table 1 Dimensions

Square type Flange type

Counterbore specifications (rail top face)

Tapped hole specifications (rail bottom face)
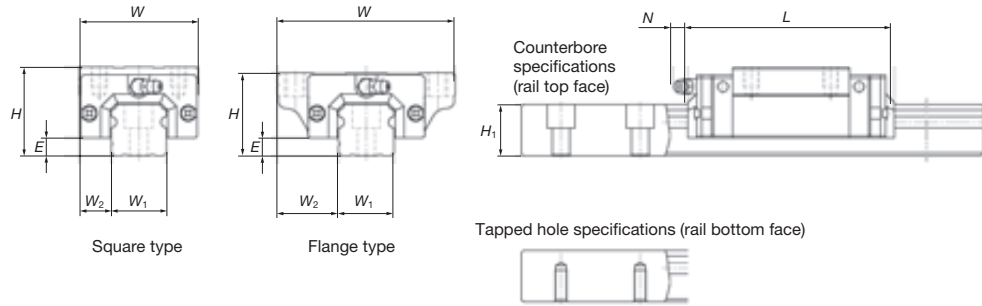
unit : mm

Model No.	Ball slide type and shape		Assembly			Ball slide		Rail		Basic load rating				
			Height H	E	W_2	Width W	Length L	Grease nipple N	Width W_1	Height H_1	Dynamic C (N)	Static C_0 (N)	Static moment (N·m)		
													Roll	Pitch	Yaw
VH15	High-load type	Square type	28	4.6	9.5	34	70.6	1	15	15	10 800	20 700	108	95	80
		Flange type	24	4.6	16	47									
	Super high-load type	Square type	28	4.6	9.5	34	89.6				14 600	32 000	166	216	181
		Flange type	24	4.6	16	47									
VH20	High-load type	Square type	30	5	12	44	87.4	11.1	20	18	17 400	32 500	219	185	155
		Flange type	30	5	21.5	63									
	Super high-load type	Square type	30	5	12	44	109.4				23 500	50 500	340	420	355
		Flange type	30	5	21.5	63									
VH25	High-load type	Square high-profile type	40	7	12.5	48	97	9.6	23	22	25 600	46 000	360	320	267
		Square low-profile type	36	7	12.5	48									
		Flange type	36	7	23.5	70									
	Super high-load type	Square high-profile type	40	7	12.5	48	125				34 500	71 000	555	725	610
		Square low-profile type	36	7	12.5	48									
		Flange type	36	7	23.5	70									
VH30	High-load type	Square high-profile type	45	9	16	60	104.4	11.4	28	26	31 000	51 500	490	350	292
		Square low-profile type	42	9	16	60									
		Flange type	42	9	31	90	117.4				35 500	63 000	600	505	425
	Super high-load type	Square high-profile type	45	9	16	60	143.4				46 000	91 500	870	1 030	865
		Square low-profile type	42	9	16	60									
		Flange type	42	9	31	90									
VH35	High-load type	Square high-profile type	55	9.5	18	70	128.8	10.9	34	29	47 500	80 500	950	755	630
		Square low-profile type	48	9.5	18	70									
		Flange type	48	9.5	33	100									
	Super high-load type	Square high-profile type	55	9.5	18	70	162.8				61 500	117 500	1 380	1 530	1 280
		Square low-profile type	48	9.5	18	70									
		Flange type	48	9.5	33	100									
VH45	High-load type	Square high-profile type	70	14	20.5	86	161.4	12.5	45	38	81 000	140 000	2 140	1 740	1 460
		Square low-profile type	60	14	20.5	86									
		Flange type	60	14	37.5	120									
	Super high-load type	Square high-profile type	70	14	20.5	86	193.4				99 000	187 000	2 860	3 000	2 520
		Square low-profile type	60	14	20.5	86									
		Flange type	60	14	37.5	120									
VH55	High-load type	Square high-profile type	80	15	23.5	100	185.4	12.5	53	44	119 000	198 000	3 600	3 000	2 510
		Square low-profile type	70	15	23.5	100									
		Flange type	70	15	43.5	140									
	Super high-load type	Square high-profile type	80	15	23.5	100	223.4				146 000	264 000	4 850	5 150	4 350
		Square low-profile type	70	15	23.5	100									
		Flange type	70	15	43.5	140									

High-Output Pinion-Type Electric Power Steering

The automobile industry is facing an increasingly challenging business environment in which product development must address the concerns of energy conservation and carbon dioxide emissions controls. One example is a California law, Assembly Bill 1493, which requires the Air Resources Board (ARB) of that state to limit emissions from California passenger cars that contribute to global warming. This and other regulations from the European Union and Japan will have a big impact on the automobile industry over the next 10 years and beyond. It is under these circumstances that electric power steering (EPS) systems have been attracting more attention for their higher energy efficiency in comparison to conventional hydraulic systems. EPS systems have been equipped in not only minivehicles, but also in some midsize and large luxury vehicles. It is in this shifting climate that NSK has developed and marketed a high-output pinion-type EPS system for 2.3-liter class hybrid SUVs. This article briefly discusses our product.

1. Outline of the System

Fig. 1 illustrates the structure of the newly developed high-output pinion-type EPS system.

This system is comprised of a torque sensor, an electric control unit (ECU), an actuator, and a reduction gear that is used in conventional systems as well. The system is configured to provide the proper amount of assist during steering based on information of the vehicle's running condition via the controller area network (CAN). The electronic units are rated at 80 amperes of driving current in order to ensure the sufficient output of higher torque required for large-class vehicles with 330-volt batteries.

Photo 1 High-output pinion-type EPS
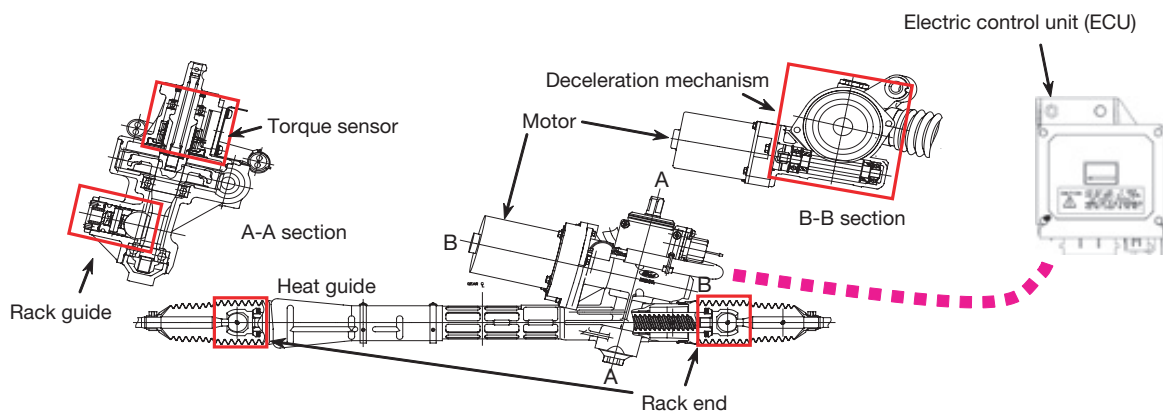
Fig. 1 Structure of high-output pinion-type EPS

2. Features of Components

1) Environmental condition of installation

Due to the EPS system being in close proximity to the exhaust manifold, EPS components must be able to withstand the high-temperature conditions within the engine bay. NSK's EPS incorporates a heat shield around plastic boots that house the system components. The shield helps to keep temperatures below 80 ˚C and

Fig. 2 Rack guide details
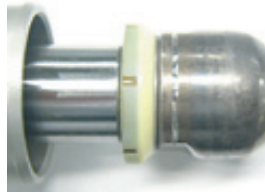
Fig. 3 Rack end details
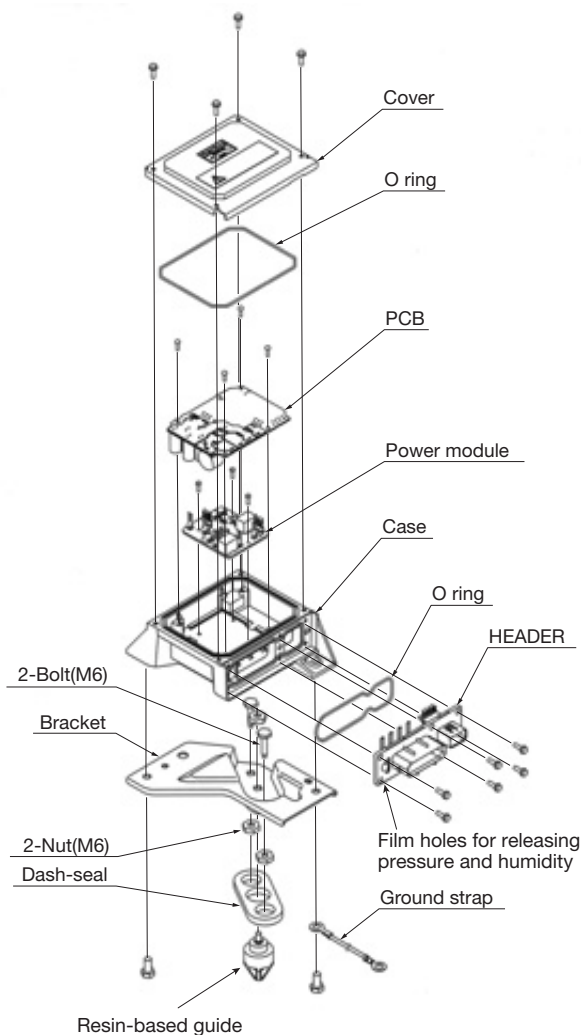
Fig. 4 Disassembled control unit

protects components against radiant heat. In addition to high-temperature durability, the plastic housing of the components helps to prevent any water intrusion.

2) Rack guide

An o-ring is positioned around the circumference of the rack guide to reduce the level of rattling noise caused by forces generated as the tire reacts to changes in the road surface (Fig. 2).

This structure provides more efficient torque transmission and higher wear-resistance than conventional sliding shafts.

3) Deceleration mechanism

A rubber steering damper supports the worm gear shaft and is employed to suppress rattling noise caused by suspension jounce and rebound.

Resin-based materials used for the worm and worm wheel in the reduction gear were selected for further reducing noise levels, for maintaining sufficient durability against the high-temperature operating conditions in the engine bay, and for being highly resistant to water intrusion.

4) Rack end

Due to the high output and increased weight, impact energy generated at the end of the rack stroke becomes large enough to raise concern over the strength of the reduction gears. Therefore, a damper is used at the end of the rack to absorb impact energy from the stopper (Fig. 3).

5) Motor

This system employs a brush motor that generates 4.14 N·m of torque at a rated 80 amperes.

In addition to electromagnetic shielded wire harness, the motor structure is configured to ensure sufficient resistance against heat and water in the engine compartment.
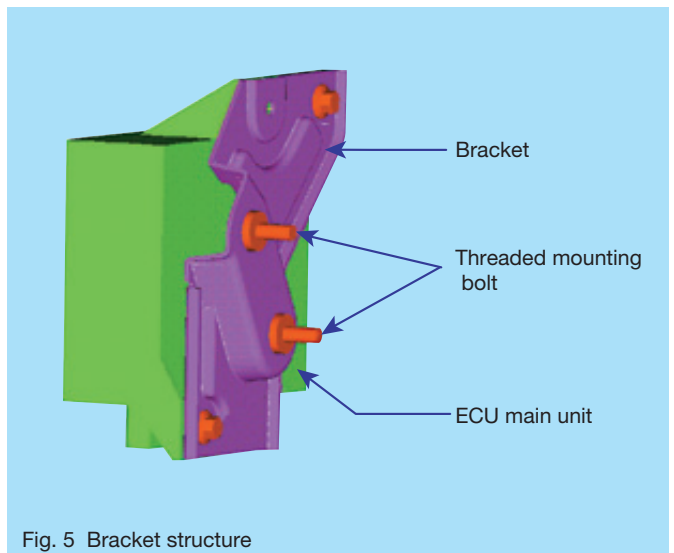
Fig. 5 Bracket structure

Table 1 High-output pinion-type EPS system specifications

	Items	Details
Assembly	Rack thrust (theoretical value)	7 985 N
	Operating temperature range	Gear: –40 ℃ to 110 ℃ ECU: –40 ℃ to 95 ℃
Gear	Type	Pinion gear
	Stroke ratio	44.0 mm/rev
	Type	Worm gear
	Reduction ratio	46 : 3
Motor	Type	DC brushless motor
	Rated current	80 A
	Rated speed	1 210 rpm
	Rated torque	4.14 N·m
Torque sensor	Type	Non-contact self-inductance
	Power supply voltage	9.5 V
Controller	Rated voltage	13.5 V
	Control range of motor current	0 A to 80 A
	Communications functions	CAN (vehicle speed signal, diagnostic tool)
	Self-diagnosis and fail-safe functions	Initial check, monitoring EPS system, test mode

6) Torque sensor

The system uses a contactless torque sensor unit that is field-proven and has low hysteresis characteristics. A laser trimming process is used to adjust neutral voltage and gain of the torque sensor in the circuit board of the torque sensor unit. Laser trimming is a newly adopted method used to adjust resistance value by trimming resistor materials instead of using variable resistance of the conventional control method. The laser trimming method ensures reliable adjustment of torque sensor characteristics even under severe operating conditions.

7) Electronic control unit (ECU)

The ECU complies with the operational requirements of hybrid vehicles and diagnostics under U.S. OBD-II regulations. The driving circuit is equipped with some 80-ampere MOSFETs connected in parallel at each gate. The housing is resistant to water and equipped with film holes for releasing internal pressure and humidity in order to meet environmental conditions in the engine bay and to offer necessary resistance against car washings.

Since the system is mounted in the engine bay, a specially shaped bracket is provided at the base of the housing, which is equipped with a plastic guide for proper alignment and easier assembly (Fig. 4 and 5).

3. Specifications

Specifications of the high-output pinion-type EPS are summarized in Table 1.

4. Summary

NSK has commercially developed the high-output pinion-type EPS with ECUs that can be mounted in the engine bay. On the basis of this model, NSK will strive to standardize products that can provide high-output performance and resistance to severe environments, particularly high resistance to water.

Hydroformed Steering Column

Manufacturers have been facing an increasingly severe business environment resulting from the recent surge in material costs due to a shortage of steel materials along with growing ecological concerns.

Given these trends, NSK started developing a weld-free, hydroformed steering column with the intention of addressing environmental concerns by eliminating the need for welding and reducing the number of parts through single-unit construction. NSK has recently been successful in commercially fabricating a weld-free steering column made from a single part that delivers higher performance than a conventional steering column, and has pursued further advances based on this achievement.

This article discusses the details of the new product.

1. Structure and Specifications

Unlike a conventional steering column in which components are welded together, our newly developed steering column represents a weld-free solution by using the hydroforming process, pressure fitting, and swaging of joints to join components into a single unit.

2. Features

(1) Benefits of switching from a welding process to hydroforming process

- Reduced load on the environment
- Improved reliability
- Greater accuracy (Adjustments to the position of the steering wheel is improved by the enhanced accuracy of sliding parts.)

Photo 2　Conventional steering column

Photo 1　Newly developed steering column
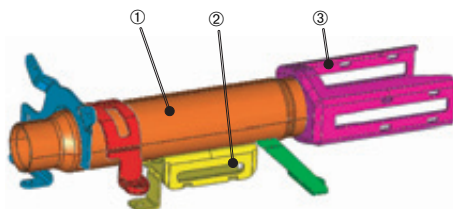
Conventional steering column

· The six individually colored parts are joined by welding.
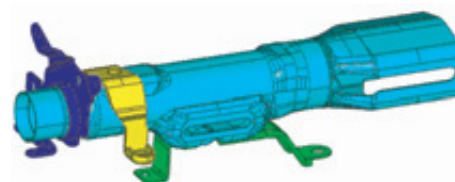
Newly developed steering column

· Parts 1, 2, and 3 (left image) are integrated into one piece by hydroforming.
· The other three parts are joined by clinching or press-fitting processes.

Fig. 1　Comparison between hydroformed and welded steering columns

(2) Reduced number of parts

Three separate parts that were traditionally welded together are all now fabricated from a single part.

(3) Improved performance

- Fabricating what were three structurally separate parts from one hydroformed piece ensures greater structural rigidity of the steering column (table 1).
- Improved accuracy of parts, which makes it easier for the driver to reposition the steering wheel, was achieved using the same die for the hydroforming process and for the process of making holes and slots (photo 3).

3. Summary

NSK will continue to develop products in response to the changing business environment and market needs.

Table 1 Rigidity

	Rigidity	
	Horizontal direction	Vertical direction
Conventional steering column	1	1
Newly developed steering column	1.3	2
Result	30 % improvement	Twofold improvement

Slots used for position adjustments of the steering wheel.
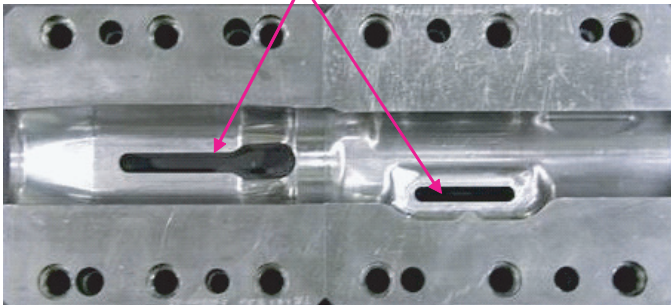
Photo 3 Tubular blank positioned in the die cavity (after hydroforming process)

PS Series of Megatorque Motors™

Demand has been increasing recently for highly productive manufacturing equipment that can perform micromachining tasks. However, conventional actuators, such as servomotors and speed-reducing systems or mechanical indexes, are reaching their limits of high performance, which are starting to fall short of user demand due to insufficient mechanical accuracy and backlash. Thus, direct drive motors are increasingly popular these days. NSK has successfully developed the new PS series of Megatorque Motors, which is a new type of direct-drive (DD) motor that can satisfy the need for higher performance indexing at higher speeds and higher accuracy (photo 1).

This article discusses the new PS series in greater detail.

1. Features

1) High-torque motor

High acceleration and deceleration are essential for achieving high-speed positioning, therefore, the motor needs to output higher torque. Finite element method (FEM) analysis was used in the development of the PS series to analyze magnetic fields (Fig. 1). A powerful permanent magnet was included when designing the optimal magnetic field. As a result, the PS series generates thrust per unit of area (thrust density) that is twice that of a conventional motor. Consequently, the PS series achieves high torque without increasing motor size.

2) Quicker high-speed positioning

A new method was developed for improving motor-control characteristics (Fig. 2) in order to achieve quicker positioning by a motor that is capable of rapid acceleration and deceleration.

- High-performance follow-up control substantially improved response to a rotation command for positioning. For example, the positioning error in a 180 ° positioning operation while responding to a rotation command is about 20 000 pulses for a conventional motor. However, the positioning error is only 40 pulses for the PS series.
- Friction compensation control enables quicker settling (the time required to reach a targeted accuracy range upon completion of a rotation command for positioning) to 1 ms, which is less than one-fifth that of a conventional control.

Photo 1 PS series of Megatorque Motors™
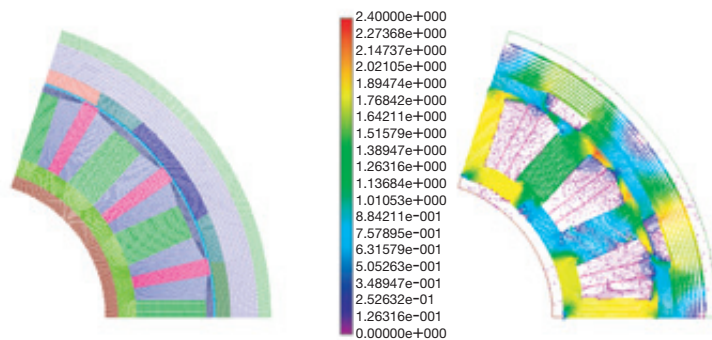
Fig. 1 FEM model and magnetic flux density distribution chart
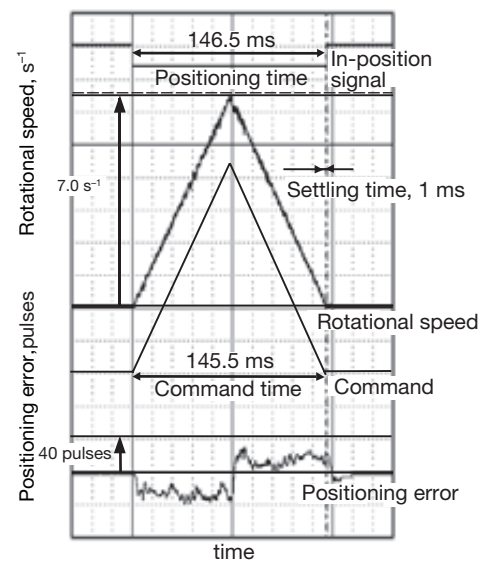
Fig. 2 Positioning test results

Table 1 Specifications of the PS series of Megatorque Motor series

Item \ Model		PS1006	PS1012	PS1018	PS3015	PS3030	PS3060	PS3090
Motor outer diameter	[mm]		ϕ100			ϕ150		
Motor height	[mm]	85	110	135	85	102	136	170
Motor bore diameter	[mm]		ϕ35			ϕ56		
Maximum output torque	[N·m]	6	12	18	15	30	60	90
Rated output torque	[N·m]	2	4	6	5	10	20	30
Maximum rotational speed	[s⁻¹]		10		10		8	5
Position sensor resolution	[count/rev]		2 621 440			2 621 440		
Absolute positioning accuracy [''(seconds of arc)]			90			90		
Rotor inertia	[kg·m²]	0.0024	0.0031	0.0038	0.011	0.014	0.019	0.024
Motor mass	[kg]	2.4	3.5	4.5	5.5	6.9	11.0	13.8

3) Highly accurate, high-speed, position detection

The PS series achieves a maximum rotational speed of 10 s⁻¹ at a resolution of 2.62 million counts/rev by controlling the resolution of the resolver at four stages according to speed.

The PS series achieves a sensor accuracy of 90 arc seconds due to optimally designed gear tooth profile for the resolver, in addition to a gear tooth number and a pole number ratio that eliminates higher harmonic components.

2. Product Specifications

Table 1 shows specifications of the PS series of Megatorque Motors. Table 2 compares the PS series and a conventional motor. As shown in this table, size and weight are reduced by 2/3 and 1/2, respectively, while output torque remains the same.

3. Applications

The PS series of Megatorque Motors is widely used in semiconductor manufacturing equipment, CD/DVD manufacturing equipment, assembling machines, inspection equipment, printers, and medical equipment.

4. Summary

In response to demand for higher performance positioning and transport equipment, NSK will continue to develop new types of actuators as a pioneer in direct motors.

Table 2 Comparison between new Megatorque Motor (PS1006) and conventional motor (JS2006)

Item		PS Series (PS1006)	(JS2006)
Motor outer diameter	[mm]	ϕ100	ϕ130
Motor height	[mm]	85	100
Motor bore diameter	[mm]	ϕ35	ϕ40.5
Maximum output torque	[N·m]	6	6
Maximum torque/Volume	[N·m/m³]	7.5	5.0
Position sensor resolution	[count / rev]	2 621 440	614 400
Absolute positioning accuracy	[''(seconds of arc)]	90	150
Maximum rotational speed	[s⁻¹]	10	3
Motor mass	[kg]	2.4	4.8

Notes

Worldwide Sales Offices and Manufacturing Plants

NSK LTD.-HEADQUARTERS, TOKYO, JAPAN www.nsk.com
Nissei Bldg., 1-6-3 Ohsaki, Shinagawa-ku, Tokyo 141-8560, Japan
INDUSTRIAL MACHINERY BEARINGS DIVISION-HEADQUARTERS
P: 03-3779-7227   F: 03-3779-7644   C: 81
AFTERMARKET BUSINESS DIVISION-HEADQUARTERS
P: 03-3779-8893   F: 03-3779-7644   C: 81
AUTOMOTIVE BUSINESS DIVISION-HEADQUARTERS
P: 03-3779-7189   F: 03-3779-7917   C: 81
PRECISION MACHINERY & PARTS DIVISION-HEADQUARTERS
P: 03-3779-7163   F: 03-3779-7644   C: 81

Africa
South Africa:
NSK SOUTH AFRICA (PTY) LTD.
JOHANNESBURG   25 Galaxy Avenue, Linbro Business Park, Sandton, Gauteng, P.O. Box 1157, Kelvin, 2054, South Africa
P: 011-458-3600   F: 011-458-3608   C: 27

Asia and Oceania
Australia:
NSK AUSTRALIA PTY. LTD. www.au.nsk.com
MELBOURNE   11 Dalmore Drive, Scoresby, Victoria 3179, Australia
P: 03-9764-8302   F: 03-9764-8304   C: 61
SYDNEY   24-28 River Road West, Parramatta, New South Wales 2150, Australia
P: 02-8843-8100   F: 02-9893-8406   C: 61
BRISBANE   1/69 Selhurst Street, Coopers Plains, Queensland 4108, Australia
P: 07-3347-2600   F: 07-3345-5376   C: 61
PERTH   Unit 1, 71 Tacoma Circuit, Canning Vale, Western Australia 6155, Australia
P: 08-9434-1311   F: 08-9434-1318   C: 61

China:
NSK HONG KONG LTD.
HONG KONG   RM 814, World Commerce Centre, Harbour City, T.S.T, KLN, Hong Kong
P: 2739-9933   F: 2739-9323   C: 852
SHENZHEN   Room 8B08-09, Jueshi Tower, Jiabing Road, Luohu, Shenzhen, China (518001)
P: 0755-25904886   F: 0755-25904883   C: 86
KUNSHAN NSK CO., LTD.
OFFICE/PLANT   258 South Huang Pu Jiang Rd., Kunshan Economic & Technical Development Zone, Jiang Su, China (215335)
P: 0512-5771-5654   F: 0512-5771-5689   C: 86
CHANGSHU NSK NEEDLE BEARING CO., LTD.
OFFICE/PLANT   No. 66 Dongnan Road, Changshu Southeast Economic Development Zone, Changshu City, Jiangsu, China (215500)
P: 0512-5230-1111   F: 0512-5230-6011   C: 86
NSK STEERING SYSTEMS DONGGUAN CO., LTD.
OFFICE/PLANT   High-tech Park, Shilong Road, Guanlong Section, Dongguan, China (523119)
P: 0769-2262-0960   F: 0769-2316-2867   C: 86
ZHANGJIAGANG NSK PRECISION MACHINERY CO., LTD.
JIANGSU PLANT   No. 34 Zhenxing Road, Zhangjiagang Economic Development Zone, Zhangjiagang City, Jiangsu, China (215600)
P: 0512-5867-6496   F: 0512-5818-0970   C: 86
SUZHOU NSK BEARINGS CO., LTD.
JIANGSU PLANT   No. 22 Taishan Road, Suzhou New District, Jiangsu, China (215129)
P: 0512-6665-5666   F: 0512-6665-9138   C: 86
NSK CHINA TECHNOLOGY CENTER
JIANGSU   258 South Huang Pu Jiang Rd., Kunshan Economic & Technical Development Zone, Jiang Su, China (215335)
P: 0512-5771-5654   F: 0512-5771-0748   C: 86
NSK (SHANGHAI) TRADING CO.
SHANGHAI   10th Fl. Building No. A, Shanghai Far East International Plaza, 319 Xian Xia Road, Shanghai, China (200051)
P: 021-6235-0198   F: 021-6235-1033   C: 86
NSK REPRESENTATIVE OFFICES
BEIJING   Room 2118, Beijing Fortune Bldg., 5 Dong San Huan Bei Lu, Chao Yang District, Beijing, China (100004)
P: 010-6590-8161   F: 010-6590-8166   C: 86
GUANGZHOU   Room 2009-2011, Guangdong Telecom Plaza, 18 Zhongshan Er Road, Guangzhou, China (510080)
P: 020-3786-4833   F: 020-3786-4501   C: 86
CHENGDU   Room1901, Green Land Hotel, No.99 Zhonglieci Xi Street, Chengdu, China (610016)
P: 028-8661-4200   F: 028-8661-4343   C: 86
NSK (CHINA) INVESTMENT CO., LTD www.nsk.com.cn
HEAD OFFICE   10th Fl. Building No. A, Shanghai Far East International Plaza, 319 Xian Xia Road, Shanghai, China (200051)
P: 021-6235-0198   F: 021-6235-1033   C: 86
CHANGCHUN   Room 1001, Building A, Zhongyin Building, 727 Xi'an Road, Changchun, Jilin Province, China (130061)
P: 0431-8898-8682   F: 0431-8898-8670   C: 86
NSK CHINA SALES CO., LTD.
SHANGHAI   10th Fl. Building No. A, Shanghai Far East International Plaza, 319 Xian Xia Road, Shanghai, China (200051)
P: 021-6235-0198   F: 021-6235-1033   C: 86
TIAN JIN   Room 06, 09F The Exchange Tower 2, No. 189 Nan jing Road, Heping District, Tianjin, China (300050)
P: 022-8319-5030   F: 022-8319-5033   C: 86
NSK-WARNER (SHANGHAI) CO., LTD.
PLANT   No. 2518 Huancheng Road (West) Fengxian District, Shanghai,China (201401)
P: 021-3365-5757   F: 021-3365-5262   C: 86
AKS PRECISION BALL (HANGZHOU) CO., LTD.
PLANT   No. 189 Hongda Road, Qiaonan Area of Economic & Technological Development Zone, Hangzhou, Zhejiang, China (311231)
P: 0571-2280-1288   F: 0571-2280-1268   C: 86

India:
RANE NSK STEERING SYSTEMS LTD.
CHENNAI   14, Rajagopalan Salai, Vallancherry, Guduvancherry, Tamil-Nadu, 603 202, India
P:044-274-66002   F:044-274-66001   C:91
NSK LTD. INDIA BRANCH OFFICE
CHENNAI   Giriguja Enclave, 56, First Avenue, Shastri Nagar, Adyar, Chennai-600 020, India
P:044-2446-6862   F:044-2446-6861   C:91
DELHI   311, JMD Pacific Square, Sector 15 (II), 32nd Milestone, National Highway-8, Gurgaon, Haryana (Delhi), India
P:0124-4104-530   F:0124-5104-532   C:91
KOLKATA   502, Trinity Towers, 83, Topsia Road, Kolkata-700 046, India
P:033-4001-2062   F:033-4001-2064   C:91
MUMBAI   321, A Wing, Ahura Centre, 82, Mahakali Caves Road, Andheri East, Mumbai-400 093, India
P:022-2838-7787   F:022-2838-5191   C:91
NSK-ABC BEARINGS LTD.
HEAD OFFICE   Giriguja Enclave, 56, First Avenue, Shastri Nagar, Adyar, Chennai-600 020, India
P:044-2446-6862   F:044-2446-6861   C:91

Indonesia:
PT. NSK BEARINGS MANUFACTURING INDONESIA
JAKARTA PLANT   Blok M4, Kawasan Berikat MM2100 Industrial Town Cikarang Barat, Bekasi 17520, Indonesia
P: 021-898-0155   F: 021-898-0156   C: 62
PT. NSK INDONESIA
JAKARTA   Summitmas II, 6th Floor, Jl. Jend Sudirman Kav. 61-62, Jakarta 12190, Indonesia
P: 021-252-3458   F: 021-252-3223   C: 62

Korea:
NSK KOREA CO., LTD. www.kr.nsk.com
SEOUL   9F (West Wing) Posco Center 892, Deachi 4 Dong Kangnam-Ku, Seoul, Korea
P: 02-3287-0300   F: 02-3287-0345   C: 82
CHANGWON   60 Seongsan-Dong, Changwon, Kyungsangnam-Do, Korea
PLANT   P: 055-287-6001   F: 055-285-9982   C: 82

Malaysia:
NSK BEARINGS (MALAYSIA) SDN BHD www.my.nsk.com
HEAD OFFICE   No. 2, Jalan Pemaju, U1/15, Seksyen U1, Hicom Glenmarie Industrial Park, 40150 Shah Alam, Selangor, Malaysia
P: 03-7803-8859   F: 03-7806-5982   C: 60
PRAI   No.36, Jalan kikik, Taman Inderawasih, 13600 Prai, Penang, Malaysia
P: 04-3902275   F: 04-3991830   C: 60
JOHOR BAHRU   88 Jalan Ros Merah 2/17, Taman Johor Jaya, 81100 Johor Bahru, Johor, Malaysia
P: 07-3546290   F: 07-3546291   C: 60
KOTA KINABALU   Lot 10, Lrg Kurma 4, Likas Ind. Centre, 5/12 Miles Jln Tuaran, 88450 Inanam, Sabah, Malaysia
P: 088-421260   F: 088-421261   C: 60
IPOH   Gr. Floor, 89 Jalan Bendahara, 31650 Ipoh, Perak, Malaysia
P: 05-2555000   F: 05-2553373   C: 60
NSK MICRO PRECISION (M) SDN. BHD. www.my.nsk.com
MALAYSIA PLANT   No.43 Jalan Taming Dua,Taman Taming Jaya 43300 Balakong, Selangor Darul Ehsan, Malaysia
P: 03-8961-3960   F: 03-8961-3968   C: 60

New Zealand:
NSK NEW ZEALAND LTD. www.nsk-rhp.co.nz
AUCKLAND   3 Te Apunga Place, Mt. Wellington, Auckland, New Zealand
P: 09-276-4992   F: 09-276-4082   C: 64

Philippines:
NSK REPRESENTATIVE OFFICE
MANILA   8th Floor The Salcedo Towers 169 H.V. dela Costa St., Salcedo Village Makati City, Philippines 1227
P: 02-759-6246   F: 02-759-6249   C: 63

Singapore:
NSK INTERNATIONAL (SINGAPORE) PTE LTD.
SINGAPORE   238A, Thomson Road, #24-01/05, Novena Square Tower A, Singapore 307684
P: 6496-8000   F: 6250-5845   C: 65
NSK SINGAPORE (PRIVATE) LTD. www.nsk-singapore.com.sg
SINGAPORE   238A, Thomson Road, #24-01/05, Novena Square Tower A, Singapore 307684
P: 6496-8000   F: 6250-5845   C: 65

Taiwan:
TAIWAN NSK PRECISION CO., LTD.
TAIPEI   11F., No. 87, Songjiang Rd., Jhongshan District, Taipei City 104, Taiwan R.O.C.
P: 02-2509-3305   F: 02-2509-1393   C: 886
TAICHUNG   107-6, Sec. 3, Wen Xing Rd., Taichung 407, Taiwan R.O.C.
P: 04-2311-7978   F: 04-2311-2627   C: 886
TAINAN   48, Lane 62, Fusing Rd., Sinshin Township, Tainan County 744, Taiwan R.O.C.
P: 06-589-2703   F: 06-589-2719   C: 886
TAIWAN NSK TECHNOLOGY CO., LTD.
TAIPEI   11F., No. 87, Songjiang Rd., Jhongshan District, Taipei City 104, Taiwan R.O.C.
P: 02-2509-3305   F: 02-2509-1393   C: 886

Thailand:
NSK BEARINGS (THAILAND) CO., LTD.
BANGKOK   25th Floor RS Tower, 121/76-77 Rachadaphisek Rd., Dindaeng, BKK 10400, Thailand
P: 02641-2150   F: 02641-2161   C: 66
NSK BEARINGS MANUFACTURING (THAILAND) CO., LTD.
OFFICE/PLANT   700/430 Amata Nakorn Industrial Estate T. Donhualor, A. Muangchonburi, Chonburi 20000, Thailand
P: 038-454-010   F: 038-454-017   C: 66
SIAM NSK STEERING SYSTEMS CO., LTD.
OFFICE/PLANT   90 Moo 9, Wellgrow Industrial Estate, Km.36 Bangna-Trad Rd., Bangwao, Bangpakong, Chachoengsao 24180, Thailand
P: 038-522-343   F: 038-522-351   C: 66

NSK ASIA PACIFIC TECHNOLOGY CENTRE (THAILAND) CO., LTD.
CHONBURI   700/430 Moo 7, Amata Nakorn Industrial Estate, T.Donhualor, A.Muangchonburi, Chonburi 20000, Thailand
P: 038-454-631   F: 038-454-634   C: 66
Vietnam:
NSK VIETNAM CO., LTD.
HEAD OFFICE   Techno Center, Room 204-205, Thang Long Industrial Park, Dong Anh District, Hanoi, Vietnam
P: 04-955-0159   F: 04-955-0158   C: 84
NSK REPRESENTATIVE OFFICE
HO CHI MINH CITY   Suite 307, Metropolitan Building, 235 Dong Khoi Street, District 1,HCMC, Vietnam
P: 08-822-7907   F: 08-822-7910   C: 84

Europe
NSK EUROPE LTD. (EUROPEAN HEADQUARTERS) www.eu.nsk.com
MAIDENHEAD   Belmont Place, Belmont Road, Maidenhead, Berkshire SL6 6TB, U.K.
P: 01628-509-800   F: 01628-509-808   C: 44
France:
NSK FRANCE S.A.S
PARIS   Quartier de l'Europe, 2 Rue Georges Guynemer, 78283 Guyancourt, France
P: 01-30-57-39-39   F: 01-30-57-00-01   C: 33
Germany:
NSK DEUTSCHLAND GMBH
HEAD OFFICE   Harkortsrasse 15, D-40880 Ratingen, Germany
P: 02102-4810   F: 02102-4812-290   C: 49
STUTTGART   Siellminger Strasse 65, D-70771 Leinfelden-Echterdingen, Germany
P: 0711-79082-0   F: 0711-79082-289   C: 49
WOLFSBURG   Heinrich-Nordhoff-Strasse 101, D-38440 Wolfsburg, Germany
P: 05361-27647-10   F: 05361-27647-70   C: 49
INGOLDSTADT   Ingoldstadt, D-85055 Ingoldstadt, Germany
P: 0841-901-4640   F: 0841-901-4642   C: 49
NSK PRECISION EUROPE GMBH
DÜSSELDORF   Harkortsrasse 15, D-40880 Ratingen, Germany
P: 02102-4810   F: 02102-4812-290   C: 49
NEUWEG FERTIGUNG GMBH
OFFICE/PLANT   Ehinger Strasse 5, D-89597 Munderkingen, Germany
P: 07393-540   F: 07393-5414   C: 49
Italy:
NSK ITALIA S.P.A.
MILANO   Via Garibaldi, 215, 20024 Garbagnate Milanese (Milano), Italy
P: 0299-5191   F: 0299-028373   C: 39
INDUSTRIA CUSCINETTI S.P.A.
TORINO PLANT   Via Giotto 4, I-10080, S. Benigno C. se (Torino), Italy
P: 011-982-4811   F: 011-988-0284   C: 39
Netherlands:
NSK EUROPEAN DISTRIBUTION CENTRE B.V.
De Kroonstraat 38, 5048 AP Tilburg, Netherlands
P: 013-4647647   F: 013-4647648   C: 31
Poland:
NSK EUROPE LTD. REPRESENTATIVE OFFICE
WARSAW   Ul. Migdalowa 4/73, 02-796, Warsaw, Poland
P: 022-645-1525   F: 022-645-1529   C: 48
NSK BEARINGS POLSKA S.A.
OFFICE/PLANT   Ul. Jagiellonska 109, 25-734 Kielce, Poland
P: 041-366-5001   F: 041-367-0500   C: 48
NSK EUROPEAN TECHNOLOGY CENTER, POLAND OFFICE
OFFICE/PLANT   Ul. Jagiellonska 109, 25-734 Kielce, Poland
P: 041-366-5812   F: 041-366-5206   C: 48
NSK STEERING SYSTEMS EUROPE (POLSKA) SP.ZO.O.
CORPORATE   Ul. Mariana Jachimowicza 17, 58-306 Walbrzych, Poland
OFFICE/PLANT   P: 074-664-4101   F: 074-664-4104   C: 48
Spain:
NSK SPAIN S.A.
BARCELONA   C/Tarragona 161, 2ª Planta, 08014, Barcelona, Spain
P: 093-433-5775   F: 093-433-5776   C: 34
Turkey:
NSK RULMANLARI ORTA DOGU TIC. LTD. STI.
ISTANBUL   19 Mayis Mah. Ataturk Cad. Ulya Engin Is Merkezi No. 68 Kat. 6, Kozyatagi 34734, Istanbul, Turkey
P: 0216-355-0398   F: 0216-355-0399   C: 90
United Kingdom:
NSK BEARINGS EUROPE LTD.
PETERLEE   3 Brindley Road, South West Industrial Estate, Peterlee, Co. Durham SR8 2JD, U.K.
PLANT   P: 0191-586-6111   F: 0191-586-3482   C: 44
NEWARK   Northern Road, Newark, Nottinghamshire NG24 2JF, U.K.
PLANT   P: 01636-605-123   F: 01636-605-000   C: 44
NSK EUROPEAN TECHNOLOGY CENTRE
NEWARK   Northern Road, Newark, Nottinghamshire NG24 2JF, U.K.
P: 01636-605-123   F: 01636-643-241   C: 44
NSK UK LTD.
NEWARK   Northern Road, Newark, Nottinghamshire NG24 2JF, U.K.
P: 01636-605-123   F: 01636-605-000   C: 44
NSK PRECISION UK LTD.
PLANT   Northern Road, Newark, Nottinghamshire NG24 2JF, U.K.
P: 01636-605-123   F: 01636-605-000   C: 44
NSK STEERING SYSTEMS EUROPE LTD.
HEAD OFFICE   Belmont Place, Belmont Road, Maidenhead, Berkshire SL6 6TB, U.K.
P: 01628-509-800   F: 01628-509-808   C: 44
COVENTRY   Oak Court Unit 4-5, Pilgrims Walk Prologis Park, Coventry, West Midlands CV6 4QH, U.K.
P: 02476-337-100   F: 02476-339-182   C: 44
PETERLEE   6/7 Doxford Drive, South West Industrial Estate, Peterlee, Co. Durham SR8 2PP, U.K.
PLANT   P: 0191-518-6400   F: 0191-518-6421   C: 44

North and South America
NSK AMERICAS, INC. (AMERICAN HEADQUARTERS)
ANN ARBOR   4200 Goss Road, Ann Arbor, Michigan 48105, U.S.A.
P: 734-913-7500   F: 734-913-7511   C: 1
Argentina:
NSK ARGENTINA SRL
BUENOS AIRES   Garcia del Rio 2477 Piso 7 Oficina "A" (1429) Buenos Aires-Argentina
P: 11-4704-5100   F: 11-4704-0033   C: 54
Brazil:
NSK BRASIL LTDA. www.br.nsk.com
HEAD OFFICE   Rua 13 de Maio, 1633-14th Andar-Bela Vista-CEP 01327-905 Sao Paulo, SP, Brazil
P: 011-3269-4786   F: 011-3269-4720   C: 55
SUZANO PLANT   Av. Vereador Joao Batista Fitipaldi, 66, CEP 08685-000, Vila Maluf, Suzano, SP, Brazil
P: 011-4744-2527   F: 011-4744-2529   C: 55
BELO HORIZONTE   Rua Ceara 1431-4th andar-sala 405-Funcionarios Belo Horizonte-MG, Brazil 30150-311
P: 031-3274-2477   F: 031-3273-4408   C: 55
JOINVILLE   Rua Blumenau, 178-sala 910-Centro Joinville-SC, Brazil 89204-250
P: 047-3422-5445   F: 047-3422-2817   C: 55
PORTO ALEGRE   Av. Cristovão Colombo, 1694-sala 202-Floresta Porto Alegre-RS, Brazil 90560 001
P: 051-3222-1324   F: 051-3222-2599   C: 55
RECIFE   Av. Conselheiro Aguiar, 2738-6th andar-conj. 604-Boa Viagem Recife-PE, Brazil 51020-020
P: 081-3326-3781   F: 081-3326-0547   C: 55
Canada:
NSK CANADA INC. www.ca.nsk.com
HEAD OFFICE   5585 McAdam Road, Mississauga, Ontario, Canada L4Z 1N4
P: 905-890-0740   F: 905-890-0488   C: 1
MONTREAL   2150-32E Avenue, Lachine, Quebec, Canada H8T 3H7
P: 514-633-1220   F: 514-633-8164   C: 1
VANCOUVER   3353 Wayburne Drive, Burnaby, British Columbia, Canada V5G 4L4
P: 604-294-1151   F: 604-294-1407   C: 1
Mexico:
NSK RODAMIENTOS MEXICANA, S.A. DE C.V. www.mx.nsk.com
MEXICO CITY   Av. Presidente Juarez No.2007 Lote 5, Col. San Jeronimo Tepetlacalco, Tlalnepantla, Estado de Mexico, Mexico, C.P.54090
P: 55-5390-4312   F: 55-5390-8175   C: 52
United States of America:
NSK CORPORATION www.us.nsk.com
HEAD OFFICE   4200 Goss Road, Ann Arbor, Michigan 48105, U.S.A.
P: 734-913-7500   F: 734-913-7511   C: 1
NSK AMERICAN   4200 Goss Road, Ann Arbor, Michigan 48105, U.S.A.
TECHNOLOGY CENTER   P: 734-913-7500   F: 734-913-7511   C: 1
CLARINDA PLANT   1100 N. First Street, Clarinda, Iowa 51632, U.S.A.
P: 712-542-5121   F: 712-542-4905   C: 1
FRANKLIN PLANT   3450 Bearing Drive, Franklin, Indiana 46131, U.S.A.
P: 317-738-5000   F: 317-738-5050   C: 1
LIBERTY PLANT   1112 East Kitchel Road, Liberty, Indiana 47353, U.S.A.
P: 765-458-5000   F: 765-458-7832   C: 1
NSK PRECISION AMERICA, INC. www.npa.nsk.com
OFFICE/PLANT   3450 Bearing Drive, Franklin, Indiana 46131, U.S.A.
P: 317-738-5000   F: 317-738-5050   C: 1
SAN JOSE   780 Montague Expressway, Suite 508, San Jose, California 95131, U.S.A.
P: 408-944-9400   F: 408-944-9405   C: 1
NSK STEERING SYSTEMS AMERICA, INC. www.nssa.nsk.com
OFFICE/PLANT   110 Shields Drive, Bennington, Vermont 05201, U.S.A.
P: 802-442-5448   F: 802-442-2253   C: 1
ANN ARBOR   4200 Goss Road, Ann Arbor, Michigan 48105, U.S.A.
P: 734-913-7500   F: 734-913-7102   C: 1
NSK-WARNER U.S.A., INC.
TROY   3001 West Big Beaver Road, Suite 701, Troy, Michigan 48084, U.S.A.
P: 248-822-8888   F: 248-822-1111   C: 1
NSK LATIN AMERICA, INC. www.la.nsk.com
MIAMI   2500 NW 107th Avenue, Suite 300, Miami, Florida 33172, U.S.A.
P: 305-477-0605   F: 305-477-0377   C: 1

P: Phone   F: Fax   C: Country Code   Printed in Japan

Motion & Control

No. 20 August 2007

Published by NSK Ltd.